UTS UNIVERSITY OF TECHNOLOGY SYDNEY

Effect of Alkali-Silica Reaction on Chloride-Induced Corrosion in Reinforced Concrete

by Ata Aminfar

Thesis submitted in fulfilment of the requirements for the degree of

Master's by Research (MRes)

under the supervision of A/Prof. Shami Nejadi
Co-Supervisor Dr Nadarajah Gowripalan

University of Technology Sydney
Faculty of engineering and information technology (FEIT)

February 2022

CERTIFICATE OF ORIGINAL AUTHORSHIP

I, *Ata Aminfar* declare that this thesis, is submitted in fulfilment of the requirements for the award of Master's by Research, in the School of civil and environmental engineering, faculty of engineering and information technology (FEIT) at the University of Technology Sydney.

This thesis is wholly my own work unless otherwise referenced or acknowledged. In addition, I certify that all information sources and literature used are indicated in the thesis.

This document has not been submitted for qualifications at any other academic institution.

This research is supported by the Australian Government Research Training Program.

Signature:

Production Note:
Signature removed prior to publication.

Date: 20/02/2022

To my lovely family

Acknowledgement

During my two year journey as a master by research student at UTS, I have learned many new things and met some great individuals that helped me throughout this challenging but delightful journey.

I want to thank my knowledgeable principal supervisor, Professor Shami Nejadi, for his guidance throughout this journey, it was indeed a pleasure to be supervised by someone who genuinely cares about his students. A special thanks to Dr. Nadarajah Gowripalan for his support. I also want to extend my gratitude to Dr. Farhad Nabavi. Lastly, I want to mention Professor Hadi Khabbaz for his support as deputy head of school (research) during my time of need.

Without my dear parents and my brother Ali's support, non of these would have been possible as they supported me monetarily and mentally throughout this long journey. I could not have done any of this without their support. I want to thank my dear friends that made the journey less cumbersome.

A big thanks to UTS Tech Lab staff, especially Muller and Ann who helped me immensely in the concrete service life laboratory to conduct my experiments and Van for being patient and always helping out everyone with the faculty procedures.

Finally, I want to note that my arrival to Australia was when Covid peaked in Sydney in early 2020. This influenced my work as a master by research student by a vast amount as the course duration was two years, and my experiments alone took around a year to be conducted. Thankfully I was able to finish my work with the guidance of my supervisors and extract good results from my experiments.

List of Submitted Publications

Aminfar, A., Nejadi, S,. ‘Effect of Alkali-Silica Reaction on Chloride-Induced Corrosion in Reinforced Concrete’ Paper and poster for the 16th International Conference on Civil Engineering and Materials ICCEM, December 2022 Sydney Australia.

List of Papers Being Prepared for Submission

Aminfar, A., Nejadi, S. and Habibagahi, M., ‘Effect of Alkali-Silica Reaction on Corrosion of Steel Reinforcement in Concrete Structures’, being prepared for Construction and Building Materials journal.

Table of Contents

Table of Figures

List of Tables

Abstract

Alkali-silica reaction (ASR) and reinforced concrete (RC) corrosion are two of the major concrete deterioration phenomena that can affect concrete structures such as jetties, bridges, and dams, causing harm to the structure lowering the lifespan and the structural integrity, which eventually results in billions of dollars of rehabilitation cost. Although ASR and RC corrosion mechanisms are well-known and have been studied significantly in the past years individually, there have been small amounts of research regarding ASR and RC corrosion combined effects and how ASR can affect the corrosion of steel in RC structures. This study aims to determine how ASR can impact chloride-induced corrosion in RC structures utilizing accelerated laboratory test methods. ASR generates an expansive gel that causes concrete to expand and crack over time. These cracks may open the way to other deteriorating effects, such as chloride ions. Previous research on ASR speculates that ASR cracks could accelerate chloride ions ingress leading to faster corrosion of the reinforcement embedded in concrete. However, recent research show otherwise and suggest that ASR can cause higher tortuosity in concrete that tributes to the lowering of diffusion/migration coefficient of concrete which causes concrete affected by ASR to resist the ingress of chloride ions. The investigation in this study is planned to be carried out using experimental approaches. The experimental study is based on a "Comparative Method" and will compare the time to corrosion-induced cracking and migration coefficient in concrete specimens utilizing accelerated methods for concrete with highly reactive dacite and non-reactive aggregate with 1.25% alkali boosting. The chloride migration coefficient of reactive specimens decreased over the 150-day test duration compared to specimens prepared with non-reactive aggregate. Furthermore, accelerated chloride-induced corrosion (ACIC) tests on reactive specimens show a higher time to cover crack due to corrosion than non-reactive specimens over the 150-day testing. Additionally, the mechanical properties of the specimens prepared with a reactive and non-reactive aggregate such as compressive strength, tensile strength and modulus of elasticity were measured. The compressive and tensile strength of the reactive specimens, which expanded by 0.12%, shows little change while the modulus of elasticity decreased over the 150-

day testing period compared to non-reactive specimens. The results of this experiment indicate that ASR within the concrete environment can lower the chloride migration of the concrete and increase the time to chloride-induced corrosion crack of the concrete cover.

Chapter 1
Introduction

1.1 Introduction

Reinforced concrete (RC) structures are one of the essential and widely used materials for construction in this era. This is because, despite its flaws, RC has good compressive strength per unit cost, its constituent can be found almost in every part of the world, it can be shaped with ease to reach the desired shape for the cause of the structure, and it is reasonably resistant to harsh environments compared to other materials (McCormac, 2016).

Due to its extensive use throughout its lifespan, RC endures numerous deleterious effects such as carbonation, corrosion, aberration and erosion, chemical attacks, alkali-aggregate reactivity (AAR), freeze-thaw deterioration and other degrading effects. The level of strength loss and degradation due to these deleterious effects is related directly to the aggressiveness of the environment and used materials in the RC structure. Among the mentioned phenomenon, corrosion of embedded steel and AAR (mainly Alkali-Silica Reaction (ASR)) are two of the significant causes of RC deterioration that affects its overall performance and durability (Gjørv, 2014; Portland Cement Association, 2002; Swamy, 1991).

Maintenance and rehabilitation of RC structures damaged by the aforementioned phenomena are costly and can escalate to vast amounts if left unchecked. According to the American Society of Civil Engineers infrastructure report card, the backlog of rehabilitation projects in the united states for dams and bridges combined is estimated to be over $212 billion (ASCE, 2017). As stated in the infrastructure maintenance report in Australia by GHD, large parts of regional Australia are affected by salinity, and salinity impacts are likely to increase by climate change heavily affecting reinforced concrete infrastructure. Because of the mentioned conditions and high costs, it is imperative to prevent RC structures premature deterioration and appropriately design them to endure their expected design service life (GHD, 2015) Because it is not economical to demolish and reconstruct the damaged structure affected by combined effects of ASR and chloride-induced corrosion, all measures should be taken to understand the process of how ASR would have an effect on chloride-induced corrosion and taken into account for the sake of monitoring and remedial purposes. ASR is not a common deteriorating effect compared to chloride-induced corrosion when it comes to RC structures and it is rare, but it still poses a great threat for structures around the globe as well as in Australia.

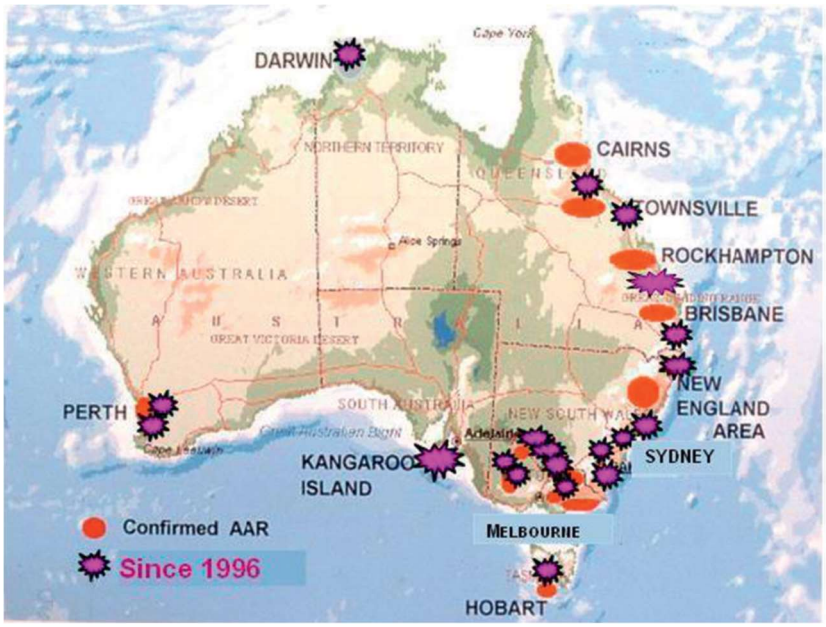

Figure 1-1 Most of the structures affected by AAR reside near coastlines, making them prone to corrosion in Australia (Poole & Sims, 2016)

Multiple structures in Australia have been diagnosed with ASR since 1980, but not much research has been conducted on the combined effect of ASR and chloride-induced corrosion on the diagnosed structures, as most of them are near the Australian coastlines, and corrosion effects on such structures should be considered as it plays a significant role on the lifespan of the structures. Lucinda Jetty, located at Lucinda, Queensland, Australia, is an example of a structure diagnosed with ASR and chloride-induced corrosion combined effect. Lucinda Jetty was constructed in 1979 and has been monitored since the late 1980s and it has been found that the prestress strands and stirrups have been subjected to extensive corrosion due to being exposed to seawater splashes, it has also been confirmed that the concrete of the Jetty structure has been subjected to ASR as well because of reactive aggregate usage (Berndt, 2019). According to the investigations and reports done by Berndt (2019), the repair and replacement of Lucinda Jetty girders damaged due to combined effects of ASR and corrosion pose a great issue because of high costs. In Figure 1-2, a depiction of joint ASR and chloride-induced corrosion deteriorating effect on Lucinda Jetty girder can be seen.

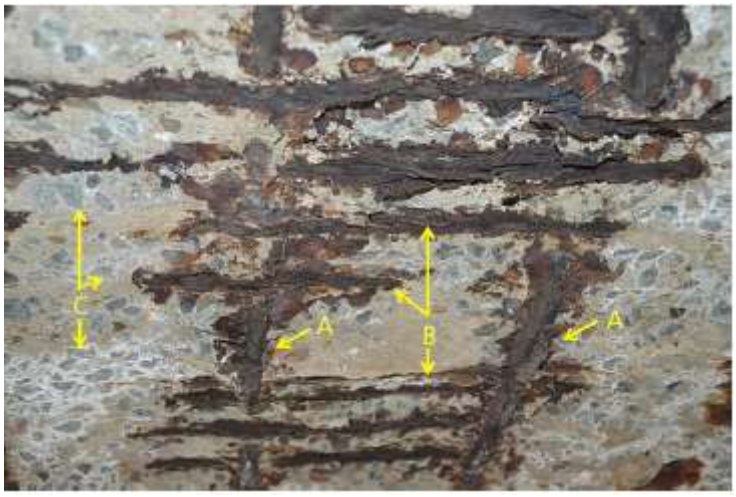

Figure 1-2. ASR and chloride-induced corrosion combined effects. (A) corrosion of prestressing strands, (B) corrosion of stirrups and (C) white ASR gel deposits (Berndt, 2019)

Considerable research has been conducted on the effects of ASR and chloride-induced corrosion on RC structures separately. However, limited observations have been made on the synergetic effects of ASR and corrosion in reinforced RC structures

premature failure, raising the question of how their joint effect can negatively impact the serviceability of RC structures and influence them.

The few early speculations and empirical evidence by Somerville suggest that corrosion has a low chance of occurrence when concrete cover is cracked due to ASR (Somerville, 1985). Research done by the institution of structural engineers in 1992, on the other hand, suggests that as the effect of ASR on the corrosion rate of RC structures may not be clear, actions such as appropriate concrete cover and good concrete quality should be taken so that the effect of ASR on corrosion rates would not be serious (ISE, 1992).

Many pieces of literature on the effects of ASR and corrosion also suggest that cracks induced by ASR can facilitate the corrosion of reinforcement within the concrete, thus regarding ASR as a means of introducing the risk of corrosion to the concrete environment (Poole & Sims, 2016; Saouma, 2020; Swamy, 1991). However, few of the studies on ASR and subsequent corrosion indicate that ASR gel can indeed slow the ingress of chloride ions which results in higher tortuosity resulting in a higher Diffusion Coefficient (D_a) in the concrete environment. ASR not only affects D_a but also influences, critical chloride threshold (C_T) and corrosion initiation time of the RC (Trejo et al., 2017). The value change in these parameters can play a crucial role in the corrosion process of concrete influenced by ASR.

1.2 Research Scope and Objectives of the Project

This research aims to investigate the effect of ASR and subsequent chloride-induced corrosion on RC specimens through accelerated methods, including evaluating time to chloride-induced corrosion crack in concrete cover utilizing Accelerated Chloride-Induced Corrosion (ACIC) test and chloride migration coefficient utilizing the standard NT Build 492. These tests will give us an insight into the combined effects of ASR and subsequent corrosion, indicating if ASR and its product ASR gel can impact the chloride diffusion and time to chloride-induced corrosion crack in concrete cover.

1.3 Research Significance and Contributions

There are a limited number of publications regarding combined deterioration due to ASR and chloride-induced corrosion, which makes this research essential. As the number of structures around the globe diagnosed by ASR increases due to ASR's time dependant reaction, which may take decades to surface and considering that reinforcement corrosion is an inevitable deteriorating effect in RC structures, it is important to evaluate such structures that are undergoing ASR and subsequent corrosion to better assess their conditions and propose the necessary remedial actions in future studies based on the latest research for current and future structures to come.

1.4 Structure of the Thesis

The thesis is presented in five chapters.

Chapter 1: A brief introduction of the topic, scops and research significance.

Chapter 2: Contains a detailed literature review on the ASR and RC corrosion, the ASR and corrosion mechanisms, the effect of ASR on mechanical properties of concrete, effects of ASR and corrosion combined effects on mechanical properties.

Chapter 3: A full description of ACIC test method measuring time to chloride-induced corrosion crack on specimens containing reactive and non-reactive aggregate to see whether ASR and its by-product ASR gel can impact the corrosion process in the concrete environment, evaluating the non-steady-state chloride migration coefficient on reactive and non-reactive specimens to determine if specimens undergoing ASR can impact the chloride migration/diffusion of the concrete by comparing the non-steady-state chloride migration coefficient and lastly conducting compressive strength, indirect tensile strength and modulus of elasticity tests on concrete specimens undergoing ASR and comparing the results with specimens containing non-reactive aggregate to see the impact of ASR on concrete mechanical properties.

Chapter 4: Results and discussion on ACIC test, NT build 492 non-steady-state chloride migration coefficient test and concrete mechanical properties.

Chapter 5: Summary and conclusion of the experimental project with recommendations for future research.

Chapter 2
Literature Review

2.1 Overview

ASR and RC corrosion are vastly different concrete deteriorating mechanisms, which cause premature deterioration of the structure. A detailed explanation will be presented for both mechanisms separately, following their combined effects on mechanical properties and structural behaviour. When ASR and chloride-induced corrosion occur in concrete simultaneously, it can devastate the concrete as both expand the concrete considerably. In the next sections, ASR and corrosion of the RC and their combined effects are explained in detail.

2.1.1 ASR History

ASR is one of the common forms of alkali-aggregate reaction (AAR) in concrete. AAR naturally consists of alkali-silica reaction, alkali-silicate reaction and alkali carbonate reaction (Gillott, 1975).

ASR was first brought to light by Stanton in 1940. It was Stanton who first stated that ASR is a deleterious reaction between the alkali hydroxyl and certain forms of

hydrous silica that causes expansion and ultimately results in the premature deterioration of the concrete, the first case of ASR damage that caught Stanton's attention was the pavement damage in the north of the town of Bradley in Salinas valley built-in 1936- 1937 after two winters in 1938 some parts of the pavement showed immoderate expansion and cracking through the pavement slabs. There were also earlier structures like the King's Bridge built in 1919-1920 that succumbed to partial failure due to ASR, but it was the Salinas valley pavement failure that led to the ASTM C227 (Standard Test Method for Potential Alkali Reactivity of Cement-Aggregate Combinations) or the (Mortar-Bar Method), which was withdrawn since 2018 and was replaced by ASTM C1260 (Standard Test Method for Potential Alkali Reactivity of Aggregates) that is still in use.

Research regarding ASR in Australia started in the year of 1943 by Commonwealth Scientific and Industrial Research Organisation (CSIRO). Most of the research was spearheaded by Harold Vivian. The research conducted in Australia from 1943 to the late 1950s on ASR concluded that many factors might influence the ASR, such as humidity and temperature, alkali content, water to cement ratio and particle size but then understanding the mechanisms and how it can effects the RC structures were in its infancy, and some aspects of it are still purely understood.

Since then, many recommendations and methods for evaluating and treating the structures affected by ASR have been published worldwide, such as the Standards Australia handbook for ASR (Pacheco-Torgal et al., 2014), RILEM reports (Nixon & Sims, 2016; Saouma, 2020), A World review on ASR (Poole & Sims, 2016), United States Federal Highway Administration (Thomas, Folliard, et al., 2013; Thomas, Fournier, et al., 2013; Thomas et al., 2011) and many other reviews, publications and testing procedures that have paved the way to better understand and take action to treat the structures affected by this phenomenon and lower the risks related to it.

2.1.2 The ASR Mechanism

ASR, in its nature, is a deleterious long term phenomenon that occurs when the metastable silica from the concretes aggregates reacts with the alkalis (Na^+ and K^+) and hydroxide ions in the pore solution of the hydrating cement to produce a hydrous alkali silicate gel, which can swell and absorb large amounts of water, this irreversible expansion can lead to cracks if the internal stress caused by the expansion exceeds the tensile capacity of the concrete (Hou et al., 2004).

According to Rajanpour et al. (2015), the solubility of silica (SiO_2) increases in a high alkali environment, resulting in hydroxide (OH^-) ions nucleophilic attack to causes the silica arrangement in concrete to break down and dissolve, which would result in the network dissolution of non-crystalline and cryptocrystalline silica, the highly degraded silica structure can behave as a hygroscopic silica gel, the dissolved silica can cross-link and become semi-solid and form ASR gel. This gel usually forms around the Interfacial Transition Zone (ITZ) between the paste and aggregate, the ASR gel can absorb the available water causing the gel to swell, resulting in expansion of the concrete, which leads to cracking that can cause serious damage to the structure (Rajabipour et al., 2015). In Figure 2-1, the reaction process of ASR can be seen.

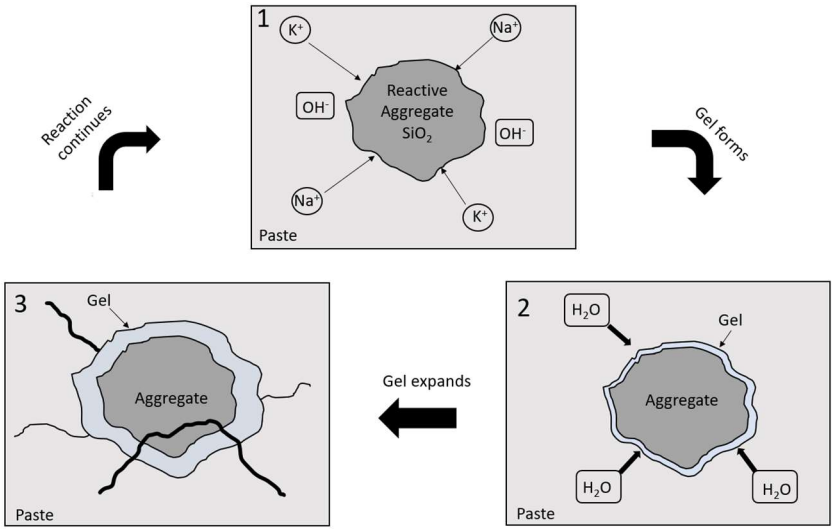

Figure 2-1 The ASR procedure: (1) Reaction of metastable silica (reactive aggregate) with alkali hydroxide resulting in network dissolution of silica, (2) Hygroscopic gel forms at (ITZ), absorbing water from pore resulting in swelling and expanding and (3) Cracking of aggregate and the surrounding cement paste as gel expands (Kreitman, 2011)

The chemical equation of ASR can be written as follows (Rajabipour et al., 2015).

$$Network\ dissolution: (\equiv \mathrm{Si-OH})_s + 3(\mathrm{OH^-})_{aq} \leftrightarrow (\mathrm{Si(OH)_4})_{aq} \quad (2.1)$$

$$Ion\ exchange: (\mathrm{Si(OH)_4})_{aq} + \mathrm{Na^+}_{aq} \leftrightarrow ((\mathrm{HO}) \equiv \mathrm{Si-O^-} \ldots \mathrm{Na^+})_{aq} + \mathrm{H^+}_{aq} \quad (2.2)$$

Rajabpour et al. (2015) stated that as ASR progresses, the pH of the concrete is reduced because of the network dissolution of silica as well as its reaction with dissolved alkalis ions. It is also suggested that calcium ions may replace some of the alkalis incorporated in silica gel, this exchange would result in recycling alkalis back to the pore solution and calcium deficiency in concrete, increasing the pH and further continuing the ASR by producing alkali calcium silicate hydrate gel, this can change the reaction products and properties of ASR gel and effect expansion due to ASR (Dron & Brivot, 1992; Rajabipour et al., 2015; Wang & Gillott, 1991).

$$Alkali\ recycling: 2((\mathrm{OH})_3 \equiv \mathrm{Si-O} \ldots \mathrm{Na})_{aq} + \mathrm{Ca^{2+}} \leftrightarrow 2\mathrm{Na^+} + ((\mathrm{HO})_3 \equiv \mathrm{Si-O} \ldots \mathrm{Ca} \ldots \mathrm{O-Si} \equiv (\mathrm{OH})_3) \quad (2.3)$$

2.1.3 ASR Conditions

According to (Thomas et al., 2011), for ASR to thrive, some conditions must be met:

1) Sufficient alkalis content which can be found in ingredients of concrete as well as supplementary cementitious material (SCM) and external sources (e.g. seawater and de-icing salt).
2) The presence of a sufficient amount of reactive aggregates such as opal, cristobalite, tridymite and many other types can contain metastable silica that would react with hydroxide.
3) A sufficient amount of moisture is required for ASR to thrive, at least 80 per cent relative humidity is needed for ASR progress within the concrete environment, the reaction intensity increases as relative humidity levels increase above 80 per cent.

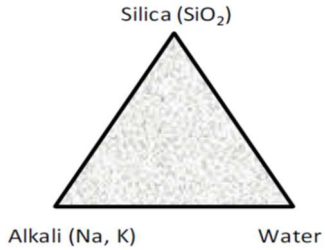

Figure 2-2 ASR progression will be halted if one of the three conditions in the triangle ceases to exist in the concrete environment (Thomas et al., 2011)

In addition to the conditions mentioned above, heat is also one of the environmental parameters that can directly affect ASR progression, increasing ASR kinetic and influencing gel development (Maia Neto et al., 2021). Feldspar rich aggregates such as granite can release a significant amount of alkalis to the pore solution at higher temperatures (Bérubé et al., 2002), this increase in temperature also influences the alkalis released from aggregates to concrete pore solution significantly (Sinno & Shehata, 2021).

2.1.3.1 Alkalis

As mentioned, one of the essential factors that cause ASR to occur is the supply of alkalis. Stanton (1940) discovered that most of the alkalis that are supplied to the concrete are from portland cement (Stanton, 1940). Research by Bérubé & Frenette (1994) stated that concrete specimens prepared with low alkali cement show less expansion than concrete with high alkali cement. As stated by Mehta & Monteiro (2017), the material in the clinker that is used to create the portland cement is the source of the cement's alkali environment, which are sodium (Na) and potassium (Ka) that range between 0.2 to 1.5 per cent acid-soluble sodium oxide equivalent (Na_2O_{eq}). It must be noted that both sodium oxide and potassium oxide simultaneously exist in concrete, but when expressing the alkali content of cement, it is calculated as (Na_2O_{eq}), the conversion is based on the equivalent molar mass, the ratio of Na_2O to K_2O is about 0.658 (Equation 2.4), therefore depending on the content of acid-soluble sodium oxide generally, the concretes pH level differs between 12.5 to 13.5, in the presence of such an alkali environment, siliceous aggregates do not stay stable for long (Mehta & Monteiro, 2017). The alkali supplied by the cement and also other resources can also increase the pH level of the pore solution, which in return causes the solubility

of the silica to increase. It is noteworthy to mention that even stable silica can be dissolved at a high alkali environment to contribute to the ASR process. Figure 2-3 shows the solubility level of silica species at different pH levels, the solubility increases significantly at higher pH levels due to the ionization of $Si(OH)_4$.

$$\%Na_2O_{eq} = \%Na_2O + 0.658 \times \%K_2O \quad (2.4)$$

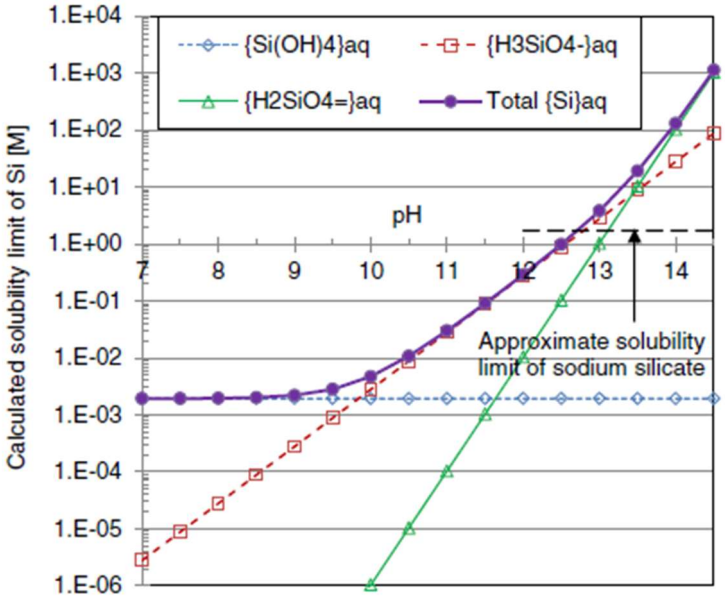

Figure 2-3 Solubility limit of amorphous silica in water at 25 °C as a function of pH, y-axis and x-axis represent Si activity and pH, respectively (Maraghechi, 2014; Rajabipour et al., 2015)

As the alkali content of cement plays a crucial role, it was recommended by Stanton (1940) to limit the alkali hydroxide content of cement to less than 0.6% Na_2O_{eq} to prevent expansion (Stanton, 1940). Hence, since ASR is a long term reaction, to facilitate accelerated ASR in the laboratory, it is essential to increase the Na_2O_{eq} to more than 0.6% (usually 1.25%), by adding NaOH to the mixing water in accelerated experiments such as ASTM C1293 and AS 1141.60.2 or by immersing the concrete in one molar NaOH solution in experiments such as ASTM 1260 and AS 1141.60.1 to obtain faster results.

2.1.3.2 Aggregate Size and Content

Aggregate size, type and proportion can be important when it comes to aggregate reactivity. Regarding the aggregate type, the mineral constituents of the aggregate should be considered, as mineral constituents of the aggregate can play an important role in the ASR expansion and gel composition (Swamy, 1991). As mentioned, some aggregate types can even increase the alkalinity of the pore solution, further accelerating the dissolution of silica. Amorphous and metastable silica is considered the most reactive among the aggregate, these reactive aggregates can range from flint, basalt, marl, shale, rhyolite, greywacke, and other various rock types (Rajabipour et al., 2015).

Assessing the aggregate proportion and size and how it can affect ASR is another key parameter of ASR. To understand this first, we must understand the meaning of pessimum aggregate size and pessimum aggregate content. Pessimum aggregate size and content is defined as maximal expansion in concrete formed from a specific proportion or size of a reactive aggregate (French, 1980). At Stanton's expansion tests on magnesian limestone, it was found that the minimal amount of magnesian limestone needed to cause ASR expansion was only 1% by the mass of the aggregate, the expansion was at its maximum at 20% (the pessimum proportion), and there was little or no expansion when the reactive aggregate was at 40% (Stanton, 1940). Similarly, Binal (2015) experiments on various reactive aggregate types such as chalcedony, andesite, opal and chert utilizing AMBT test showed different pessimum content ratios for each of the aggregate types, as it can be seen from Figure 2-4 each aggregate type shows different pessimum content ratio at different reactive aggregate content, 50%, 22% and 40% for chalcedony, opal and chert, respectively, however andesite shows the same pessimum ratio at different reactive aggregate content, the pessimum content can influence to such extent that it can completely mitigate ASR as seen in opal at 40% reactive aggregate ratio, although it should be noted that pessimum content of an aggregate may vary based on mineralogy of the rock type due to different amount of amorphous silica (Binal, 2015).

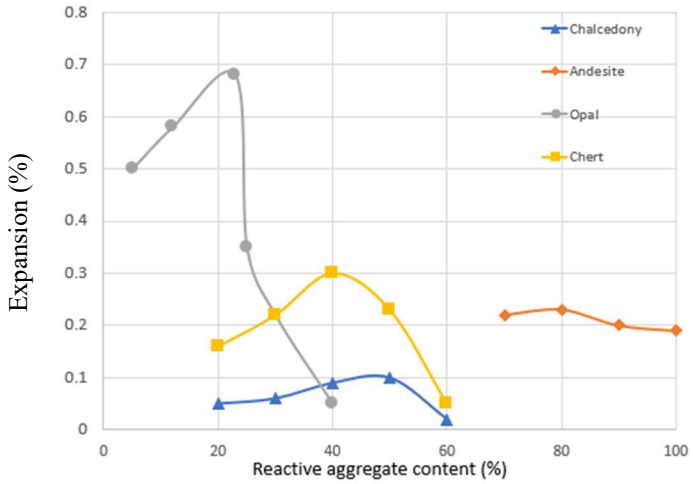

Figure 2-4 Pessimum ratio graph for chalcedony, andesite, opal and chert (Binal, 2015)

The grain size can also affect ASR expansion, as different gradations of a reactive aggregate may result in different expansions or even go to the extent of mitigating the ASR expansion. It is expected that ASR expansion would increase with the reduced size of reactive aggregate particles, as it would provide more surface area of the reactive aggregate, but that was not the case as different researchers such as French (1980) and Stanton (1940) found different results based on their experiments. Multon et al. (2008), experimental research on reactive siliceous limestone concluded that maximum expansion was seven times larger for coarse 1.25 –3.15 mm aggregate than that of the smaller 80 –160 µm ones (Multon et al., 2008). Similarly, Binal (2015) and Stanton (1940) experiments showed the same trend of more expansion in coarse reactive aggregates than the finer ones.

Many pieces of research, as mentioned above, have been conducted on pessimum aggregate size and content with different results. When evaluating an aggregates activity in experiments such as AMBT where the aggregate is crushed to finer sizes pessimum effect must be considered as not many aggregates show similar pessimum ratios.

2.1.3.3 Moisture and Humidity

Humidity and moisture are pivotal for ASR progression as not enough supply may halt the ASR progress, as shown in Figure 2-5.

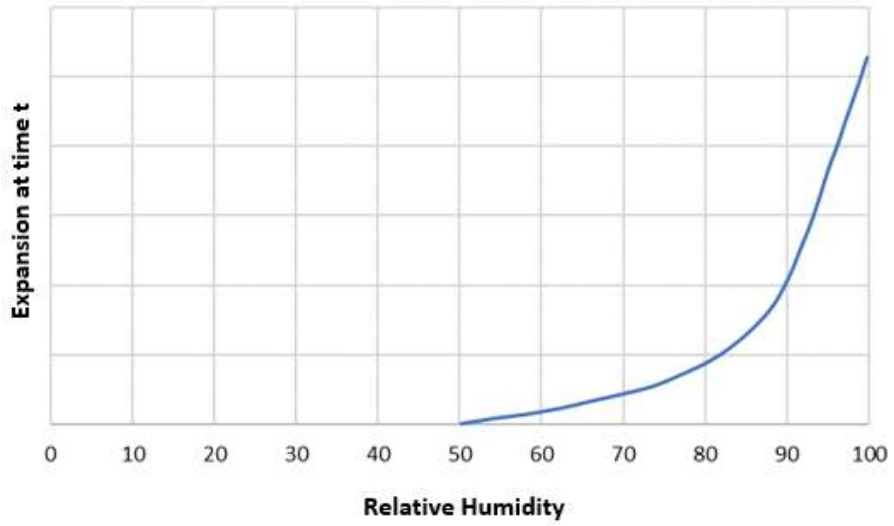

Figure 2-5 Correlation between relative humidity and expansion due to ASR (Swamy, 1991)

If sufficient moisture is not supplied, the ASR progression will cease. Thus, extra care should be taken when a structure is in contact with an external water supply, such as maritime environment, leakages, groundwater, and condensation (Poole & Sims, 2016). Because of the mentioned reasons, it is important to protect and minimize the exposed parts of the structure against moisture and humidity by any means to prevent ASR. Figure 2-6 depicts a bridge abutment in which its right side was exposed to environmental conditions, resulting in a much more severe ASR than the abutment's left side (Thomas et al., 2011).

Figure 2-6 ASR is much more severe on the right side of the bridge abutment where it is exposed to environmental conditions, the left part covered by the bridge deck has minor ASR cracking when compared to the right side (Thomas et al., 2011)

2.1.3.4 Laboratory Test to Accelerate ASR Conditions

Since the discovery of ASR, multiple standards and recommendations have been developed to assess the aggregate's reactivity, including Concrete Prism Test (CPT) such as ASTM C1293 and AS 1141.60.2 and Accelerated Mortar Bar Test (AMBT) such as ASTM 1260 and AS 1141.60.1, which are considered more reliable than other test methods and widely used by engineers to assess the reactivity of the aggregate and categorize them based on the expansion (Thomas et al., 2008). Although these tests have their flaws, for instance, crushing the aggregate may reduce the reactivity, not detecting late expansive aggregates, alkali leaching, and long test results in the case of CPT. Recent test method AASHTO TP 110 Miniature Concrete Prism Test (MCPT) method can remedy these deficiencies and give accurate and promising results on the reactivity of aggregates in less time (about eight weeks) with more accuracy than AMBT and CPT as it considers the alkali leaching and aggregate size as well and show good correlation with CPT test which takes one year (Latifee, 2013).

To sum up, the conditions that may affect ASR can be narrowed down in Figure 2-7, ASR prevention can be achieved by controlling these three major factors and subfactors. To prevent and minimize ASR, precautions such as using low alkali cement, limiting the amount of moisture supplied to concrete and utilizing SCM in the concrete mix design should be considered (Poole & Sims, 2016).

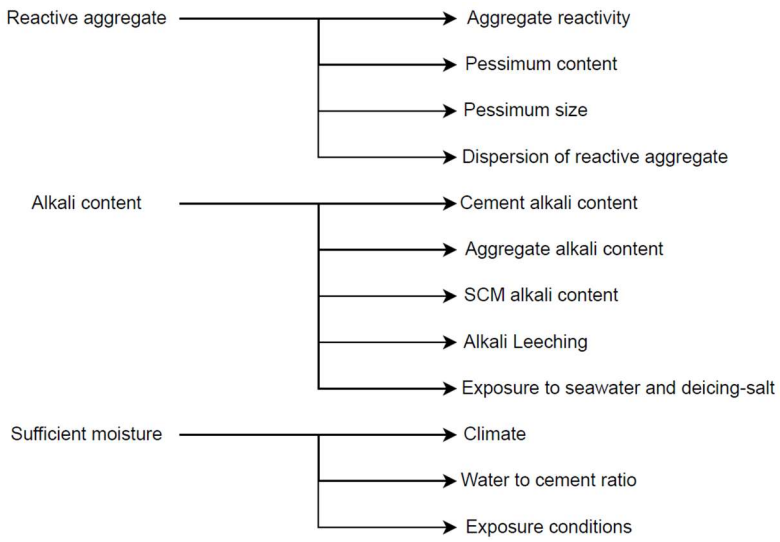

Figure 2-7 Conditions that directly influence ASR

2.1.4 Expansion and Cracking Due to ASR

As ASR occurs in the concrete environment and ASR gel is produced by absorbing the water from the environment, it swells and expands, causing internal stress to the concrete. If the internal stress caused by expansion exceeds the tensile strength of the concrete, it will result in micro and macro cracking in the concrete environment, as ASR progresses within the concrete, it takes time to show itself on the surface as cracks, these cracks vary based on whether the concrete is reinforced or not, if the concrete is not reinforced, the map cracking will occur, and if the reinforcement is present, the cracks will be parallel to the reinforcement direction as it can be seen in figure 2-8 (Fan & Hanson, 1998; Saouma, 2020).

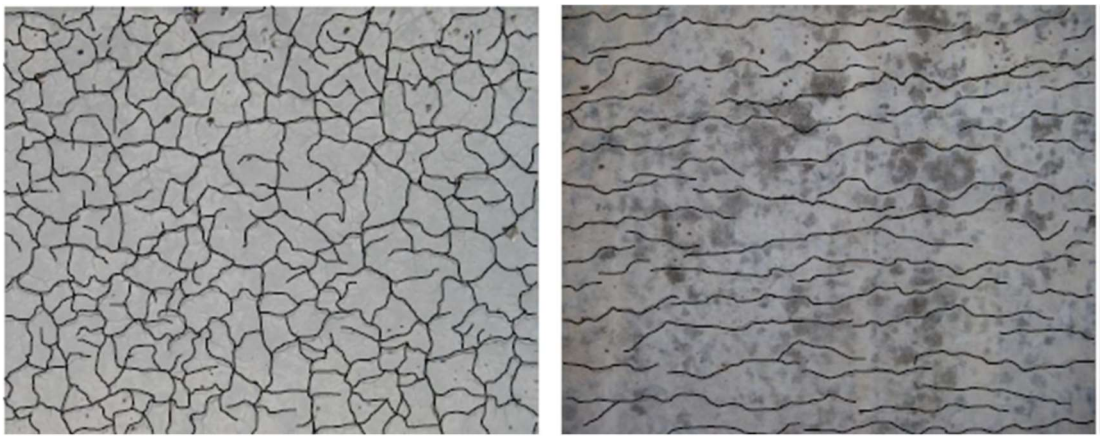

Figure 2-8 Orientation of cracks in reinforced and plain concrete: Map cracking on the left picture and cracking in the direction parallel to the rebar in the reinforced concrete on the right (Kreitman, 2011)

The surface cracking due to ASR should not be confused with the structural cracking as the interior of the structure cracks in a different way when compared to ASR cracks (Courtier, 1990). As the complex chemical reaction of ASR progresses within the concrete by the reaction between reactive siliceous aggregates and alkali hydroxides, it generates ASR gel that applies pressure to the surrounding aggregate as it absorbs moisture, causing microcracking (L. F. M. Sanchez et al., 2015).

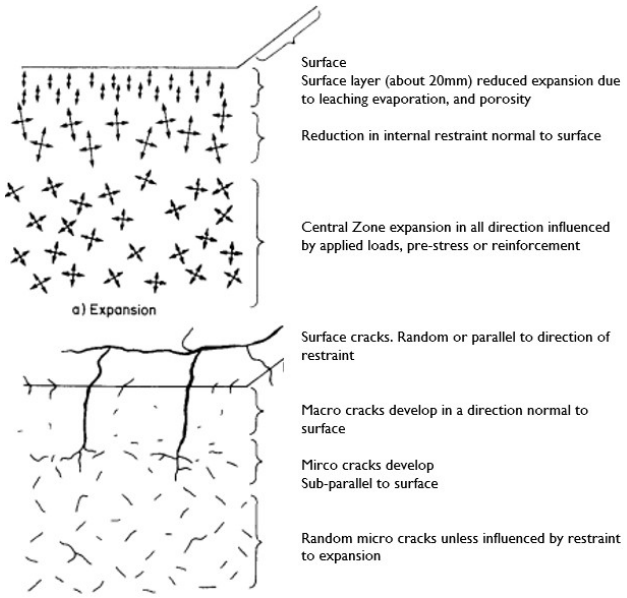

Figure 2-9 Influence of internal tension generated due to ASR on crack development and propagation (Courtier, 1990)

These microcracks originate from the reactive aggregate and can either generate at the surface or inside the reactive aggregate, in many volcanic and synthetic glasses, the silica at the surface of the aggregate can quickly react with the alkaline pore solution that leads to alkali-silica gel formation, but when reactive silica is not at the surface of the aggregate and is present as reactive particles located within a non-reactive aggregate in aggregates like greywackes and siliceous limestones alkali pore solution cannot reach the reactive interior easily (Rajabipour et al., 2015). Additionally, Maraghechi et al. (2012) research on soda-lime glass proves that, unlike other natural aggregates, soda-lime glass experiences ASR within the cracks inside the glass and not at the aggregate surface, making their reactivity dependent on the availability of cracks within the aggregate (Maraghechi et al., 2012).

2.1.5 Effect of ASR on Mechanical Properties of Concrete

As ASR progresses in concrete, it causes localized expansion and microcracking inside of the concrete that results in tensile stress in the surrounding material. As the materials in concrete become stressed and expand, these internal stresses cause anisotropic expansion, this anisotropic behaviour directly affects the concrete's mechanical behaviour (Kongshaug et al., 2020). Many pieces of research have been

conducted on how ASR can affect the mechanical properties of the concrete since the discovery of ASR by Stanton in 1940. Some of the important literature can be found in Table 2-1 below.

Table 2-1 Research done regarding mechanical properties of concrete affected by ASR by chronological order adapted from (Mohammadi et al., 2020)

Researches	ASR Condition	Aggregate	Samples	Mechanical properties
Cao et al. (2021)	High-pressure autoclave at 70 and 80 °C with three cycles	Reactive aggregate	Cylinder and prism	Modulus of elasticity, compressive strength, and tensile strength
Kongshaug et al. (2020)	60°C and 100% RH	crushed reactive cataclasite	Extracted cylinder cores from lab cast cubes	Modulus of elasticity
Barbosa et al. (2018)	Extracted cores	Reactive aggregate	Extracted concrete cores from severely damaged bridges	Compressive strength
Islam and Ghafoori (2018)	In water RH 100% at 20 °C and in 1.0 N NaOH at 80 °C	Fourteen reactive aggregate groups	Mortar bar (ASTM C1260)	Modulus of elasticity
Shi et al. (2018)	Conditions comply with ASTM C1260	Reactive natural sand	Activated slag mortars	Compressive strength

Researches	ASR Condition	Aggregate	Samples	Mechanical properties
Munir et al. (2018)	Conditions comply with ASTM C1260 and ASTM C227	Five different sources	mortar cubes and prisms	Compressive strength and modulus of rupture
Li et al. (2016)	Submerged in water at 80 °C and in 1 N NaOH solution at 80 °C	Reactive sand containing volcanic glass	cementitious mortar	Flexural strength
Alaud & van Zijl. (2016)	1N NaOH at 80°C	Greywacke and Granite coarse aggregates	Cylinders	Compressive strength and modulus of elasticity
Islam and Ghafoori. (2015)	submerged in 1.0 N NaOH at 80 °C	Fourteen reactive aggregate groups	Mortar bar (ASTM C1260)	Compressive strength
Yurtdas et al. (2013)	60 °C, RH 95%	Reactive and non-reactive material	Prisms and cylinders	Compressive strength, modulus of elasticity, and flexural strength
Giaccio et al. (2008)	Conditions comply with ASTM C1293	None, slow and highly reactive aggregates	Prism and cylinder	Flexural, compressive, modulus of elasticity and Poisson's ratio
Marzouk and Langdon (2003)	Submerged in NaOH solution at 80 °C for 12 weeks	Highly and moderately reactive aggregate	Normal and high strength concrete	Compressive strength, Modulus od elasticity, Uniaxial tension and modulus of rupture

Researches	ASR Condition	Aggregate	Samples	Mechanical properties
Ahmed et al. (2003)	Submerged in water, 38° C	Highly and slow reactive aggregate	Prism, cylinder and cube	Compressive strength, direct tensile strength, tensile splitting strength, flexural tensile strength, static modulus of elasticity.
Fan and Hanson (1998)	0.5 N NaOH solution at 38 °C	Reactive and non-reactive aggregate	Reinforced concrete beams and cylinders	Compressive strength, splitting tensile strength and dynamic modulus

The main findings regarding the mechanical properties of concrete affected by ASR based on the literature provided in the Table 2-1 are presented below:

2.1.5.1 Modulus of Elasticity

Across the literature (Alaud & van Zijl, 2016; Giaccio et al., 2008; Islam & Ghafoori, 2018; Jones & Clark, 1998; Kreitman, 2011; Marzouk & Langdon, 2003; Saint-Pierre et al., 2007), it is unanimous that ASR reduces the modulus of elasticity of concrete. For instance, Marzoul & Langdon (2003) experiments on the modulus of elasticity of highly and moderately reactive aggregates on 75×150 mm concrete cylinders exposed to NaOH and water at 80 °C over twelve weeks determined that the modulus of elasticity of normal strength concrete containing highly reactive aggregate and moderately reactive aggregate decreased by 80% and 20% respectively. Similarly, experiments conducted by Aluad & van Zijl (2016) show the same trend of low modulus of elasticity. However, specimens containing modestly reactive aggregate's modulus of elasticity decreased at late ages than that of highly reactive ones (Alaud & van Zijl, 2016). Interestingly the modulus of elasticity measurement of highly degraded specimens due to ASR was deemed inaccurate due to the formation of large cracks (Islam & Ghafoori, 2018). Additionally, conducting modulus of elasticity experiments on cylindrical cores extracted from three different severely damaged bridge structures affected by ASR build from 1966 to 1976 determined that modulus

of elasticity is strongly correlated with the crack orientation, extracted cylindrical specimens with perpendicular cracks showed significantly reduced Young's modulus than that of the specimens with parallel cracks (Barbosa et al., 2018).

2.1.5.2 Compressive Strength

Experimental program conducted by Fan & Hanson (1998) on cylindrical specimens containing reactive aggregate and submerged in 38°C alkali solution determined that before visible ASR cracks appeared on the concrete surface, the change in mechanical properties of concrete cylinders compressive strength was insignificant, but after cracking a substantial amount of compressive strength over 24% was lost (Fan & Hanson, 1998). Likewise, the compressive strength of highly reactive aggregates in experiments conducted by Marzoul & Langdon (2003) was reduced by 28%, but the compressive strength of specimens containing moderately reactive aggregate was unchanged and unaffected by ASR (Marzouk & Langdon, 2003). The orientation of the cracks caused by ASR can significantly affect the compressive strength as it does Young's modulus (Ahmed et al., 2003; Barbosa et al., 2018). However, Giaccio et al. (2008) experiments on slow reactive coarse aggregate show increased strength gain on a par with control specimens made with non-reactive aggregate, while other mechanical properties were reduced (Giaccio et al., 2008). Also, high-strength concrete placed in NaOH solution surprisingly showed an increase of 10% to 21% in compressive strength (Ahmed et al., 2003). These conflicting results may be due to the severity of the ASR damage to the specimens, as crack orientation and the damage severity of the specimens can heavily influence the test results (Barbosa et al., 2018; Schmidt et al., 2014).

2.1.5.3 Flexural strength

As mentioned, when ASR progresses in a concrete environment, it causes internal tensile stress, which can be aggravated due to the factors mentioned in 2.1.3 (Swamy, 1991). Because flexural and tensile strength tests are related to concretes tensile strength, these mechanical properties are expected to reduce due to expansion (Mohammadi et al., 2020). Experimental research conducted by Ahmed et al. (2003) on 100×100×500 mm^3 prisms with highly reactive aggregates shows a reduction of

81.85% in flexural strength and 53.64% in tensile splitting strength (Ahmed et al., 2003). Marzoul & Langdon (2003) experiments on normal strength concrete showed a slight reduction of 8.77% in flexural strength, which is relatively low when it is compared to Ahmed et al. (2003) experiments. Aggregates reactivity and expansion may affect the flexural strength results as some aggregates show late expansive behaviour than other reactive aggregates. The alkali content of the cement mix can also be an influential factor in the flexural strength of specimens affected by ASR, as Li et al. (2016) observed that an increase in the alkali content of cement resulted in the loss of flexural strength due to ASR (Li et al., 2016).

2.1.5.4 Tensile Strength

After careful examination of the literature, it can be said that the tensile strength of the concrete can be reduced due to ASR (Ahmed et al., 2003; Cao et al., 2021; Fan & Hanson, 1998; Islam & Ghafoori, 2018). Marzoul & Langdon (2003) conducted tests that showed a reduction of 31% and 37% in tensile strength of moderately reactive and highly reactive specimens, respectively. Cao et al. (2021) experiment on reactive aggregate utilizing accelerated autoclave test showed a reduction in tensile strength after further expansion of the specimens. Similarly, Fan and Hanson (1998) observed an average reduction of 24% compared to the corresponding 28-day results.

2.1.5.5 Summary of ASR Mechanical properties

Overall, ASR can reduce the mechanical properties of concrete such as compressive strength, Young's modulus of elasticity, flexural and tensile strength, reducing their values as ASR progress in the concrete environment. Factors that may affect these parameters are explained in chapter 2.1.3. To evaluate ASR damage and set a criteria for the evaluation of ASR cracks in concrete modulus of elasticity and tensile strength can be considered as they are the most sensitive out of all mechanical properties and show less fluctuation in results from across the literature, other mechanical properties vary from literature to literature, and some show slight or high decreases, and some do not even show any change in mechanical properties, rendering them not as sensitive to evaluate the progress of ASR (Mohammadi et al., 2020; Rivard et al., 2010; Saouma, 2020). However, some researchers argue that compressive strength is a better indicator

for evaluating ASR cracks than Young's modulus and tensile strength (Barbosa et al., 2018). Nevertheless, a more reliable test method is still needed for assessing ASR in concrete. Stiffnes Damage Test (SDT) is a non-destructive test method in which five cyclic loading and unloading are done with 40% of concretes compressive strength on extracted cores or cylinders with a length to diameter ratio of two (Sanchez et al., 2014). From the output of the SDT, it is possible to extract the Stiffness Damage Index (SDI) and Plastic Deformation Index (PDI), which appraise the amount of distress in concrete based on extracted cores from structures affected by ASR or specimens created in the lab (Sanchez et al., 2016).

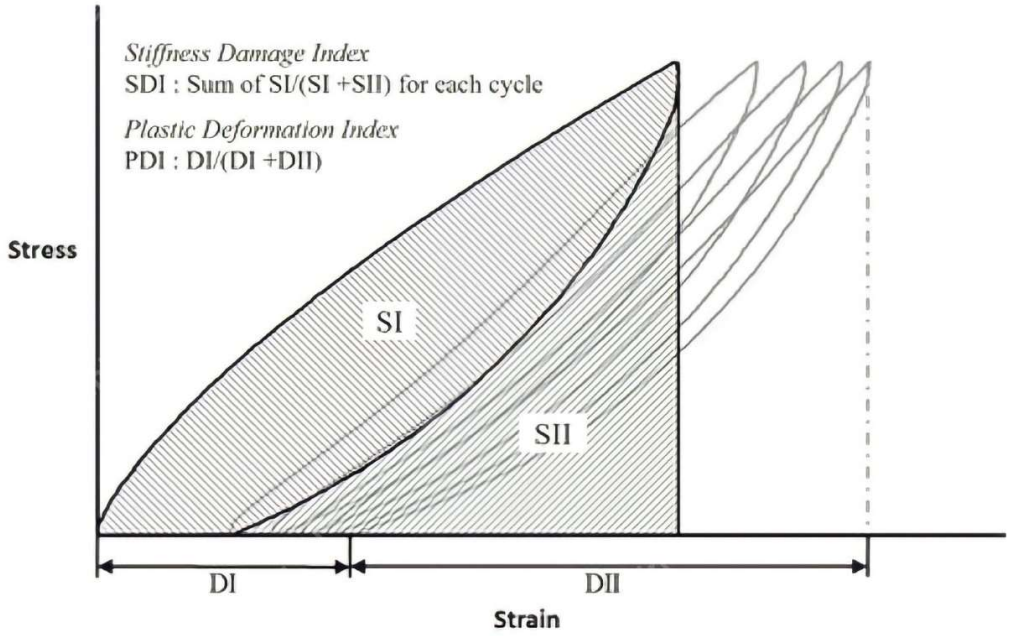

Figure 2-10 The procedure of calculation SDI and PDI after five cyclic loadings and unloading (Giannini et al., 2018)

Research conducted by Sanchez et al. (2016), Sanchez et al. (2015) and Sanchez et al. (2014) on STD concluded that SDI and PDI show better results than hysteresis area and plastic deformation due to taking dissipated energy/total energy into account and show a better result in evaluating the ASR and is considered a powerful tool to assess structures affected by ASR, but SDT still needs further experimentation and study to be implemented in practical use in engineering (L. anchez et al., 2015; Sanchez et al., 2014; Sanchez et al., 2016).

2.2 Corrosion in RC Structures

Chloride-induced corrosion of RC structures is one of the dominant deterioration effects in concrete structures (Babaee & Castel, 2018). Corrosion of the reinforced embedded steel in concrete due to carbonation and exposure to environments that can supply chloride ions such as aggregates containing salt, maritime environments, and deicing salt can cause serious damage leading to high repair costs (Böhni, 2005).

When steel is exposed to the natural environment, it will corrode and return to its lower level of energy, in the case of steel, it is oxides, but typically even if sufficient moisture and oxygen are present in the environment good quality steel embedded in concrete will not corrode that easily, this is because of the alkali nature of the concrete pore solution that usually ranges between 12.5 and 13.5, in such alkaline environment a thin oxide layer called the passive film surrounds the embedded steel that protects it against corrosion, when this passive layer is destroyed by the moisture and oxygen attacks it depassivates and the thin film gets destroyed and opens the way to the steel corrosion. (Raupach, 1996). Table 2-2 shows the corrosion of steel reinforcement at different pH levels. In the absence of Chloride ions in the solution, the passive layer on the steel is stable as long as the pH is above 11.5, normally the pH of the concrete is above 12 as long as there is around 20 weight per cent solid calcium hydroxide $Ca(OH)_2$If the calcium hydroxide is leeched or concrete is very permeable, the pH of the concrete will be reduced, and the steel will start to lose the passive protective film opening the way to corrosion (Mehta & Monteiro, 2017).

Table 2-2 Reinforcement corrosion at different pH levels (Pullar-Strecker, 1987)

Concrete pH	State of reinforcement corrosion
9.5	Commencement of steel corrosion
At 8.0	Severe corrosion
Below 7	Catastrophic corrosion

The whole electrochemical process in a steel reinforcement can happen in two ways (Hansson et al., 2006); 1) If two different metals are embedded in concrete like steel and aluminium or when significant variations exist on the steel's surface characteristics, which is called macrocell; 2) If there are different concentration of ions

in concrete near the steel reinforcement, cells may form to exchange ions which is called microcell. It should be noted that it is also possible to form macrocells on in single bar exposed to different environments within the concrete or where part of the reinforcement extends outside of the concrete. This results in one of the two different reinforcing steels, or the one steel with different concentrations of ions, in concrete becoming anodic and catholic. Depending on what state the oxidation is, as the iron transforms into rust, the volume increase can reach 600 per cent of the actual metal. As corrosion products build up they increase the internal stress of the concrete over time, eventually resulting in cracking of the concrete cover, which propagates from the bar to the nearest surface, which can accelerate the ingress of other deleterious material.

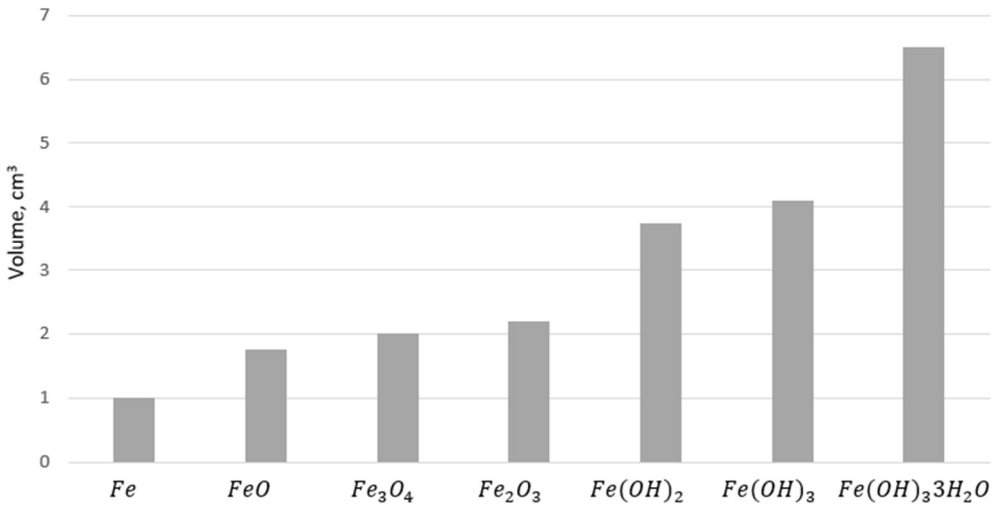

Figure 2-11 The increase in volume depending on the oxidation state of the embedded steel (Mehta & Monteiro, 2017)

2.2.1 Corrosion Mechanism

The electrochemical process of chloride-induced corrosion in concrete operates much like a battery, the anode and cathode are created by different surface areas of steel creating poles, the voltage of the corrosion cell is created by a difference in potential of steel surfaces in reinforced concrete (Raupach, 1996).

This difference in potential voltage can set up microscopic electrochemical cells or microcells between anode and cathode, this is caused by the heterogeneity of the steel

material, the heterogeneity differences in the surface of the steel can be places that have scratches on the bar or even places that have residual stress, the pore solution acts as electrolyte in the concrete, in chemistry anode and cathode reactions are called half-cell reactions, the reaction that causes the corrosion of metal is the anodic reaction which the oxidation happens and cathodic reaction is the reduction process. it is called the reduction process because it results in a reduction of dissolved oxygen forming hydroxyl ions (Nabavi, 2014).

The electrochemical corrosion process in RC can be described as below (Ji et al., 2013; Nabavi, 2014; Neville, 1995):

The cathodic and the anodic sites are connected via the concrete pore solution, which acts as the electrolyte. The anodic reaction consists of metal being consumed to release electrons. The ferrous ions (Fe^{2+}) from reaction (2.5) passes into the solution from the anodic site, to be converted into rust in furthered reactions:

$$Fe \rightarrow Fe^{2+} + 2e^{-} \quad (2.5)$$

These electrons pass into the cathodic site across the metal while the ferrous ions in the pore solution are dissolved. Oxygen in the pore solution at the cathodic site combines with the electrons to form hydroxyl (OH^{-}) ions.

$$2H_2O + O_2 + 4e^{-} \rightarrow 4(OH^{-}) \quad (2.6)$$

Ferrous (Fe^{2+}) and hydroxyl (OH^{-}) ions pass across the pore solution in opposite directions, and ferrous hydroxide ($Fe(OH)_2$) precipitates.

$$Fe^{2+} + 2OH^{-} \rightarrow Fe(OH)_2 \quad (2.7)$$

In addition, since there is moisture and oxygen, the ferrous hydroxide is oxidized to ferric oxide.

$$4Fe(OH)_2 + 2H_2O + O_2 \rightarrow 4Fe(OH)_3 \quad (2.8)$$

$$2Fe(OH)_3 \rightarrow Fe_2O_3 + 3H_2O \quad (2.9)$$

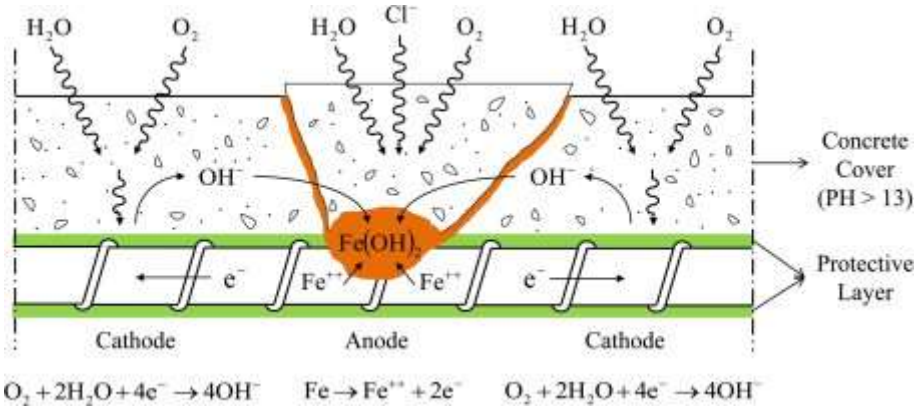

Figure 2-12 The process of corrosion in concrete where pore solution acts as an electrolyte (Cao et al., 2013)

2.2.2 Fick's Law of Diffusion

Fick's law of diffusion states that the diffusion of a substance across a surface or membrane is proportionate to the concentration gradient (Davis et al., 1995). Fick's first law is presented below (Equation 2-5). In this equation, the concentration does not change with time and is (steady-state) (Philibert, 2005).

$$\mathrm{J} = -\mathrm{D}\frac{\partial \emptyset}{\partial \mathrm{x}} \quad (2.10)$$

where:

- J is the diffusion flux ($\frac{mol}{m^2.s}$)
- D is the diffusion coefficient ($\frac{m^2}{s}$)
- $\emptyset$ is concentration ($\frac{mol}{m^3}$)
- x is the depth from the concrete surface (m)

Fick's second law of diffusion can be used to measure the diffusion as concentration as time passes (non-steady-state).

$$\frac{\partial \emptyset}{\partial \mathrm{t}} = D\frac{\partial^2 \emptyset}{\partial x^2} \quad (2.11)$$

Crank's solution for Fick's second law can be written as below (Crank, 1975).

$$C_x = C_s \left[1 - \text{erf}\left(\frac{x}{\sqrt{4tD}}\right)\right] \quad (2.12)$$

where:

- C_x is the chloride at a certain depth
- x depth
- C_s surface chloride concentration
- D Chloride diffusion coefficient
- t is period of exposure

2.2.3 Chloride Threshold Level in RC Corrosion

As predicting the service life of RC structures are essential in this era, CTL is one of the essential tools in service life assessment, the chloride threshold level (CTL) is defined as the amount of chloride content that is needed to destroy the passive protective film around the steel reinforcement to start the corrosion initiation (Sagüés et al., 2014).

CTL can be expressed in different forms, such as Cl^-/OH^-, total chloride percentage, percentage of free chlorides and the weight of the concrete's binder, among these, Cl^-/OH^- appears to be more precise as but due to difficulty of OH^- measurement, free and total chloride is used in the industry, and it is measured and obtained via natural and accelerated tests (Alonso & Sanchez, 2009)

Hausmann first did the measurement of CTL in 1967 by using a synthetic concrete solution. Since then, many experiments have been conducted on CTL. Since then, many experiments have been conducted on the evaluation of CTL. However, the values vary in the literature as there are many factors that can influence the CTL. The values that can directly affect the CTL can range from the type of cement, water to cement ratio, steel chemical composition and various other factors (Bertolini, 2013). This fact makes it hard to be able to predict the service life of a structure precisely as there are different values of CTL due to the mentioned factors. According to Angst et al. (2009), because of the factors influencing the results of CTL experiments, more

research is needed to measure free chlorides precisely, raising the need for a reliable test method for CTL measurement as it is an essential factor in predicting the service life of RC structures.

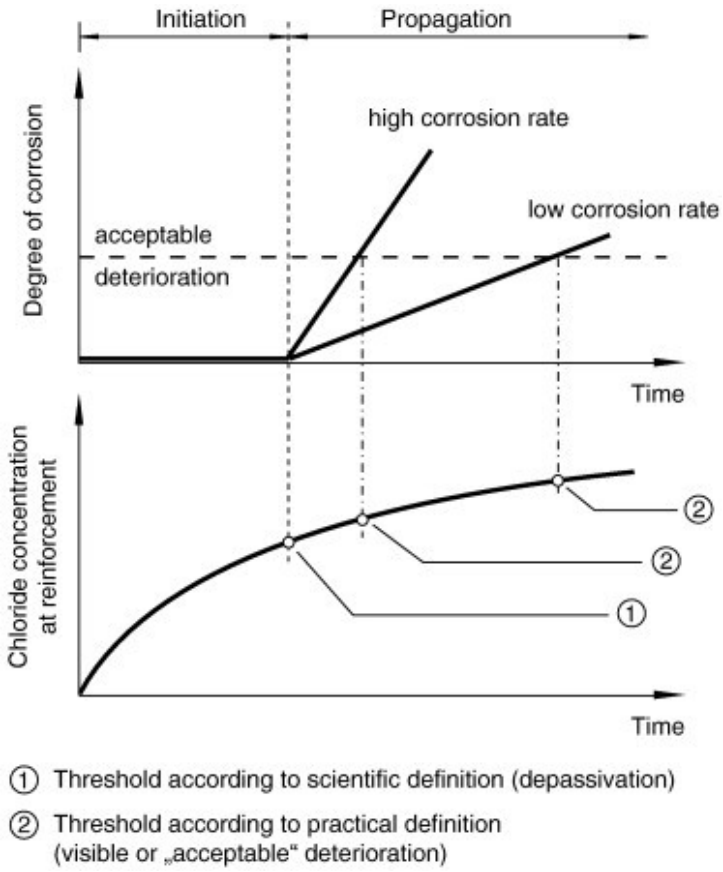

Figure 2-13 Time vs degree of corrosion and chloride concentration at reinforcement (Angst et al., 2009)

2.2.4 Surface Chloride Concentration

Surface chloride concentration (C_s) is another factor that can influence chloride diffusion in concrete. C_s is dependent on the exposure time of the structure, but factors such as concrete mix and curing methods can also influence C_s (Nabavi, 2014).

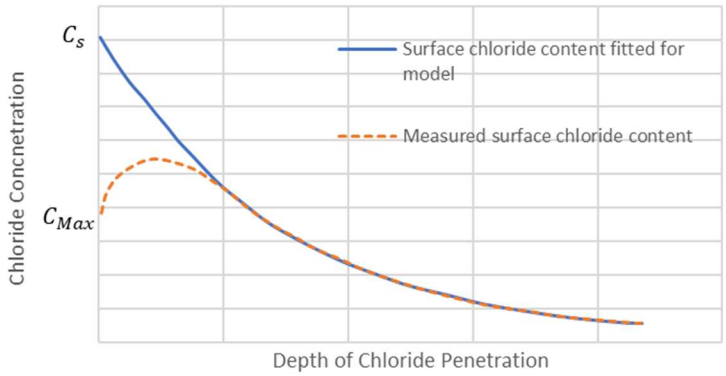

Figure 2-14 Surface chloride concentration based on models and measured data (Gjørv, 2014)

2.3 Combined Effects of ASR and Chloride-induced Corrosion

ASR and chloride-induced corrosion are explained in detail in previous sections. There are limited publications on the combined effects of ASR and chloride-induced corrosion on how this combined deterioration can affect the durability and mechanical properties of an RC structure. Based on assumptions and some field results, it is commonly accepted that the expansion and crack caused by ASR can lead to the ingress of other deleterious material into the concrete, including chloride ions (Poole & Sims, 2016; Saouma, 2020; Thomas et al., 2011). However, that may not be the case as there are conflicting results in the literature (Berndt, 2019; Mazarei et al., 2017; Mikata et al., 2018; Mikata et al., 2020; Tordoff, 1990; Trejo et al., 2017). In the following section, the publications regarding the combined effect of ASR and corrosion, which are limited, will be reviewed.

2.3.1 Combined Deterioration Effect on Non-Mechanical Properties

2.3.1.1 Assessing prestressed post-tensioned bridges affected by ASR and chloride-induced corrosion, Tordoff (1990)

Tordoff (1990) conducted research on seven sixteen-year-old prestressed post-tensioned concrete bridges built-in 1974/75 suffering from ASR in the united kingdom. The first cracks in the structure were observed in 1982. Initially, in 1983 the cause of the cracks was diagnosed to be due to plastic shrinkage and drying shrinkage

for longitudinal cracking and map cracking, respectively. Later in the year 1988, after remediation works for the previous diagnosis, the cause of the cracks was diagnosed as ASR, with the majority of the ASR cracks being hairline cracks and the maximum width of the cracks being approximately 1 mm containing ASR gel with some other cracks being empty with no signs of ASR gel. The crackings due to ASR did not cause any length change, the reduction of 40 mm beam length shows that additional prestressing did not occur due to ASR expansion.

Surface chloride levels were assessed from the said bridges to evaluate the durability of the structures. The results showed an interesting aspect of the structure affected by ASR. The chloride levels from extracted cores of all six bridges were so low that it would suggest the bridge was not in an aggressive environment, while at least two of the bridges were in an area where de-icing salt was used frequently. Tordoff's (1990) argued that concrete suffering from ASR can resist deleterious external attacks such as the ingress of chloride ions. In his research, he argues that in concrete suffering from ASR, the voids in the concrete could act as a reservoir for ASR gel and prevent the ingress of chloride to an extent before severe cracking due to ASR. The research also shows that despite cracking due to ASR, the strength of the beams has not been reduced. Cracks caused by ASR can also widen due to gel pressure in concrete pores as ASR progresses, particularly in unreinforced members. However, in reinforced members, the gel is more likely to migrate.

Below is the chloride content by the weight of cement of the six bridges at 5-30 mm and 30-60 mm depth compared to the corrosion risk at different amounts of chloride content, which is within the negligible threshold.

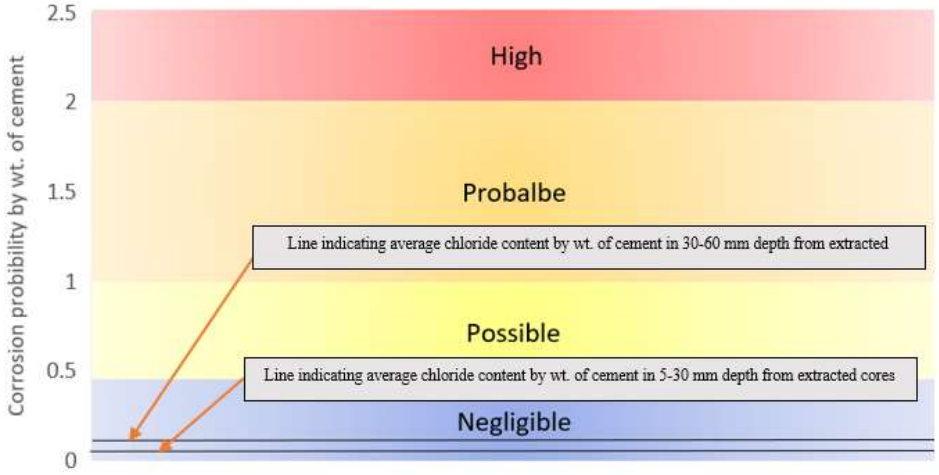

Figure 2-15 Figure depicting the risk of reinforcement corrosion with different amounts of chloride content by weight of cement with the two black lines indicating the average chloride content at 5-30 mm and 30-60 mm by the weight of cement (Tordoff, 1990)

2.3.1.2 Assessing conditions of Jetty affected by ASR and chloride-induced corrosion, Berndt (2019)

Another real-world case of combined effects of ASR and chloride-induced corrosion can be seen in Lucinda Jetty, located in tropical Coral sea Lucinda, Queensland, Australia. According to Brendt (2019), the Lucinda jetty was one of the first structures in Australia diagnosed with ASR. Lucinda jetty construction was completed in 1979 with cracking due to ASR starting to show after two years of construction. Except at the abutment, where the headstocks and piles are reinforced concrete, the jetty is built up of precast prestressed concrete girder units supported by steel headstocks and piles. Type A ordinary portland cement was used for the construction with total alkali content of 0.59 to 0.84 ($NaOH_{eq}$). the girders were produced by two companies ASTM C289 tests were conducted on the used aggregates, and the aggregates passed the test. Widespread cracking of the prestressed girders was observed after two years of construction, with the cracking cause contributing to ASR. As the jetty is located in a harsh maritime environment, it was subjected to seawater splashes and extensive corrosion of prestressing strands and stirrups.

Early examination of the Jetty conducted by Tordoff et al. (1989) on extracted cores demonstrated that the ASR damage is due to reactive volcanic rhyolitic tuff. It was also found that the ASR gel composition and appearance were dependent on its

location. Tordoff et al. (1989) observed that low calcium causes the ASR gel to be fluid and easily extrude out of the cracks caused by ASR. In contrast, high calcium content caused ASR gel to have binding properties similar to hydrated cement paste, concluding that calcium content affects the ASR gel expansion, as was later demonstrated by Thomas (2019) and Rajabpour et al. (2015) that calcium can play a key role in ASR expansion and may aggravate the ASR expansion. Calcium ions may replace some of the alkalis incorporated in silica gel, this exchange would result in recycling alkalis back to the pore solution and calcium deficiency in concrete, increasing the pH and further continuing the ASR by producing alkali calcium silicate hydrate gel (Rajabipour et al., 2015; Thomas, 2019). Investigations show that the structure in its current conditions is heavily corroded and affected by ASR in jetty abutment where they were in contact with splash zones due to the higher moisture content at abutment ASR has progressed severely when compared to other areas.

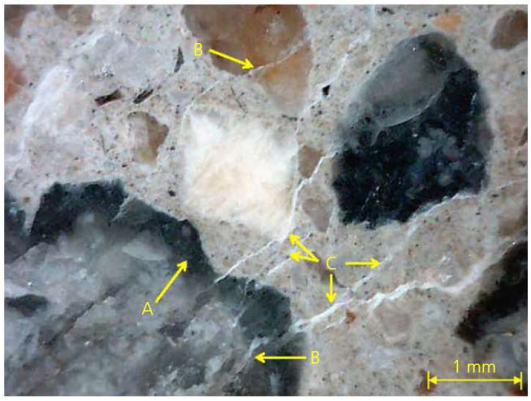

Figure 2-16 Extracted core from Lucinda jetty with (A) ASR gel forming around the aggregate, (B) crack formation inside aggregate and (C) ASR gel forming in the interface of paste and aggregate (Berndt, 2019)

Figure 2-17 Corrosion of stirrups and prestress strands with heavy stirrup corrosion at the bending location (Berndt, 2019)

Field investigations by Brendt (2019) on the combined effects of ASR and chloride-induced corrosion show that corrosion products were accommodated in the partially filled or empty cracks caused by ASR expansion. This can be explained why extensive corrosion was observed without delamination or spalling due to corrosion as ASR cracks accommodated corrosion products. ASR expansion also has caused the fracture of stirrups due to the combined effects of corrosion and transverse expansion. Additionally, ASR can affect chloride diffusion, lowering its value by filling up the gaps and preventing the ingress of chloride ions.

2.3.1.3 Assessing the combined effects of ASR and chloride-induced corrosion in laboratory conditions, Trejo et al. (2017)

Trejo et al. (2017) is one of the first publications to simulate the combined effect of ASR and corrosion of reinforced concrete in the laboratory environment. the main objective of the research was to investigate the general belief that as cracks can provide a pathway to RC corrosion (Win et al., 2004), ASR cracks can also contribute to this cause as well. To be able to achieve a comprehensive result, the corrosion initiation time, critical chloride threshold and diffusion coefficient were measured during the experiment for reactive and non-reactive specimens.

Because of the lack of a global standard for the combined effects of ASR and chloride-induced corrosion in RC structures, ASTM G109 and ASTM C1293 standards were modified to be able to simulate the combined effect in the lab environment. Ten 285×152×114 mm specimens were fabricated with five specimens containing fine-reactive aggregate and five specimens containing non-reactive aggregate. The reactivity of the specimens was tested via ASTM C1260 and ASTM C1293. In each specimen, three N 4 reinforcement were embedded while casting, the end of rebars were drilled, and stainless steel screws were installed a 100-ohm resistor then connected to the top and bottom rebars as per ASTM G109 specifications to measure the current. To boost the alkalinity of the concrete mix to accelerate the ASR, sodium hydroxide was added to increase the alkalinity of the concrete mix by 1.25% ($NaOH_{eq}$) by mass of cement. The specimens were subjected to 38°C and 95% relative

humidity after the initial curing, during this exposure condition, the specimens were ponded with 3% sodium chloride (NaCl) solution for two weeks on the top reservoir provided for the chemical admixture as per the requirement of ASTM G109 and rotated to pond the bottom side with distilled water to prevent warping. The conditioning specimens was according to the ASTM C1293 to be able to measure the length change due to ASR. The schematic of the specimens with the top and bottom reservoir can be seen in Figure 2-18.

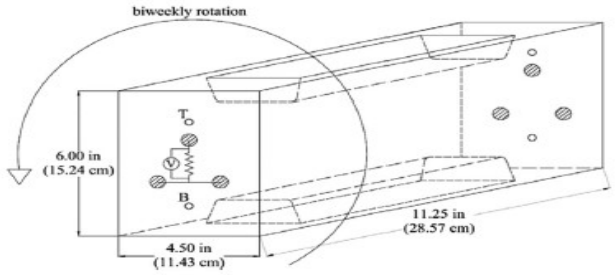

Figure 2-18 schematics of the specimens (Trejo et al., 2017)

To be able to measure the time to corrosion initiation, the readings from the 100-ohm resistor were monitored and converted to coulombs as per ASTM G109 specifications when the average integrated microcell current reaches 150 coulombs. After observing the corrosion initiation, the chloride content in various depths was measured to be able to obtain the chloride diffusion coefficient.

The obtained results show that the reactive specimens expanded by 0.35 to 0.52 per cent while the non-reactive specimens showed no expansion after 225 days of curing age which is the corrosion initiation time in the reactive and non-reactive specimens, indicating that accelerated ASR conditions did not have any effect on the corrosion initiation. However, reactive specimens showed higher mean coulombs up to day 80 of exposure while non-reactive specimens showed higher mean coulombs after 80 days, this can be explained by the formation of ASR gel that can fill the gaps and pores, resulting in lowering the transport of the chloride ions within the concrete environment. The chloride diffusivity of the reactive and non-reactive specimens was also measured after the corrosion initiation. The results show that the specimens containing reactive aggregate have a lower diffusion coefficient than the non-reactive specimens due to ASR gel filling the existing gaps and pores. This is also supported

by Energy Dispersive X-Ray (EDX) analysis, which shows that chloride levels in ASR gel are low, resulting in ASR gel blocking the transport of chloride ions.

ASR gel also affected the critical chloride threshold at the time of the corrosion initiation. The results of the critical chloride threshold at the time of corrosion initiation show that the reactive specimens had a lower critical chloride threshold compared to the non-reactive specimens as the result of the pH of the surface of the steel reinforcement being reduced due to ASR (Wang & Gillott, 1991).

2.3.1.4 Assessing the combined effects of ASR and chloride-induced corrosion in laboratory conditions utilizing SCM, Trejo et al Mazarei et al. (2017)

All conditions of the experiment conducted by Mazarei et al. (2017), such as alkali boosting, mixing procedure and curing, were the same as the experiment conducted by Trenjo et al. (2017), with the difference being an addition of two types of specimens with reactive aggregate containing 20% class F fly ash and 40% class F fly ash were created to assess the effect of ASR on corrosion with added fly ash. The results of the experiment show that the addition of the fly ash on non-reactive specimens lowers the diffusion coefficient and the critical chloride threshold, with the lowering the diffusion coefficient being more beneficial as it extends the time to corrosion initiation. Specimens containing reactive aggregate with 20% fly ash showed longer corrosion initiation time compared to reactive specimens containing 40% fly ash, this is due to ASR gel formation in 20% fly ash specimens compared to specimens with 40%, which showed no signs of ASR. Specimens containing 20% fly ash also showed a higher critical chloride threshold compared to reactive specimens without fly ash as ASR gel in specimens containing 20% fly ash did not reduce the pH of the pore solution as much as the non-reactive specimens containing no fly ash.

2.3.1.5 Summary

From assessing the limited literature regarding the combined effects of ASR (Berndt, 2019; Tordoff, 1990; Trejo et al., 2017) and chloride-induced corrosion, it is unanimous that ASR gel can block the diffusion of the chloride ions within the concrete environment due to ASR gel filling the cracks and voids and act as a barrier

against the diffusion of the chloride ions. Additionally, due to ASR lowering the pH of the concrete, the critical chloride threshold of the reinforcement is also lowered. Interestingly the corrosion initiation time in reactive and non-reactive specimens in Trejo et al. (2017) experiment occurred at the same time it is due to lower critical chloride threshold and diffusion coefficient in the reactive specimens that compensate each other so that the corrosion initiation time occurs at the same time as the non-reactive specimens. The need for more extensive research on the combined effects of ASR and chloride-induced corrosion can be seen. More research in this area is needed to develop a universal testing method to be able to assess the combined effects of ASR and chloride-induced corrosion. Conditions such as different reactive aggregate, curing environment and concrete mix must also be studied for the role of ASR in chloride-induced corrosion of reinforced structures. The main findings consist of:

- ASR gel can block the transportation of chloride ions due to filling the concrete pore and existing void resulting in reducing the chloride diffusion coefficient of the concrete.
- ASR may reduce the pH of the concrete pore at the steel-concrete interface resulting in a lower critical chloride threshold.
- The corrosion initiation time of reactive and non-reactive specimens occurred at the same time, which indicates that the low critical chloride threshold and low diffusion coefficient of the concrete can counteract each other to reach the same corrosion initiation time as non-reactive specimens.
- The addition of 20% fly ash by weight of cement can maximize the durability of the concrete by increasing its corrosion initiation time due to the formation of ASR gel which lowers chloride transportation. This effect was not observed in specimens with 40% fly ash as there were no signs of ASR occurring in the concrete due to fly as completely negating ASR.

2.3.2 Effect of Combined Deterioration on Flexural Capacity

Mikata et al. (2020) and Mikata et al. (2018) are the first publications to evaluate the effect of combined deterioration due to ASR and chloride-induced corrosion on the Shear capacity and flexural capacity of RC beams. More research is needed to evaluate

the combined effects of ASR and chloride-induced corrosion on RC mechanical properties as there are limited publications regarding this topic.

2.3.2.1 Mikata et al. (2020)

Due to over 30 structures currently damaged by ASR and succumbing to subsequent corrosion and steel bar fracture in Japan, the study of the combined deterioration is vital to evaluate the state of the damaged structures and propose remedial actions and be able to clarify the residual performance of shear capacity of RC members affected by the combined deterioration effect due to ASR and corrosion.

A total of twelve beams were cast, the details of the specimens and the ultimate shear capacity of the specimens are provided in Table 2-3 and Figure 2-19.

Table 2-3: Test specimens and ultimate shear capacity (Mikata et al., 2020)

Series	Specimens	Anchorage of shear reinforcement	Mix proportion type of concrete	Ultimate shear capacity	
				P_{us}	V_y
Normal (N)	N-1-14	Sound	Normal	102	50.8
	N-2-14	Fractured	Normal	102	50.8
	N-1-15	Sound	Normal	113	56.7
	N-2-15	Fractured	Normal	113	56.7
ASR (A)	A-1-14	Sound	Reactive coarse aggregate	101	50.5
	A-2-14	Fractured	Reactive coarse aggregate	101	50.5
	A-1-15	Sound	Reactive fine and coarse aggregate	105	52.6
	A-2-15	Fractured	Reactive fine and coarse aggregate	105	52.6
ASR and corrosion (AC)	AC-1-14	Sound	Reactive coarse aggregate	102	51
	AC-2-14	Fractured	Reactive coarse aggregate	102	51
	AC-1-15	Sound	Reactive fine and coarse aggregate	101	50.4
	AC-2-15	Fractured	Reactive fine and coarse aggregate	101	50.4

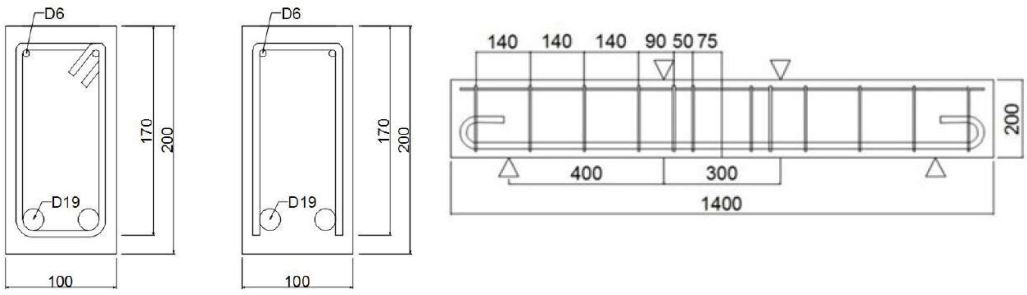

Figure 2-19 Specimen dimensions (Mikata et al., 2020)

All specimens were cured for four weeks under normal moist-curing conditions at 20°C. The A-series were placed in a chamber with 40°C and 90% humidity. As for the AC series, they were placed in 40°C and 90% humidity chamber at weekends and sprayed with 3% saline water and transferred outside on weekdays.

The expansion of the specimens containing reactive fine and coarse aggregate was larger than that of specimens containing only reactive coarse aggregate. The axial strain of specimens can be seen in Figure 2-20 ASR axial strain, which have expanded considerably due to ASR.

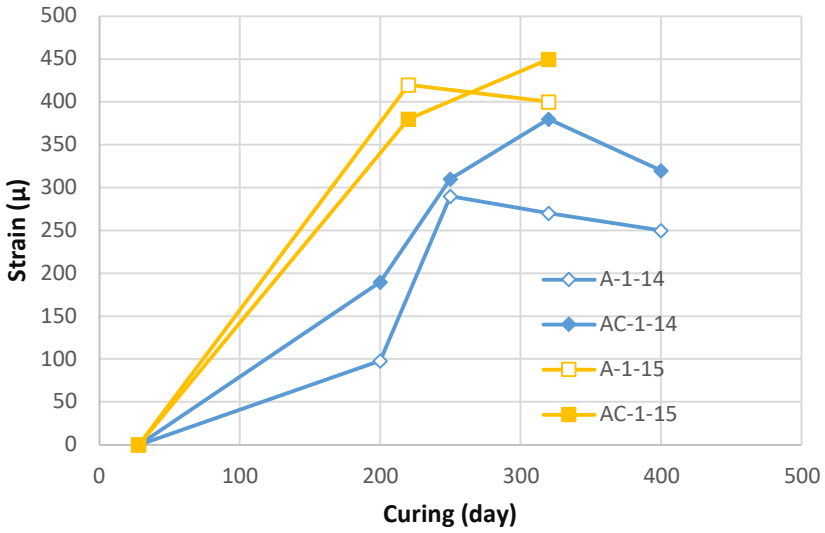

Figure 2-20 ASR axial strain (Mikata et al., 2020)

The failure models of the specimens in the experiment were different due to specimens being both affected by ASR, corrosion and anchorage conditions. The

specimens containing fractured was lower in fractured anchorage specimens than that of the sound specimens. Additionally, in A and AC series specimens, the shear stress carried were complicated due to ASR and corrosion cracks. It should be noted that the ultimate load capacity of the AC-series was much lower than A and N series due to corrosion.

2.3.2.2 Mikata et al. (2018)

To evaluate the combined effects of ASR and chloride-induced corrosion on the flexural capacity of RC beams, four series of specimens. Normal (N) series, corrosion (C) series, ASR-series and combined deterioration (AC) series. N-series contained ten specimens, while other series each had eight. Half of the specimens of each series were cast with hook, and the other half were cast with no hook. The A-series were kept in a climate chamber with 40°C and 90% humidity. The AC series were also kept in a climate chamber and sprayed with 3% saline water every weekday. As for the C-series, the specimens were placed in a curing room and sprayed with 3% saline water every weekday.

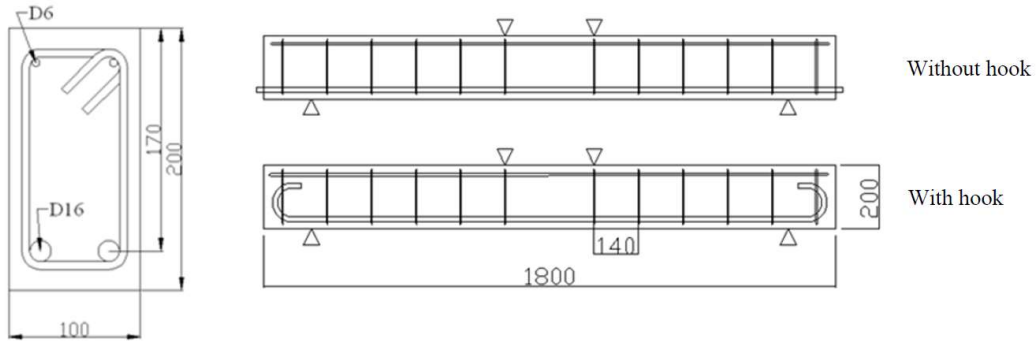

Figure 2-21 Cast specimens dimensions and cross-section (Mikata et al., 2018)

ASR expansion of the beams were measured using contact gauge tips. The rebars' corrosion was measured by removing the rebars after the loading test and removing the rust by using di-ammonium hydrogen citrate solution and comparing the weight loss with the initial weight of the rebar before casting. It is observed that the weight loss percentage of the rebars increased throughout the experiment period.

The experiments on the specimens show that the corrosion weight loss and chemical prestress due to ASR can play a key role in the flexural capacity of the beams. Due to corrosion, the ductility of the C-series were lower than other specimens. On the other hand, due to the chemical prestress of ASR in AC-series, the loading force increased after yield. However, the ultimate load of AC-series were lower than other specimens in this experiment. The ultimate load capacity of AC and C-series decreased in proportion to cross-section area loss of the reinforcement. Although chemical prestress occurred in AC-series, the ultimate load ratio on the AC-series were lower than N series due to corrosion.

2.3.2.3 Summary

It can be noted that the combined effect of ASR and corrosion can directly affect the flexural capacity and shear capacity of the RC structures. From the literature, we can conclude that despite the chemical prestress of ASR, corrosion can lower the flexural capacity of the structure by lowering the cross-section of the reinforcement. Cracks caused by the combined effects of ASR and corrosion can affect the shear capacity result of the structure. In addition, specimens containing fractured anchorage showed lower chemical prestress. More experiments are required on the topic of combined effects of ASR and corrosion on mechanical properties of the RC structures as there are very limited literature.

2.4 Summary

A comprehensive literature review has been conducted on ASR and chloride-induced corrosion and their combined effects on RC structures.

From the literature, it is evident that ASR can adversely affect the mechanical properties of RC. It has been observed that to evaluate ASR damage and set criteria for the evaluation of ASR cracks in concrete modulus of elasticity and tensile strength can be considered as they are the most sensitive out of all mechanical properties and show less fluctuation in results from across the literature.

From assessing the limited literature regarding the combined effects of ASR and chloride-induced corrosion, it can be concluded that ASR gel can block the transportation of chloride ions due to filling the concrete pore and existing voids resulting in reducing the chloride diffusion coefficient of the concrete while reducing the pH of the pore solution leading to a lower critical chloride threshold of the reinforcement embedded within the concrete affected by ASR, which sets an equilibrium in the concrete environment. Surprisingly, it was observed the addition of fly to an amount that would not halt the ASR progression in concrete can increase the time to corrosion initiation compared to specimens in which ASR progression was halted due to the addition of fly ash.

Chapter 3
Experimental Program

3.1 Overview

This experimental study is planned to utilize Accelerated Chloride-Induced Corrosion (ACIC) test to investigate the effect of alkali-silica reaction on time to corrosion-induced cracking in concrete cover due to chloride-induced corrosion and their combined effect on the deterioration of concrete structures. Additionally, the effect of ASR propagation on chloride ion migration/diffusivity is studied using NT build 492 (chloride migration coefficient from non-steady-state migration experiments) standard, which utilized an accelerated method to determine the chloride migration coefficient in concrete.

Nabavi (2014) argues that the initiation of corrosion in concrete is assumed a conservative method of estimating the end of service life of the concrete structure; however, time to corrosion-induced crack on the concrete cover can also be considered a reliable tool to be able to determine the end of service life (Nabavi, 2014). Thus, In this experimental program to be able to evaluate the combined effects of ASR and chloride-induced corrosion both during corrosion initiation and corrosion propagation stages ACIC method is used.

The results of both these tests on concrete specimens contacting reactive and non-reactive aggregate can give us an insight into how combined effects of ASR and chloride-induced corrosion can have an impact on chloride diffusivity in concrete.

This experimental study is based on a "Comparative Method" and will compare the time to corrosion-induced cracking in reinforced concrete specimens with and without reactive silicate aggregates. To accelerate the ASR process (NaOH) will be added to the concrete mix to increase the ($NaOH_{eq}$) to 1.25%, and the specimens will be submerged in 1M (NaOH) solution in the case of reactive siliceous aggregates. Control specimens with non-reactive aggregates will be cast for the purpose of the comparative method. The Accelerated Chloride-Induced Corrosion (ACIC) method is selected to compare the time to corrosion-induced cracking in both categories of samples, including reactive and non-reactive aggregate. As the mechanical properties and migration confidant of the specimens are determined over time, reinforced specimens will be tested at the same time to see the differences in time to corrosion-induced cracking at the different time periods.

The following experimental phases present the road map of the investigation:

1. A proper design of concrete mix to achieve a characteristic compressive strength of 40 MPa (structural concrete).
2. Sample preparation using both types of concretes with and without reactive silicate aggregates.
3. Investigation on mechanical properties of both concrete categories.
4. Investigation on time to corrosion-induced cracking in concrete specimens containing reactive and non-reactive aggregate utilizing the "Accelerated Chloride-Induced Corrosion" method.
5. Investigation on chloride migration coefficient utilizing NT build 492 standard in concrete specimens containing reactive and non-reactive aggregate and evaluating whether ASR can affect the chloride migration/diffusion in concrete.

3.2 Materials and Concrete Mix Design

3.2.1 Aggregate

In this experiment for casting reactive specimens, a highly reactive coarse (10mm and 20mm) dacite aggregate was used to accelerate the ASR along with none reactive fine and coarse sand. For casting the non-reactive specimens coarse (10mm and 20mm), limestone was used along with the same non-reactive fine and coarse sand Table 3-1. To achieve a less porous and good quality concrete sieve analysis of coarse and fine aggregates are done according to AS 2758.1 and presented in Figure 3-1 and Figure 3-2, respectively.

Table 3-1 Mix aggregates

Aggregate	Size	Status
20mm limestone	20 mm	Non-reactive
10mm limestone	10 mm	Non-reactive
Stockton dune sand	Fine sand	Non-reactive
Maroota coarse sand	Coarse sand	Non-reactive
20 mm dacite	20 mm	Reactive
10 mm dacite	10 mm	Reactive

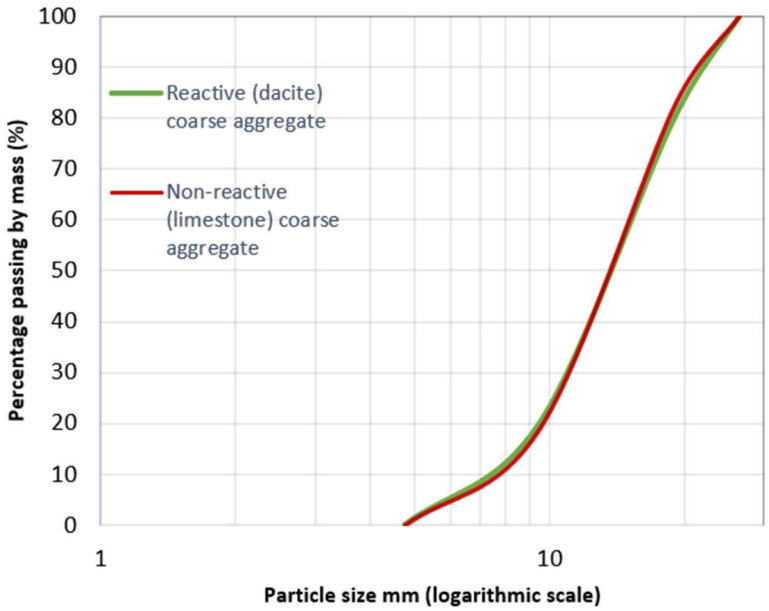

Figure 3-1 Reactive and non-reactive coarse aggregate grading curves

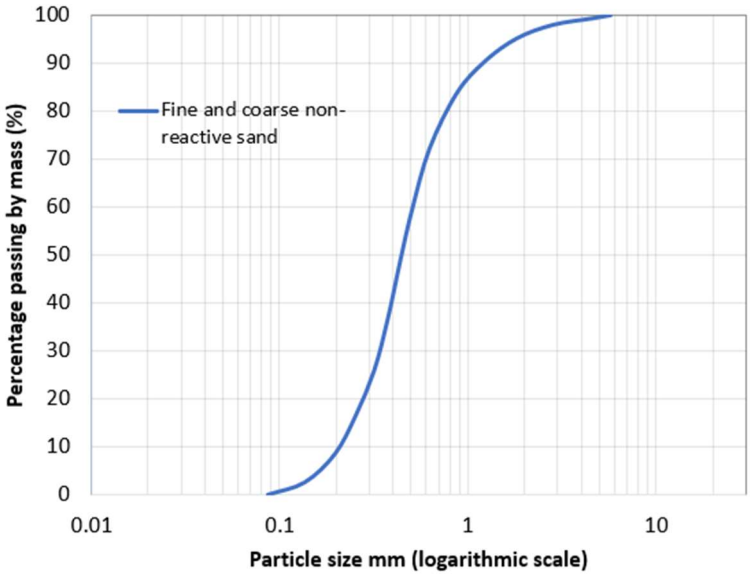

Figure 3-2 Non-reactive fine and coarse sand aggregate grading curve

.

Accelerated AMBT and autoclave experiments conducted by UTS researchers Tapes (2020) and Cao et al. (2021) show that dacite aggregate, which is used in this experiment for reactive aggregate purposes, is a highly reactive aggregate, making it is susceptible to ASR Figure 3-3 (Cao et al., 2021; Tapas, 2020).

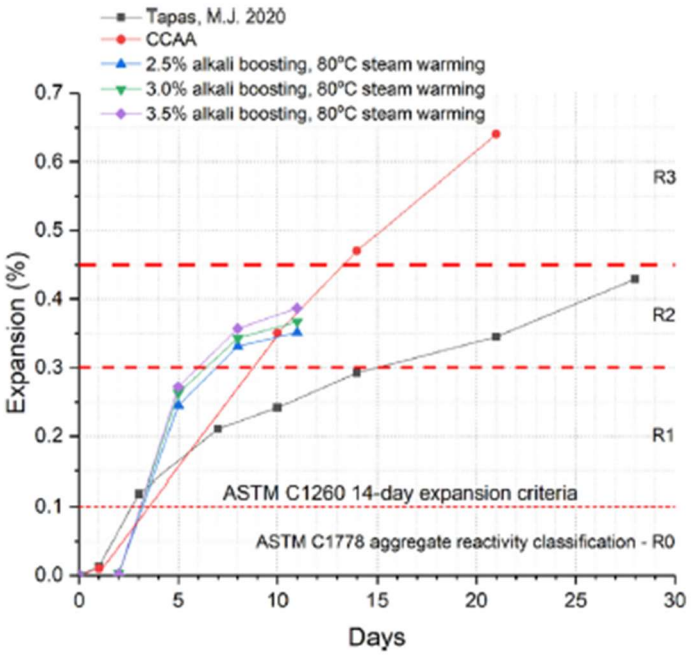

Figure 3-3 Dacite aggregate reactivity comparison in autoclave and AMBT(Cao et al., 2021)

3.2.2 Cement

General-purpose cement with an alkali content of 0.5% (Na_2O_{eq}) by the mass of cement were used to cast reactive and non-reactive specimens. The (Na_2O_{eq}) is calculated via $\%Na_2O_{eq} = \%Na_2O + 0.658 \times \%K_2O$ equation. The oxide composition analysis of the GP cement is provided in Table 3-2.

Table 3-2 GP cement oxide composition in concrete

Oxide composition	Weight Percentage (%)
CaO	64.06
SiO_2	19.65
Al_2O_3	5
Fe_2O_3	3
SO_3	2.39
MgO	0.9
K_2O	0.42
TiO_2	0.2
Na_2O	0.21
P_2O_5	0.04
Mn_2O_3	0.1
LOI	4.03
Total	100
Na_2O_{eq}	0.5

The alkalinity of the reactive concrete mix should be boosted to accelerate the ASR process. For the purpose of accelerating the progress of ASR, the alkali content of cement was increased to 1.25% Na_2O_{eq} by using (NaOH) pallets with 98% purity, (NaOH) pellets were added to the concrete mix water 24 hours prior to the mixing as (NaOH) generates a considerable amount of heat when initially mixed with water that can negatively affect the strength and quality of the concrete. The reactive specimens were also submerged in 1M (NaOH) (40gr/litre) solution (NaOH) to prevent alkali leaching.

Figure 3-4 NaOH pallets with 98% purity

3.2.3 Concrete Mix Design

For the concrete mix design, it was chosen to be as close to concrete used in the industry with characteristic compressive strength (f_c') of 40 MPa, water to cement ratio (W/C) of 0.4 and slump between 70 to 90 mm. The complete mix design and the aggregate percentage are presented in Table 3-2 and Figure 3-5, respectively.

Table 3-3 Mix design representing material needed for one cubic meter of concrete

Material	Concrete mix design
Cement	350 kg/m3
Water	140 kg/m3
Fine Sand	72 kg/m3
Coarse Sand	652 kg/m3
10mm Aggregate	220 kg/m3
20mm Aggregate	886 kg/m3
NaOH pallet	3.46 kg/m^3
superplasticizer	0.17 lit/m^3

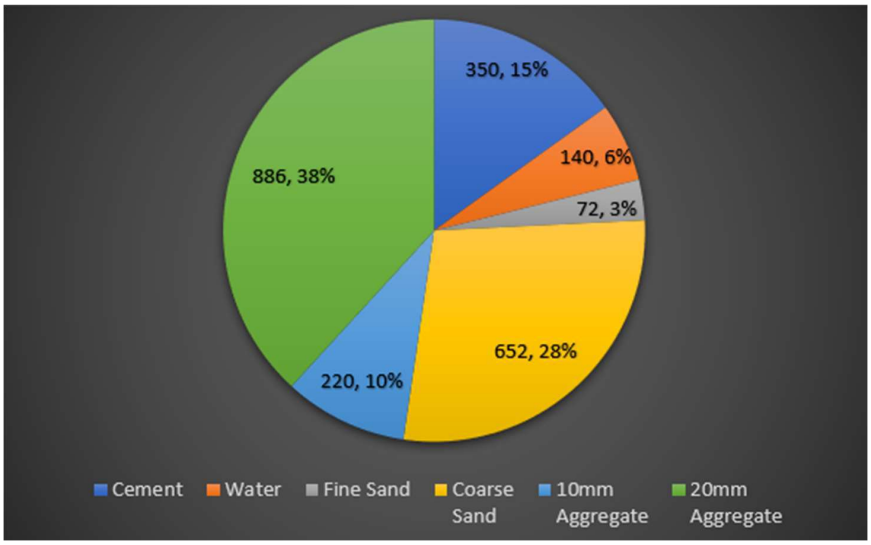

Figure 3-5 Mix design quantity and percentage

As this experiment mix design's water to cement ratio is relatively low (*W/C=0.4*), a superplasticizer/high-range water reducer is required. For this purpose, MasterGlenium SKY 8379 superplasticizer is used to reach the desired slump of 70 to 90 mm and increase the workability of the concrete while preparing the specimens.

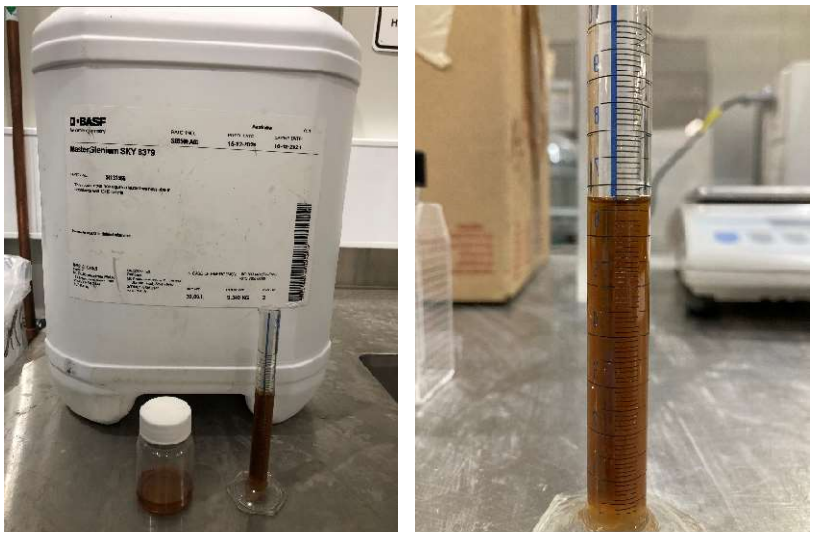

Figure 3-6 MasterGlenium SKY 8379 superplasticizer

3.3 Specimen Types and Preparation

The mixing process of concrete in this experiment was in accordance with AS 1012.2. Two types of specimens were cast for the purpose of this experiment. Normal cylindrical (Ø100mm × 200mm) for mechanical testing and NT build 492 (chloride migration coefficient from non-steady-state migration experiments). Cylindrical (Ø100mm × 200mm) specimens with an N12 steel reinforcement embedded in the central axis of the cylinder with 7cm extension from the top base and 5cm spacing from the bottom base for the ACIC test.

The N12 reinforcements were held utilizing a hollow plastic bar chair to avoid movement of the rebar when casting and transferring the mould as the placement of the rebar precisely on the central axis with the 50mm bottom spacing is crucial to the ACIC test result as any reinforcement deviation may result in faster than usual corrosion time. Also, 10cm of the rebars from the top end are coated with three layers of epoxy to ensure that corrosion will not occur during the long curing period.

The schematic of both of the specimens are presented in Figure 3-7 and Figure 3-8.

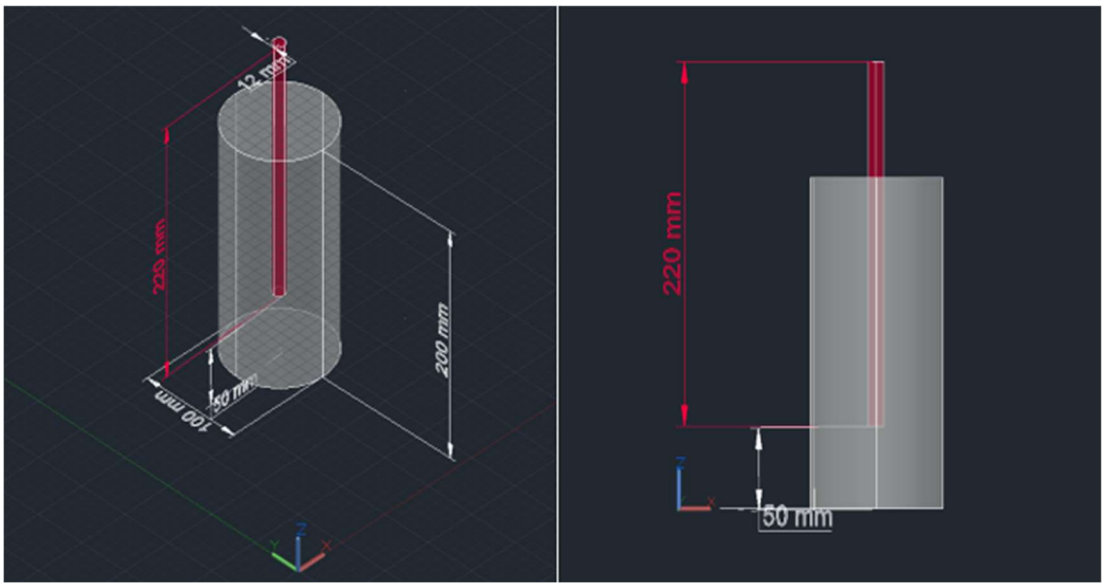

Figure 3-7 ACIC cylindrical (Ø100mm × 200mm) specimen with N12 rebar embedded in the central axis for ACIC test purposes

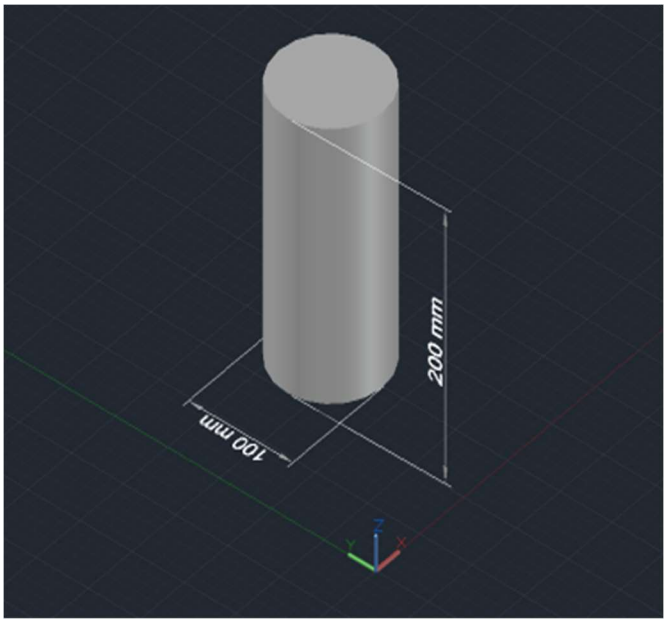

Figure 3-8 Normal cylindrical (∅100mm × 200mm) specimen for mechanical properties test

Furthermore, specimens in this experimental test can be categorized into durability and mechanical test, as presented below in Figure 3-9.

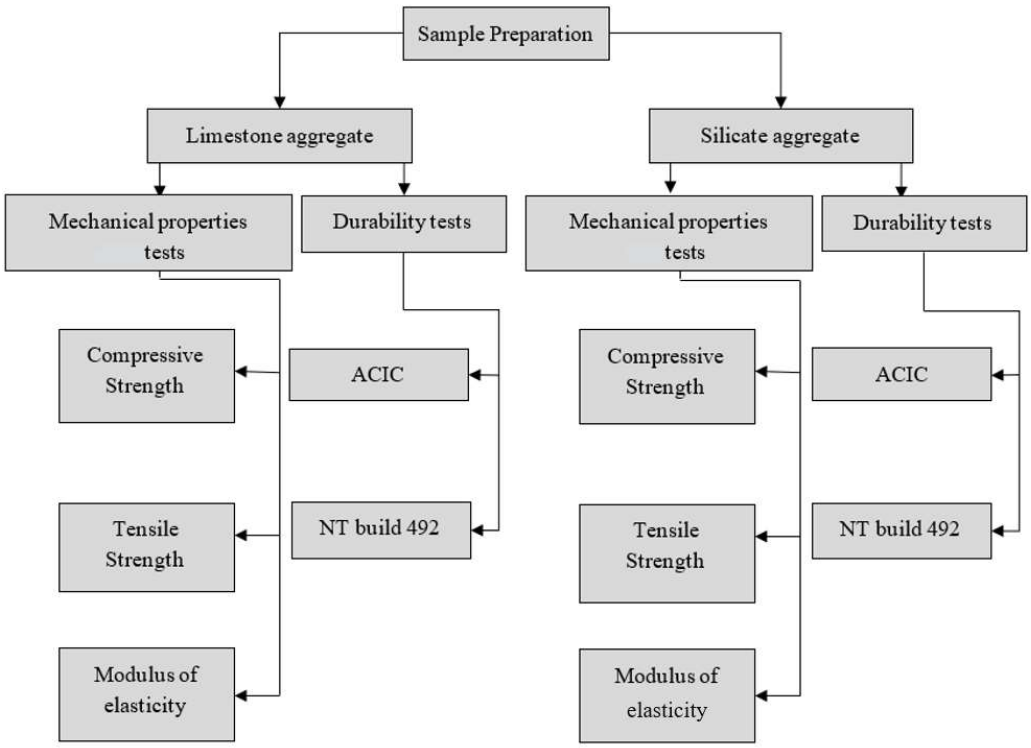

Figure 3-9 testing categories

3.4 Trial Bach

A trail mix was conducted using reactive and non-reactive specimens to evaluate the mix design's characteristic compressive strength and see if any adjustments were required in the final mix. As presented in Table 3-4, the compressive strength of both specimens containing reactive and non-reactive aggregate following the mix design presented in chapter 3.2.3 is above 40 MPa, deeming the mix design acceptable for the main reactive and non-reactive specimens' fabrication.

Table 3-4 Trial mix results

Specimen types	Average compressive strength (MPa)		
	7-day	14-day	28-day
Reactive	40.3	44.56	50.32
Non-reactive	42.4	44.98	51.89

3.5 Final Concrete Mix and Batches

Six batches of concrete specimens, including normal (Ø100mm × 200mm) cylinder for the mechanical test, (chloride migration test) and (Ø100mm × 200mm) cylinder with N12 embedded rebar for ACIC test, were cast, with four batches for reactive with batch name RB1, RB2, RB3 and RB4 four for non-reactive specimens. The other four batches were cast with non-reactive aggregate with batch names NRB1, NRB2, NRB3 and RB 4. To be able to cast concrete with good quality, all of the coarse aggregates in this experiment were washed and in a Saturated Surface Dry (SSD).

In addition, to determine the effect of chloride-induced corrosion crack time on different slump values in reactive specimens, the RB1 slump was aimed at 90 to 110 mm to see the effects on the ACIC test and how it would compare to other specimens with N12 embedded rebar.

All the mixing process was done in the UTS Tech Lab utilizing a horizontal pan mixer. The concrete was prepared in accordance with AS 1012.2. The aggregate was first poured into the mixer and mixed for two minutes. After the mixing of aggregates, the cement is added and mixed for an additional 2 minutes. During this time, water

and superplasticizer are added. For the batches containing reactive aggregate, the mixing water is boosted with (NaOH) pallets which boosts the total alkali content of the cement by 1.25% of the weight of cement. After this stage, the mix is set to rest for two minutes and then a further two minutes of final mixing. The mix's slump, air content, and density are also measured utilizing AS 1012.3 and AS 1012.4, respectively. The specimens are left for 24 hours to set before demolding and curing.

Table 3-5 presents batch numbers and expected specimens to be cast from each batch.

Table 3-5 Batch number and expected number of specimens from each batch

Batch Number	(Ø100mm × 200mm) cylinder	(Ø100mm × 200mm) cylinder with embedded N12 rebar
RB1	16	9
RB2	16	9
RB3	22	None
RB4	25	None
NRB1	16	9
NRB2	16	9
NRB3	22	None
NRB4	25	None

Figure 3-10 Pictures of concrete mixing process with slump, air content and density test measurements at UTS Tech Lab

3.6 Curing of Specimens

The specimens initial curing method will comply with AS 1012.8.1. After demolding the reactive casted specimens, are submerged in 25°C water to cure for three days, then transferred to 38°C climate chamber and submerged in water. ASR is a time-consuming process to simulate in laboratory conditions. A sufficient amount of alkali, reactive aggregate, moisture, and heat is required to accelerate the ASR progress and overcome this time-consuming process for faster results similar to other accelerated tests such as AS 1141.60.1 and AS 1141.60.2 (Rajabipour et al., 2015). Additionally, alkali leaching must also be considered in this process. Based on the literature (Latifee & Rangaraju, 2015; Thomas et al., 2006), the alkalis in concrete can leach out into the water, contributing to the delay of ASR progression, making it more time-consuming. To overcome this issue, the reactive specimens are submerged in a 1M sodium hydroxide (NaOH) solution (40gr/l) to prevent alkali leaching. All the cylindrical (Ø100mm × 200mm) specimens with an N12 steel reinforcement were submerged in a manner to prevent water from touching the epoxy coated rebars to prevent any premature corrosion despite being coated with three layers of epoxy.

Images of curing reactive and non-reactive specimens are shown in Figure 3-11.

Figure 3-11 (Top) Reactive and non-reactive specimens in 38°C climate chamber with non-reactive specimens being submerged in water and reactive specimens submerged in 1 M sodium hydroxide (NaOH) solution, (Bottom) Non-reactive and reactive specimens cured in 25°C submerged in water.

3.7 Concrete Mechanical Properties

As mentioned in chapter 2.1.4, as the concrete expands due to ASR, it can cause internal tension resulting in the expansion of the concrete. To evaluate how the progression of ASR impacts the integrity of the casted concrete specimens, compressive strength test, indirect tensile strength test and modulus of elasticity tests will be conducted to assess the concrete as ASR progresses alongside with ACIC test and chloride migration test.

3.8 Expansion Measurement

ASR may take years to exhibit damaging expansion, and it can have a negative effect both on the concrete and the reinforced structure (Fan & Hanson, 1998). In some cases, expansion can even cause the reinforced steel rebar or stirrup to yield, causing fractures. This effect combined with reinforcement corrosion has been seen in structures such as Lucinda jetty in Australia and some bridge piers in japan. Because of the mentioned reasons, it is important to monitor the expansion of specimens due to ASR.

In order to measure the free expansion of the reactive and non-reactive specimens, a Demountable Mechanical Strain Gauge (DEMEC) was used to measure the expansion of cylindrical specimens for up to 150-days. At the third day for curing DEMEC disks were adhered to the surface of the cylinders using epoxy adhesive from three sides parallel to the central axis Figure 3-12.

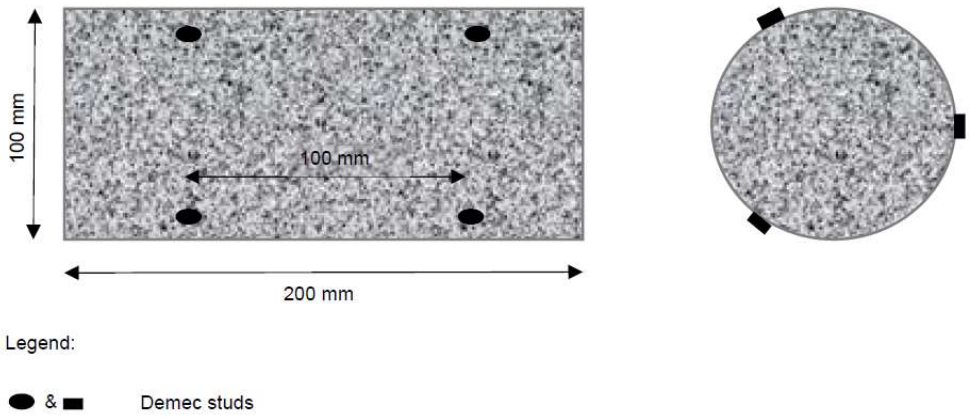

Figure 3-12 (Left) Side view of 100mm × 200mm specimen with attached DEMEC discs, (Right) Top view of 100mm × 200mm specimen

3.9 ACIC Test

To evaluate the performance of the specimens containing reactive aggregate undergoing ASR and non-reactive aggregates due to corrosion, the accelerated chloride-induced corrosion test is utilized. Across the literature, some researchers argue that the service life of a structure ends with corrosion initiation of the steel, which is also known as the corrosion-free service life of the structure, this assumption

is based on the fact that the period from corrosion initiation to cover cracking is substantially shorter than the corrosion initiation time (Funahashi, 1990; Maage et al., 1996; Nabavi, 2014). However, other researchers consider and evaluate corrosion-induced cover cracking as the end of serviceability of the concrete structure (Andrade et al., 1993; Bhargava et al., 2006; Cui & Alipour, 2018; Nabavi, 2014; Pantazopoulou & Papoulia, 2001; Zhang et al., 2010). Thus, in this experiment, the concrete cover cracking is assumed to be the end of service life based on the information from the literature.

ACIC set up in this experiment is an Impressed Current (IC) method. The embedded steel reinforcement will act as the anode, another steel bar will act as the cathode, and a 15% sodium chloride concentration will act as an electrolyte. A 30 V constant direct current will be connected to the Anode and Cathode. Any impulsive rise in electrical potential will indicate the crack generation within the concrete cover during this test. Utilizing a digital data logger, we can constantly monitor the circuit at any given time, as shown in Figure 3-14 and Figure 3-15. During this test, the concrete reinforcement acts as an anode and will attract $OH^-$and Cl^- anions, the cathode will reduce O_2 to OH^- and will attract Na^+ and H^+ cations, through these chemical reactions, the corrosion process is accelerated (Schueremans et al., 1999). The data logger utilized in this experiment is a high-resolution data logger with up to eight true differential inputs capable of monitoring voltage in the range of ±2.5. The data logger is connected to a computer containing PicoLog software which can monitor the voltage at any given time increments. The software has built-in fluctuation detection, which can help to estimate the chloride-induced cover crack more accurately by monitoring the spike in voltage Figure 3-13.

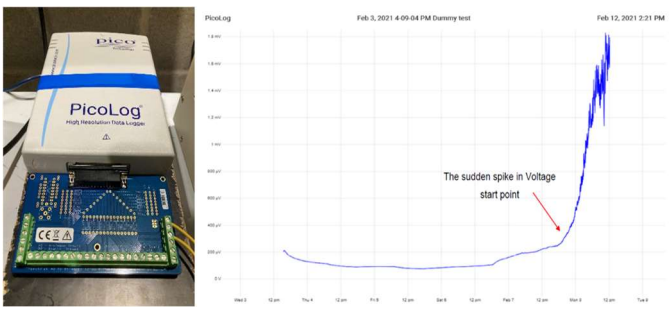

Figure 3-13 (Left) PicoLog high-resolution data logger with terminal board and (right) PicoLog software platform on computer

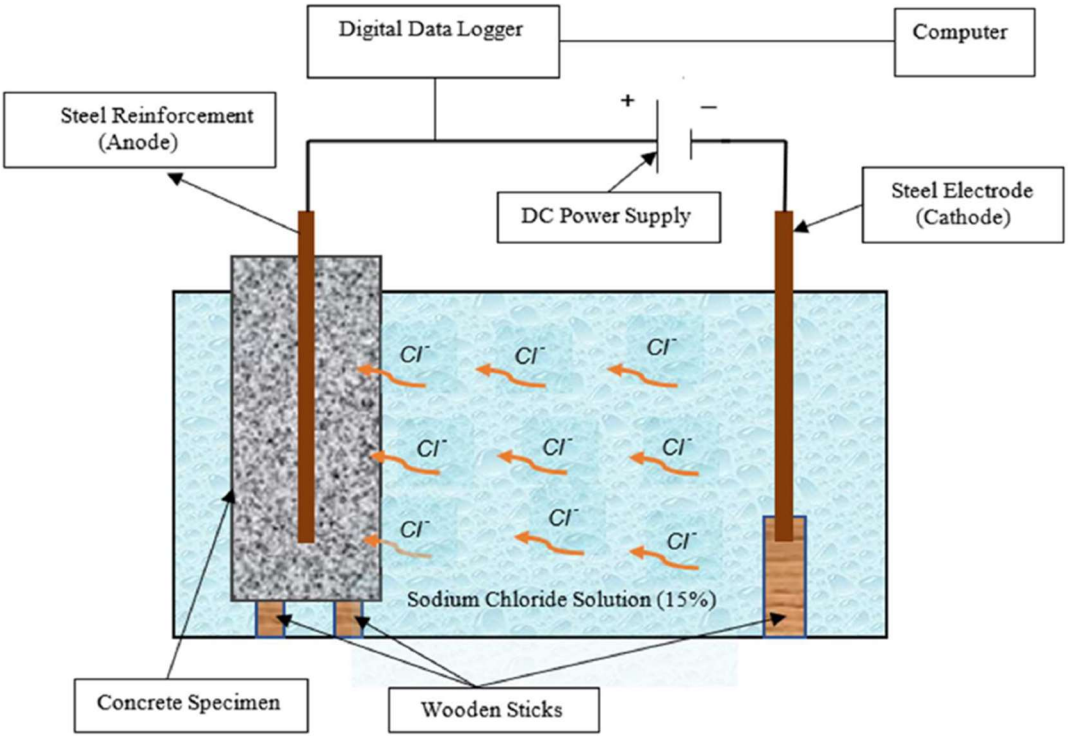

Figure 3-14 ACIC test schematic

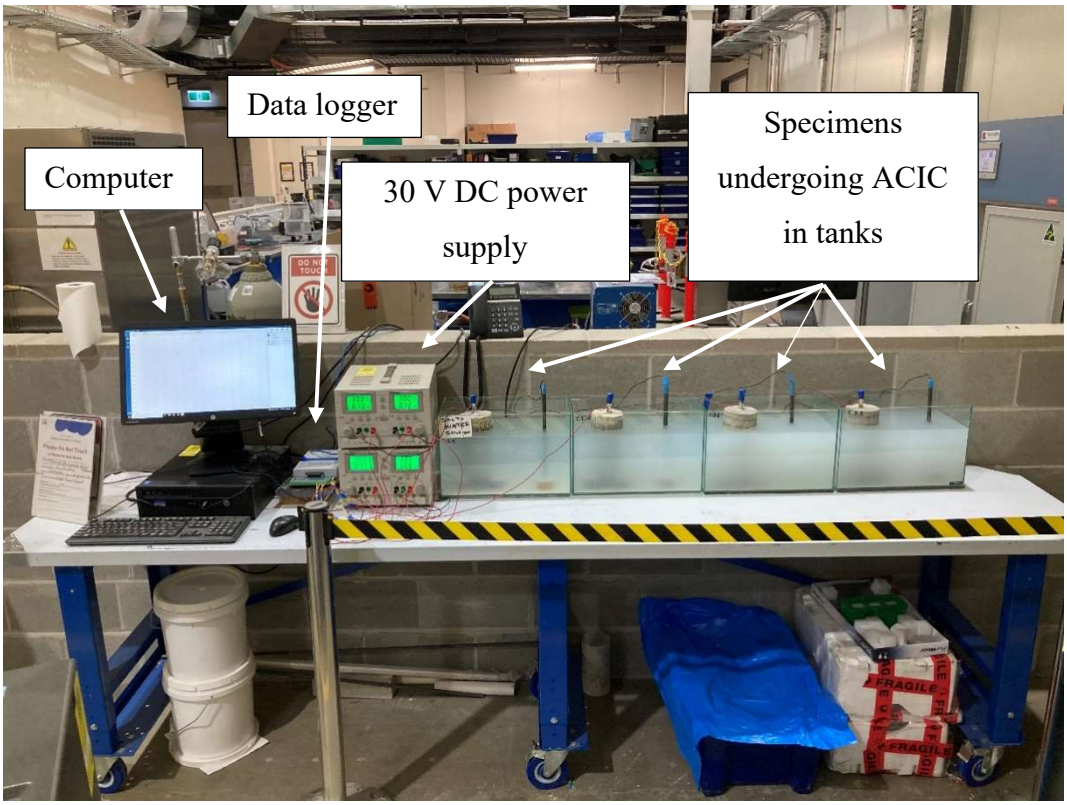

Figure 3-15 ACIC test setup at UTS Tech Lab

In this experiment, the time to chloride-induced corrosion crack is set as a criterion for assessing the combined effects of ASR and corrosion of reinforcement by comparing specimens containing reactive and non-reactive aggregate. Accelerated corrosion testing is a reliable experiment since corrosion by itself is a long term electrochemical reaction (Güneyisi et al., 2013; Saetta, 2005).

3.10 Chloride Migration Test

To elaborate more on the role of ASR on retarding the chloride ingress in concrete, the Nordtest method NT build 492 (Chloride Migration Coefficient from non-steady-state Migration Experiments) was utilized. Migration is defined as when ions within a material move by the influence of an external electrical field, whereas diffusion is the movement of ions from under a concentration gradient from a higher concentration to a lower concentration zone. Chloride ingress speed in concrete is a defining factor when it comes to concretes resistivity to chloride ingress. As this is a master's project and the limitation of time constraints the experimental progress, we use accelerated migration instead of diffusion tests such as ponding. Accelerated tests such as ASTM C1202, AASHTO T277, and NT build 492 are widely used and accepted in determining and comparing the chloride ingress rate of concrete with different build aspects and water to cement ratios.

To prepare the specimens for the migration test, the ∅100mm × 200mm cylindrical specimens were cut in half into two ∅100mm × 100mm cylinders and then by cutting 50 ± 2 mm at the end surfaces nearer to the first cut. The samples were transferred into a vacuum container with a pressure of 10-50 $mbar$ (1-5 kPa) for three hours. With the pump still running, the vacuum chamber is filled with a saturated solution of calcium hydroxide $Ca(OH)_2$, immersing the specimens, the vacuum is maintained for an additional hour before air is allowed to reenter the vacuum chamber. The specimens are to be kept in the solution for 18 to 20 hours. The specimens are then removed from the vacuum chamber and rinsed with water to clean off the excess calcium hydroxide $Ca(OH)_2$ from the surface of the specimen and then dried with a piece of cloth to prepare for the test.

Figure 3-16 Vacuum chamber for preparing the specimens for the test

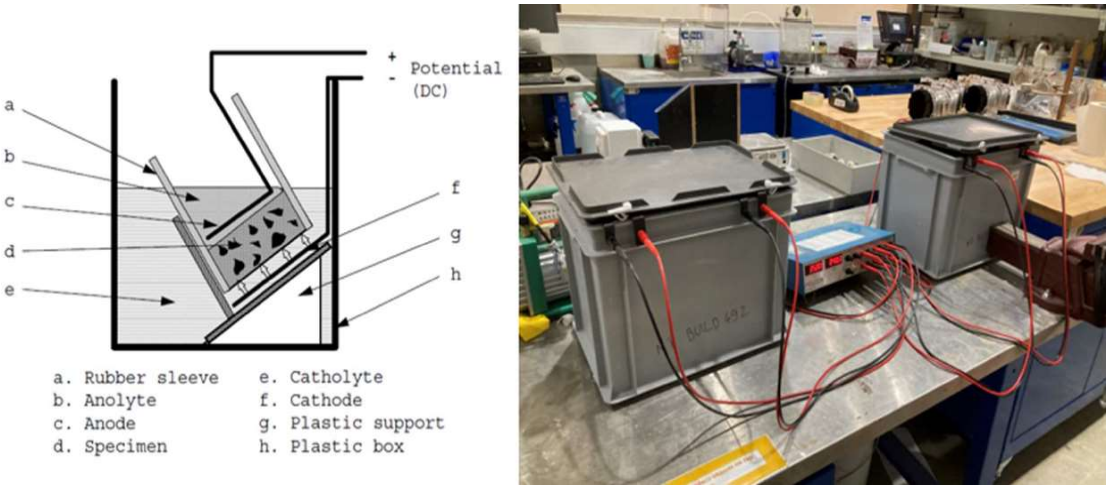

Figure 3-17 NT build 492 setup for migration coefficient measurement

The 50 mm disks are then put into a silicone rubber sleeve and tightened with stainless steel clamps. The anolyte and catholyte solutions are in this experiment were 0.3 N (NaOH) with distilled water and 10% NaCl using tap water, respectively. The

specimens are then introduced to a 30V initial electrical potential. This value is then adjusted based on the current at the time of 30V initial electrical potential. The duration of the test is also achieved with this method using the recommendations of NT build 492 Table 3-6.

Table 3-6 Test voltage based on initial current at 30V utilizing NT build 492 standard

Initial current I_{30V} (with 30 V) (mA)	Applied voltage U (after adjustment) (V)	Possible new initial current I_0 (mA)	Test duration t (hour)
$I_0 < 5$	60	$I_0 < 10$	96
$5 \le I_0 < 10$	60	$10 \le I_0 < 20$	48
$10 \le I_0 < 15$	60	$20 \le I_0 < 30$	24
$15 \le I_0 < 20$	50	$25 \le I_0 < 35$	24
$20 \le I_0 < 30$	40	$25 \le I_0 < 40$	24
$30 \le I_0 < 40$	35	$35 \le I_0 < 50$	24
$40 \le I_0 < 60$	30	$40 \le I_0 < 60$	24
$60 \le I_0 < 90$	25	$50 \le I_0 < 75$	24
$90 \le I_0 < 120$	20	$60 \le I_0 < 80$	24
$120 \le I_0 < 180$	15	$60 \le I_0 < 90$	24
$180 \le I_0 < 360$	10	$60 \le I_0 < 120$	24
$I_0 \ge 360$	10	$I_0 \ge 120$	6

At the end of the test, the silicone sleeve and steel clamps are carefully disassembled, and specimens are rinsed with water to remove the excess solutions on the surface of the specimens. The specimens are then split axially into two pieces then a 0.1 M silver nitrate solution is spayed on the split section to determine the penetration depth Figure 3-18.

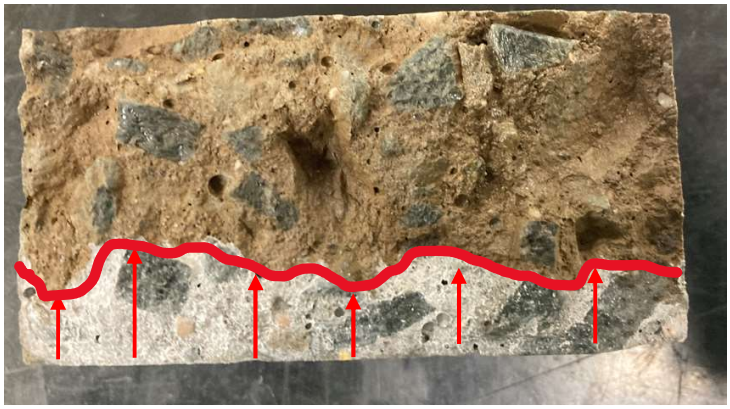

Figure 3-18 Chloride precipitation and direction of penetration

The non-steady-state migration coefficient is calculated from the equation underneath:

$$D_{nssm} = \frac{RT}{z\,FE} . \frac{x_d - \alpha\sqrt{x_d}}{t} \tag{3.1}$$

where:

- $E = \frac{U-2}{L}$
- $\alpha = 2\sqrt{\frac{RT}{z\,FE}} . \mathrm{erf}^{-1}\left(1 - \frac{2c_d}{c_0}\right)$
- D_{nssm}: non-steady-state migration coefficient, m^2/s
- z: absolute value of ion valence, for chloride, z = 1
- F: Faraday constant, F = 9.648 ×10₄ J/(V·mol)
- U: absolute value of the applied voltage, V
- R: gas constant, R = 8.314 J/(K·mol)
- T: average value of the initial and final temperatures in the anolyte solution, K
- L: the thickness of the specimen, m
- x_d: average value of the penetration depths, m
- t: test duration, seconds
- erf^{-1}: inverse of error function
- c_d: chloride concentration at which the colour changes $c_d \approx 0.07$ N for OPC concrete
- c_0: chloride concentration in the catholyte solution, $c_0 \approx 2$

The test results are then compared to see the difference in non-steady state chloride migration coefficient on reactive and non-reactive specimens and to determine if ASR can influence chloride migration/diffusion in the concrete environment.

3.11 Summary

The experimental program has been thoroughly explained in this chapter. To be able to produce good quality concrete, sieve analysis has been conducted for fine and

coarse aggregates. Trail mixes were performed to cast specimens with and without reactive aggregate, and their compressive strength was evaluated in 7, 14 and 28 days. The results were acceptable.

The ACIC test has been explained in which cylindrical specimens with embedded N12 rebar are exposed to a corrosive environment by analyzing the time to chloride-induced corrosion comparative method on reactive and non-reactive specimens. It can be determined if the combined effects of ASR and chloride-induced corrosion may impact the time to corrosion-induced crack in RC structures and their service life.

Furthermore, NT build 492 standards is utilized to evaluate the non-steady-state chloride migration confidant and to determine the influence of ASR and its by-product ASR gel on chloride migration/diffusion of concrete specimens containing reactive and non-reactive aggregates.

Chapter 4
Results and Discussion

4.1 Introduction

In this chapter, the results of the experimental program are discussed. These experiments will consist of:

- Assessing ASR's influence on concrete mechanical properties, including compressive strength, Indirect tensile strength and modulus of elasticity and comparing them with control specimens. These tests will give a good indication of how ASR can influence the mechanical properties of concrete.
- Conducting ACIC test to evaluate the time to chloride-induced corrosion crack in reactive and non-reactive specimens. This test can give us information on how the combined effects of ASR and chloride-induced corrosion can impact the cracking time of concrete cover due to chloride-induced corrosion in an accelerated test.

- Conducting the non-steady-state chloride migration test utilizing NT build 492 standard to evaluate the chloride migration coefficient of reactive and non-reactive concrete specimens in order to determine if ASR gel which is

a by-product of ASR, can influence the migration/diffusion of chloride ions in concrete.

4.2 Fresh Concrete Properties

In this section, the properties of freshly mixed concrete are presented. As it can be seen, the batches slump, air volume and density are within the same range, ensuring the consistency and homogeneity of the batches are the same. To evaluate the effect of water content on time to chloride-induced crack utilizing the ACIC test, one of the reactive batches, namely RB1, was selected to be cast with a higher slump between 90 mm to 110 mm.

Table 4-1 below presents the fresh concrete properties:

Table 4-1 Fresh concrete properties and number of specimens from each batch

Batch Number	Slump (mm)	Air volume (%)	Density (kg/m^3)	(Ø100mm × 200mm) cylinder	(Ø100mm × 200mm) cylinder with embedded N12 rebar
RB1	108	2.7	2556	15	10
RB2	88	2.7	2560	15	10
RB3	86	2.5	2558	22	None
RB4	87.5	2.6	2559	22	None
NRB1	90	2.5	2559	15	10
NRB2	87	2.6	2561	15	10
NRB3	89	2.7	2557	22	None
NRB4	89	2.5	2558	22	None

4.3 Compressive Strength

Compressive tests are done according to AS 1012.9. The top surface of the cylindrical specimens were ground utilizing a grinder device to achieve a plane surface for the compressive strength test for uniform loading. The universal testing machine apparatus can be seen in Figure 4-1.

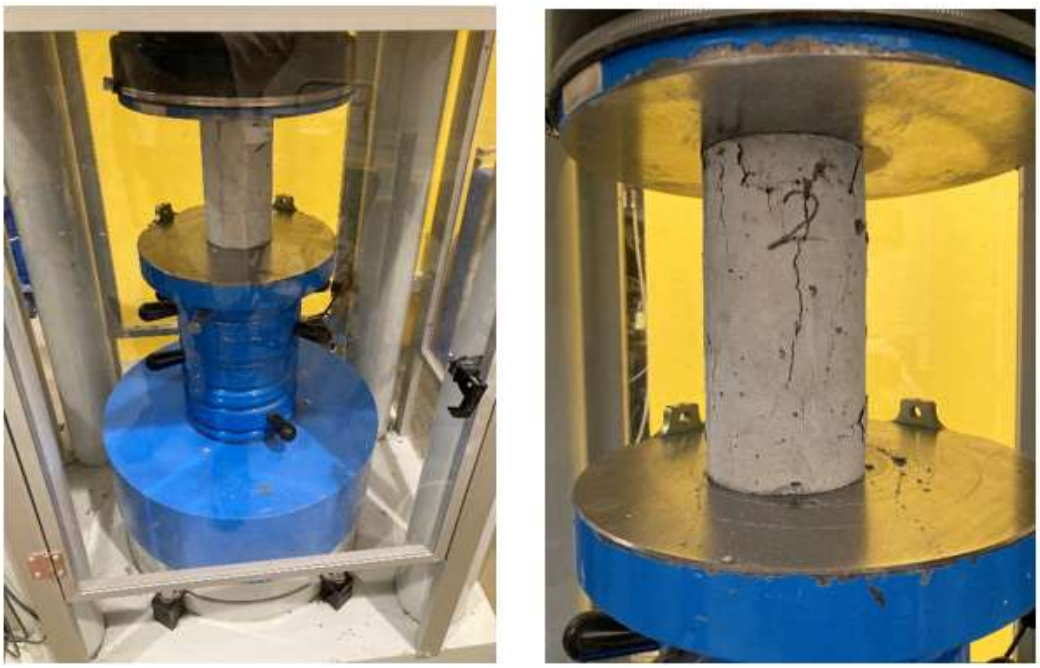

Figure 4-1 Compressive strength universal testing machine

The reactive and non-reactive specimens were tested on 7-day, 28-day, 56-day, 90-day and 150-day to evaluate the effect of ASR as it progressed over time and compare them versus non-reactive specimens. The average compressive strength results are presented in Table 4-2. As it can be seen, the targeted compressive strength of specimens are above the targeted 28-day compressive strength, which is 40 MPa.

Table 4-2 Average compressive strength test results for reactive and non-reactive specimens

Specimens type	Average compressive strength (MPa)				
	7-day	28-day	56-day	90-day	150-day
Reactive	40.01	44.82	49.1	54.02	57.21
Non-reactive	43.4	45.6	50.23	55.5	59.89

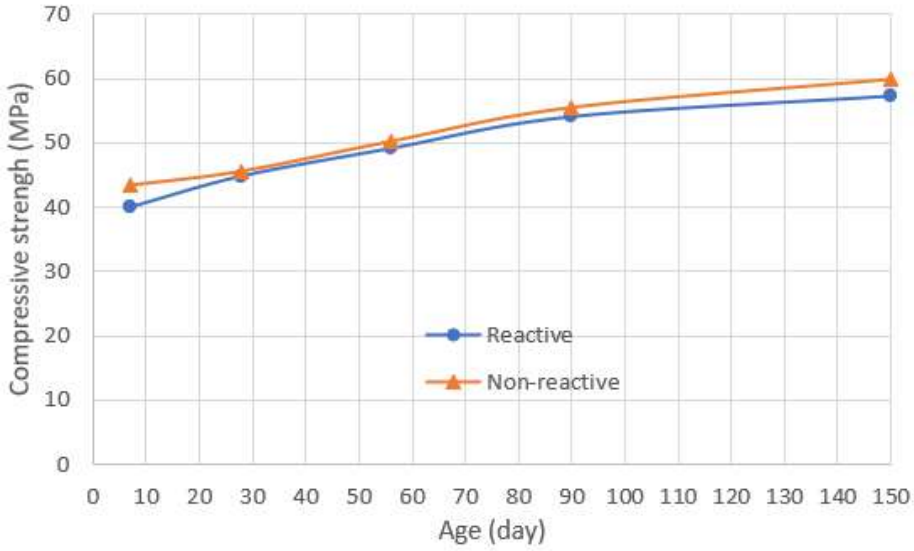

Figure 4-2 Compressive strength development in reactive and non-reactive specimens

From the acquired compressive strength test results on reactive and non-reactive specimens over 150 days, it is evident that ASR did not affect the compressive strength of the reactive specimens compared to non-reactive ones, as was expected based on chapter 2.1.5.2. Not much reduction in compressive strength can be seen in reactive specimens despite surface map cracking which appeared after approximately day-120 of curing in in a 38°C climate chamber and submerged in 1M sodium hydroxide (NaOH) solution. A total of three specimens of each type were tested for compressive strength at their respective test day.

Figure 4-3 External cracks on cylinders after 120-days submerged in 1M sodium hydroxide solution in 38°C climate chamber

It is expected that the compressive strength of the reactive specimens gets lower as time passes and ASR takes place, causing the cracks to become more severe (Barbosa et al., 2018).

4.4 Tensile Strength

To further evaluate the effect of ASR on the concrete specimens in this study, indirect tensile strength in accordance with AS 1012.10 Figure 4-4 and Figure 4-5.

Figure 4-4 Indirect tensile strength test apparatus

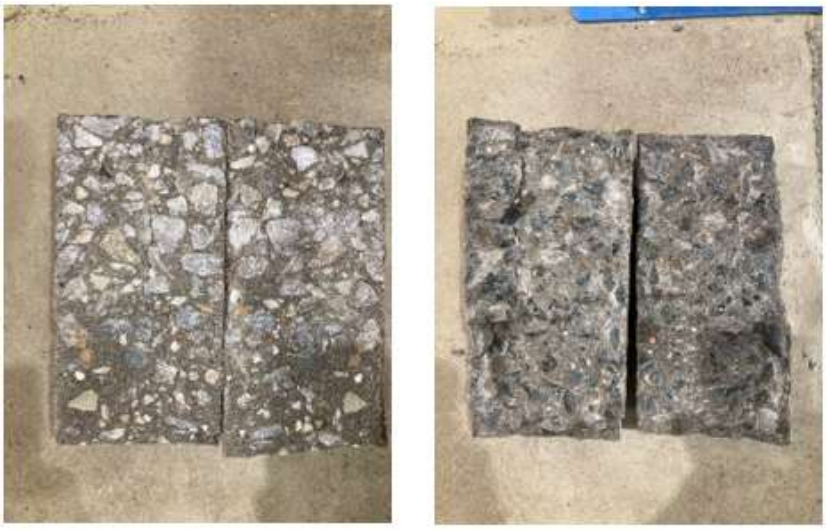

Figure 4-5 (left) Non-reactive specimen undergone indirect splitting tensile strength test (Right) Reactive specimens undergone indirect tensile strength test

The test has been conducted on reactive and non-reactive specimens in 7-day, 28-day, 56-day and 150-day. The results are presented underneath Table 4-3.

Table 4-3 Average splitting tensile strength test results

Specimens type	Average splitting tensile strength (MPa)				
	7-day	28-day	56-day	90-day	150-day
Reactive	4.59	4.49	4.46	4.45	4.39
Non-reactive	4.3	4.3	4.41	4.40	4.52

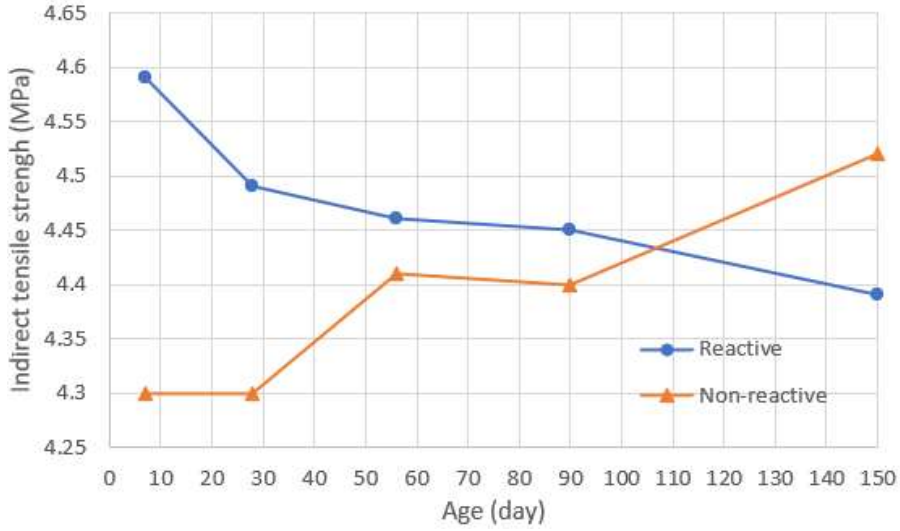

Figure 4-6 Tensile Strength development in reactive and non-reactive specimens

From the obtained results, it can be concluded that ASR progression did not affect the tensile strength of reactive specimens during 150-days of testing. A total of three specimens of each type were tested for the tensile test at their respective test day.

4.5 Modulus of Elastisity

The modulus of elasticity tests has been conducted in accordance with AS1012.17. The surface of the specimens was ground to achieve a uniform surface load. 10% and 40% of the compressive strength of the concrete specimens are used as an input for the modulus of elasticity test. The test is run in three cycles, and the gradient of the third and second cycle of the axial strain vs stress (MPa) is obtained as the modulus of elasticity of the specimen. The testing apparatus can be seen in Figure 4-7.

Figure 4-7 Modulus of elasticity testing apparatus

The test results for 7-day, 28-day, 56-day, 90-day and 150-day are presented below:

Table 4-4 Modulus of elasticity test results.

Specimens type	Average modulus of elasticity (GPa)				
	7-day	28-day	56-day	90-day	150-day
Reactive	39.81	46.43	39.8	37.25	35.98
Non-reactive	43.46	53.55	53.2	54.1	55.3

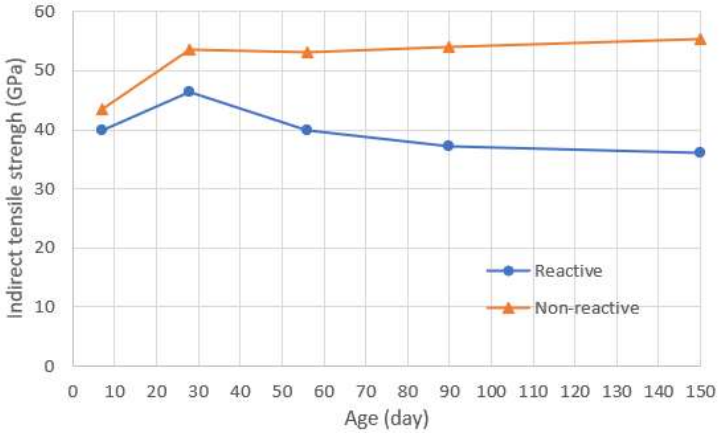

Figure 4-8 Modulus of elasticity development in reactive and non-reactive specimens

From the obtained results, it can be concluded that the average modulus elasticity of reactive and non-reactive specimens increased from 7day to 28-day due to concrete

hydration. However, the reactive specimens average modulus of elasticity is lowered by 22.5% from 28-day to 150-day. On the other hand, the non-reactive specimens show a slight increase of 3.8 from 28-day to 150-day. A total of three specimens of each type were tested for modulus of elasticity at their respective test day.

4.6 Expansion Measurement

The free expansion measurement of the reactive and non-reactive specimens for this study is conducted utilizing a demountable mechanical strain gauge (DEMEK). After the 3-day initial curing in 25°C submerged in water, DEMEC disks were adhered to the surface of the cylinders from three sides parallel to the central axis. After the 3-day initial reading, the specimens were transferred to the 38°C climate chamber. The reactive specimens were submerged in 1M sodium hydroxide (NaOH) solution, while the non-reactive specimens were submerged in water. The attachment of the DEMEC discs were similar to the study conducted by Fan and Hanson (1998). A total of six specimens, three for reactive and three for non-reactive, were measured for expansion due to ASR.

Table 4-5 Number of specimens for expansion measurement

Specimens type	Number of Specimens for expansion measurement
Reactive	3
Non-reactive	3

Figure 4-9 (Left) Mechanical DEMEC gauge for length change measurement and (Right) DEMEC disks adhered to the surface of the cylindrical specimen

The expansion result can be seen below in Figure 4-10:

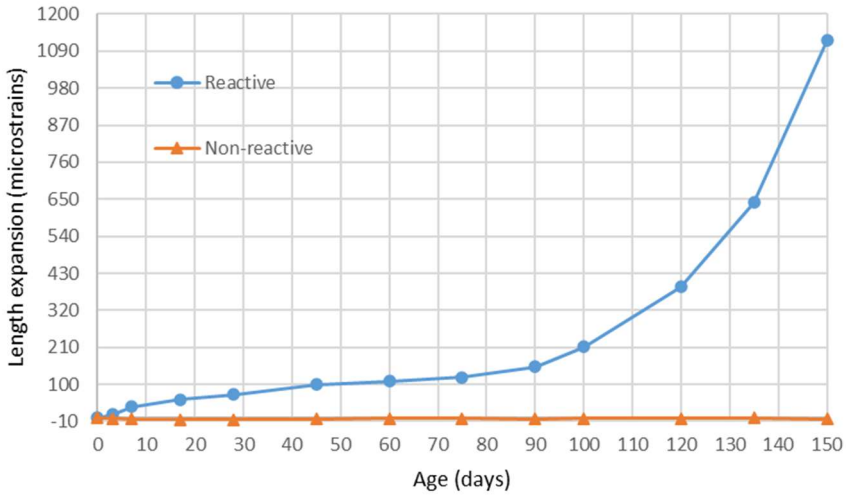

Figure 4-10 Expansion measurement for reactive and non-reactive specimens

It is observed that the reactive specimens in 38°C climate chamber submerged in 1M sodium hydroxide solution boosted with 1.25% of the weight of cement have been expanded about 0.12% due to ASR in the age of 150 days accompanied by cracking at the surface of the specimens A slight shrinkage is observed in non-reactive specimens with no expansion in the 150-day measuring the duration. The specimens are expected to expand more as the aging day progresses.

4.7 ACIC Test

4.7.1 ACIC Comparison In Pre and Post Cracking

At the first stages of the ACIC experiment, the ACIC setup has been tested systematically to better understand the behaviour of accelerated corrosion and estimate the time to corrosion-induced crack of test specimens correctly. For this purpose, up to five non-reactive ACIC specimens cured for seven days were tested and monitored for pre and post-cracking of the concrete surface due to chloride-induced corrosion while constantly monitoring the time vs. voltage through digital data logger. After each stage, the time to chloride-induced crack was measured,

the time the rebars were extracted to weigh and evaluate any signs of corrosion. The post crack specimens minimum and maximum crack width have been measured as well. To prepare the cylindrical (Ø100mm × 200mm) specimens with an N12 steel reinforcement, the epoxy on the top of the rebar is removed and cleaned with sandpaper to achive a smooth and clean surface to solder the wire to the rebar. The specimen is then connected to the positive socket (anode), and the other steel electrode (cathode) is then connected to the negative socket of the power supply. The basis of this experiment suggests that if any crack appears on the concrete surface, the voltage will spike. Thus, the connection to the data logger is from the anodic wire utilizing the differential channel input. After the wires are connected to the anode, cathode and data logger, the 15% salt (NaCl) solution is then poured into the experiment tank and filled until 4cm to 5cm from the surface of the cylindrical specimen. The PicoLog software is then updated with the experiments data and data logging intervals. After these steps, the DC power supply is turned on for the experiment to commence until a spike in the voltage is observed on the PicoLog software, indicating the surface of the concrete has cracked and opened for the way to chloride ions to freely access the N12 rebar embedded in the concrete specimen or anode. The process of preparing the specimens can be seen in Figure 4-11.

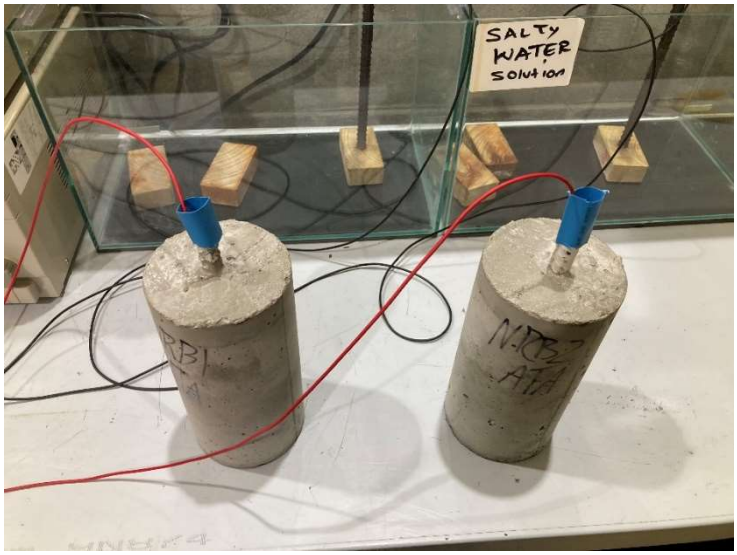

Figure 4-11 Preparing the cylindrical (Ø100mm × 200mm) specimens with N12 steel reinforcement for the ACIC test

The result of the initial stage of ACIC experiment for pre and post cracking evaluation on five non-reactive specimens can be seen in Figure 4-12 and Table 4-6.

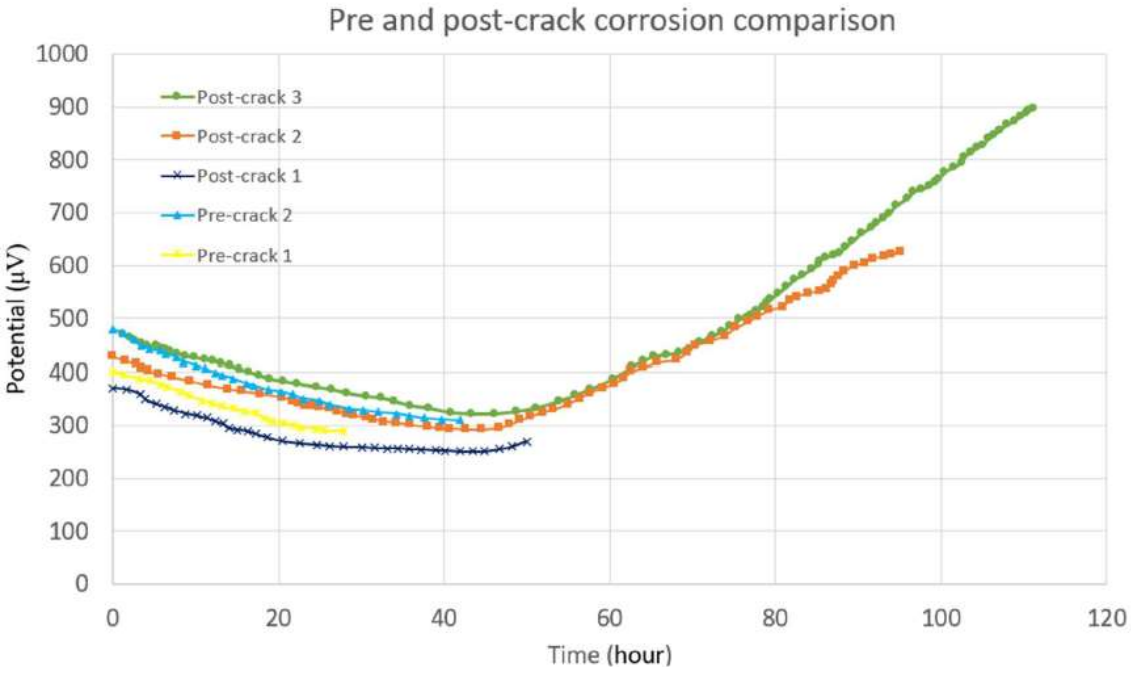

Figure 4-12 Comparison of data (potential in microvolts vs. time in hours) in pre and post-cover crack on five different non-reactive specimens with seven days of curing

Table 4-6 Rebar weight loss percentage, time to corrosion-induced crack, minimum and maximum crack width in pre and post-crack scenarios using seven days cured none-reactive ACIC specimens

Category	ACIC corrosion comparison specimen with 7-day curing				
	Pre-crack 1	Pre-crack 2	Post-crack 1	Post-crack 2	Post-crack 3
Rebar mass loss percentage	1.22%	3.41%	5.2%	7.87%	9.12%
Time (hours)	28	41	49	95	111
Minimum visible crack width (mm)	None	None	0.31	0.4	0.32
Maximum visible crack width (mm)	None	None	0.57	2	3.2

Some depictions of the experiment can be seen below Figure 4-13:

Figure 4-13 (Top left) ACIC specimen during the test with corrosion byproducts oozing out, (Bottom Left) Cleaned cracked specimen with crack pattern parallel to the embedded N12 rebar, (Top right) Extracted corroded N12 rebar with heavy corrosion and pitting signs, (Bottom right) Corroded specimen cut parallel to the central axis to extract rebar, the corrosion by-products can be seen on the surface of the concrete by brown, dark brown and black colours

From the information gained through Figure 4-12 and Table 4-6, it is evident that the time to corrosion-induced crack in the concrete cover is correlated with the items listed below:

- The chloride-induced corrosion cracks occur when the time vs. voltage curve starts to rise (49 hours).

- We can assume that the rebar mass loss percentage associated with chloride-induced corrosion crack to occur is between 3.41 and 5.2 per cent.
- As time progresses, maximum crack width and rebar mass loss increase as well.
- From observing the Post crack-1 specimen, it is evident that chloride-induced corrosion occurs as the U shaped curve starts to rise.

4.7.2 Main ACIC Test

After evaluating the specimens in pre and post-cracking situations and determining the time to chloride-induced corrosion crack patterns, the main ACIC tests are conducted. These tests were conducted in pairs with cylindrical (Ø100mm × 200mm) specimens with N12 steel reinforcement for reactive and non-reactive specimens at the age of 10-day, 30-day, 60-day, 90-day and 150-days. The reactive specimens were cured for three days in normal conditions according to the AS 1012.8.1. After the initial curing, all the reactive ACIC specimens were transferred to 38°C climate chamber. The reactive specimens were also cured in 1M sodium hydroxide (NaOH) solution in the 38°C climate chamber, while the non-reactive specimens were submerged in water at 22°C.

The epoxy at the top of the rebars were cleaned and sandpapered for a clean surface to solder the wire to the rebar, which acts as the anode. The specimens were closely monitored utilizing the data logger and PicoLog software for any spike in voltage that would indicate the cover cracking due to chloride-induced corrosion

ASR, in its nature, is a long-term deteriorating effect which is accelerated in this study by boosting the alkali concrete of the cement to 1.25% (Na_2O_{eq}) and submerging the specimens is 1M sodium hydroxide (NaOH) to prevent alkali leaching, which can contribute to lowering the ASR process in a laboratory environment since the specimens are submerged in water to have access to an unlimited supply of moisture. If sufficient moisture is not supplied to the specimens, ASR progress will cease.

The reactive specimens boosted with 1.25% (Na_2O_{eq}) and submerged in 1M sodium hydroxide (NaOH) solution showed white material, likely ASR gel exuding out of the cylinder after the age of 120-day as shown in Figure 4-14. The ASR gel gradually converts to C-S-H due to alkali recycling, and it is also carbonated when exposed to air. This means that ASR was progressing through the reactive specimens well before the age of 120-days filling the concrete pores with ASR gel until showing itself on the surface of the specimens oozing out as a white substance. Research conducted by Trejo et al. (2017) argues that ASR gel which fills the pore of the concrete, can contribute to retarding the ingress of chloride ions and act as a barrier to prevent chloride ions from entering (Trejo et al., 2017). Additionally, Energy-dispersive X-ray (EDX) analysis done by Trejo et al. (2017) shows chloride levels in ASR gel are low or non-detectable, further proving that ASR gel contributes to lowering the diffusion of chloride ions (Trejo et al., 2017).

Figure 4-14 Reactive cylindrical (Ø100mm × 200mm) specimens with an N12 steel reinforcement with ASR gel exuding and microcracking on the surface

The results from the experiment for 10-day, 30-day, 60-day, 90-day and 150-day are presented in Figure 4-15, Figure 4-16, Figure 4-17, Figure 4-18, and Figure 4-19, respectively.

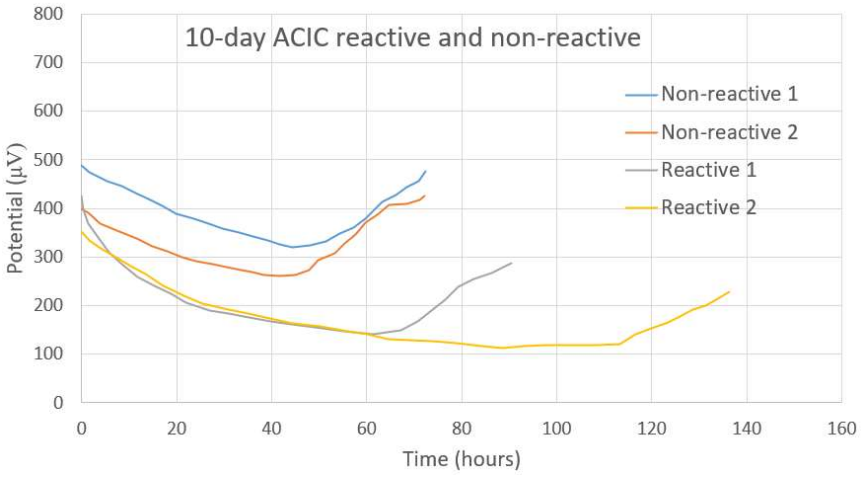

Figure 4-15 10-day ACIC test

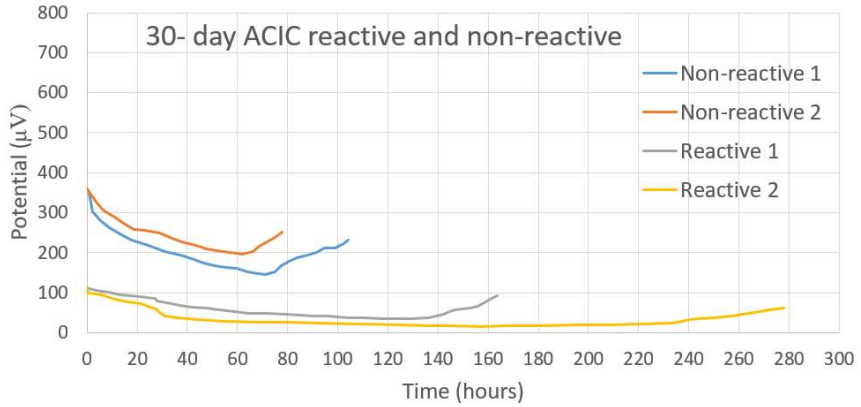

Figure 4-16 30-day ACIC test

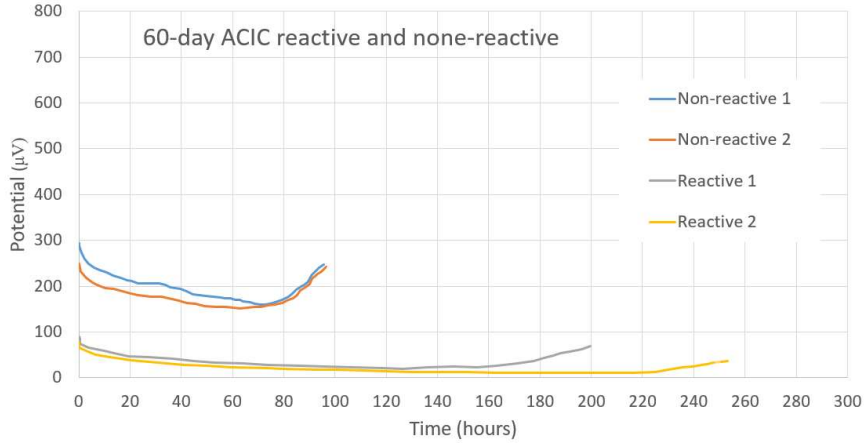

Figure 4-17 60-day ACIC test

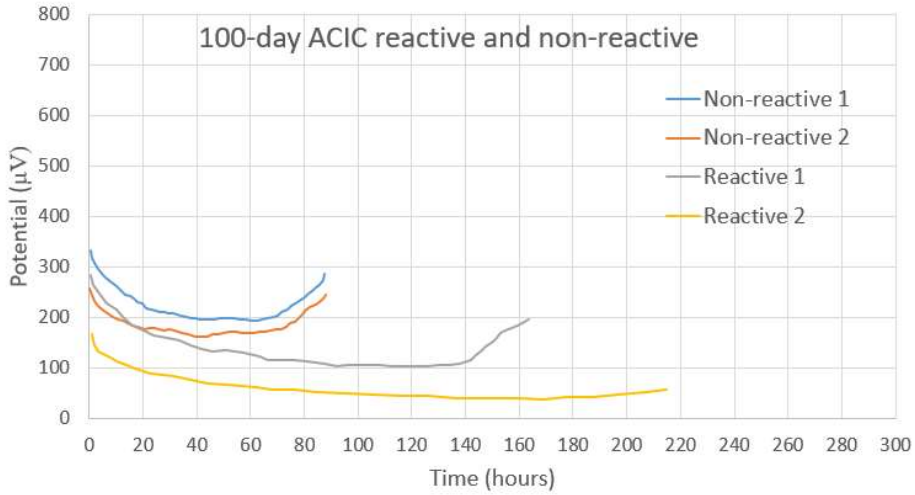

Figure 4-18 100-day ACIC test

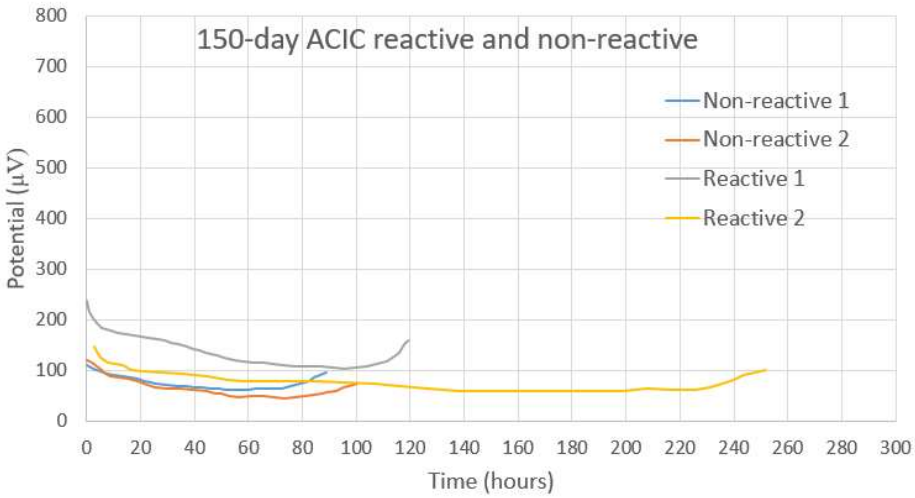

Figure 4-19 150-day ACIC test

The condition of some of the specimens after the ACIC experiment can be seen in Figure 4-20. After the experiment, the minimum and maximum crack widths are measured. Additionally, the N12 rebars are extracted for examination and rebar mass loss percentage measurement Figure 4-21.

Figure 4-20 Cover cracking of cylindrical specimens embedded with N12 rebar outlined with red colour

Figure 4-21 (Left) Extracted unclean corroded rebars, (Right) Sandblasted rebar the left side of the rebar, which was covered in epoxy, has no signs of corrosion, while the right side is heavily corroded with signs of pitting corrosion

The chloride-induced corrosion cover cracking time, rebar mass loss, and maximum and minimum crack widths are presented in Table 4-7 at the age of 10-day, 30-day, 60-day, 100-day and 150-day for reactive and non-reactive cylindrical specimens embedded with N12 rebar for ACIC test.

Table 4-7 Time to chloride-induced corrosion crack, rebar mass loss, minimum and maximum visible crack width on 10-day, 30-day, 60-day, 100-day and 150-day for reactive and non-reactive specimens in ACIC test

Curing duration	Category	Specimen number	Chloride-induced corrosion cracking time (hours)	Rebar mass loss percentage	Minimum visible crack width (mm)	Maximum visible crack width (mm)
10-day	Non-reactive	1	50	4.18	0.21	0.8
		2	45	3.97	0.34	0.71
	Reactive	1	70	4.9	0.21	0.68
		2	97	4.32	0.36	0.9
30-day	Non-reactive	1	66	5.13	0.24	0.5
		2	77	4.61	0.28	0.66
	Reactive	1	139	3.98	0.41	0.87
		2	180	4.85	0.23	0.81
60-day	Non-reactive	1	75	5.02	0.26	0.98
		2	73	4.1	0.17	0.65
	reactive	1	133	5.31	0.37	0.77
		2	219	4.94	0.44	0.87
100-day	Non-reactive	1	73	4.01	0.2	0.87
		2	67	5.05	0.19	0.76
	reactive	1	138	5.09	0.31	0.91
		2	208	4.21	0.29	0.77
150-day	Non-reactive	1	79	5.1	0.18	0.58
		2	91	4.04	0.21	0.87
	reactive	1	112	3.98	0.21	0.62
		2	240	4.83	0.35	0.7

To better illustrate the different times of cover cracking due to chloride-induced corrosion in reactive and non-reactive specimens, Figure 4-22 is presented.

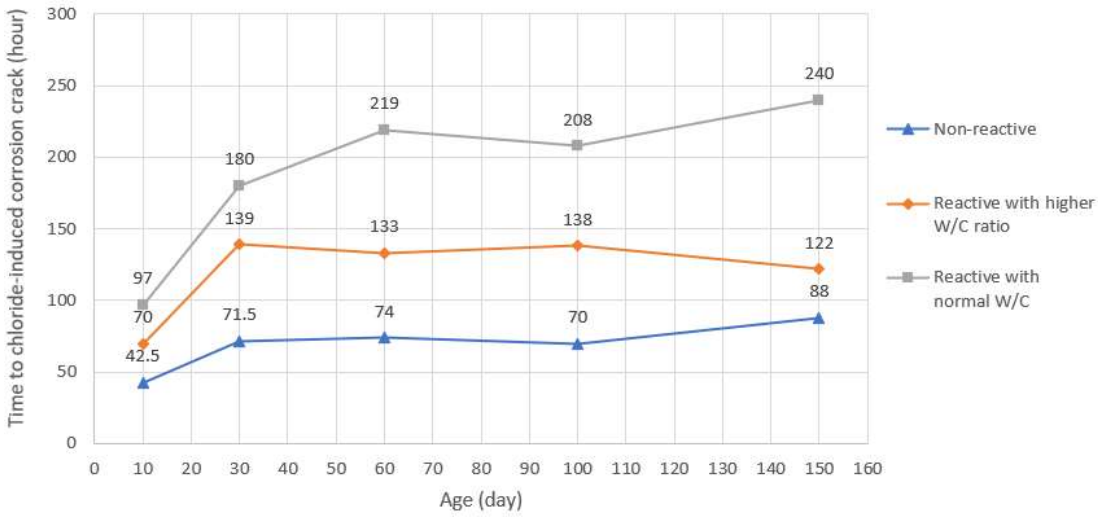

Figure 4-22 Average time to chloride-induced corrosion crack in reactive and non-reactive specimens

Based on the information provided in Table 4-7 and Figure 4-22, for the ACIC test, we can assume that the early improvement of time to crack from 10-day to 30-day in all of the specimens are due to the hydration of concrete. As the concrete sets, the pores are filled, and the tortuosity of the concrete increases resulting in a higher time to crack. Reactive specimens results in ACIC tests compared to non-reactive specimens indicate that as time passes and ASR progresses within the concrete environment, the time to chloride-induced corrosion is increased, suggesting a reduction in concretes chloride diffusivity in reactive specimens. All specimens show an average rebar mass loss of 4.86 with pitting corrosion signs and were relatively consistent throughout the experiment as the specimens were removed from the ACIC test as soon as any indications of crack were observed by monitoring the data logger. Overall it can be concluded that reactive specimens with a normal W/C ratio of 0.4 affected by ASR show about 64.58% more resistance to chloride-induced corrosion crack compared to non-reactive specimens with the same W/C ratio at the age of 150-day.

Comparing the reactive specimens with a higher W/C ratio of 0.42 and normal W/C, which is 0.4, indicates that the water content of the concrete mix can play an

essential role in the outcome of the test as the water content of the concrete increases the time to chloride-induced corrosion crack in concrete cover decreases by a considerable amount.

The alkali boosting of the reactive specimens have also been considered as they may affect the passive layer, which protects the rebar. As ASR progresses within the concrete, it consumes the available NaOH and reduces the alkalinity and pH of the concrete (Rajabipour et al., 2015). In his study, Trejo et al. (2017) also observed that the specimens affected by ASR have a lower critical chloride threshold, resulting from ASR gel lowering the pH of the concrete environment. Assuming this factor and the reduction of pH as ASR progresses, the non-reactive specimens were not boosted to have an accurate result when it comes to non-reactive specimens chloride-induced corrosion crack over a long period.

4.8 Chloride Migration Coefficient Test

To determine if ASR gel can affect the movement of chloride ions within the concrete environment, the NT build 492 test was utilized to determine the migration coefficient from the non-steady-state migration test. The testing procedure is explained in detail in chapter 3.10.

Figure 4-23 (Left) NT build 492 test tank and (Right) Specimens ready for NT build 492 test after extracting from the vacuum chamber

The tests were conducted on specimens with the age of 10-day, 30-day, 60-day, 100-day and 150-day on reactive and non-reactive specimens. The number of the testing specimens can be seen below in Table 4-8.

Table 4-8 Migration confidant values for reactive and non-reactive specimens

Curing duration	Category	Specimen number	non-steady-state migration coefficient D_{nssm} $(10^{-12}m^2/s)$	Average D_{nssm} value	Standard Deviation
10-day	Non-reactive	1	9.11	9.14	0.18
		2	8.98		
		3	9.33		
	Reactive	1	8.88	8.89	0.21
		2	9.10		
		3	8.67		
30-day	Non-reactive	1	9.21	9.48	0.64
		2	9.01		
		3	10.22		
	Reactive	1	7.31	7.5	0.33
		2	7.89		
		3	7.3		
60-day	Non-reactive	1	9.81	9.42	0.35
		2	9.32		
		3	9.13		
	reactive	1	6.8	6.58	0.32
		2	6.21		
		3	6.73		
100-day	Non-reactive	1	7.5	8.06	0.53
		2	8.11		
		3	8.57		
	reactive	1	5.98	6.11	0.18
		2	6.32		
		3	6.03		
150-day	Non-reactive	1	7.89	7.76	0.33
		2	8.01		
		3	7.38		
	reactive	1	5.56	5.46	0.3
		2	5.70		
		3	5.12		

To better interpret the results, the age vs. average migration coefficient is plotted in Figure 4-24.

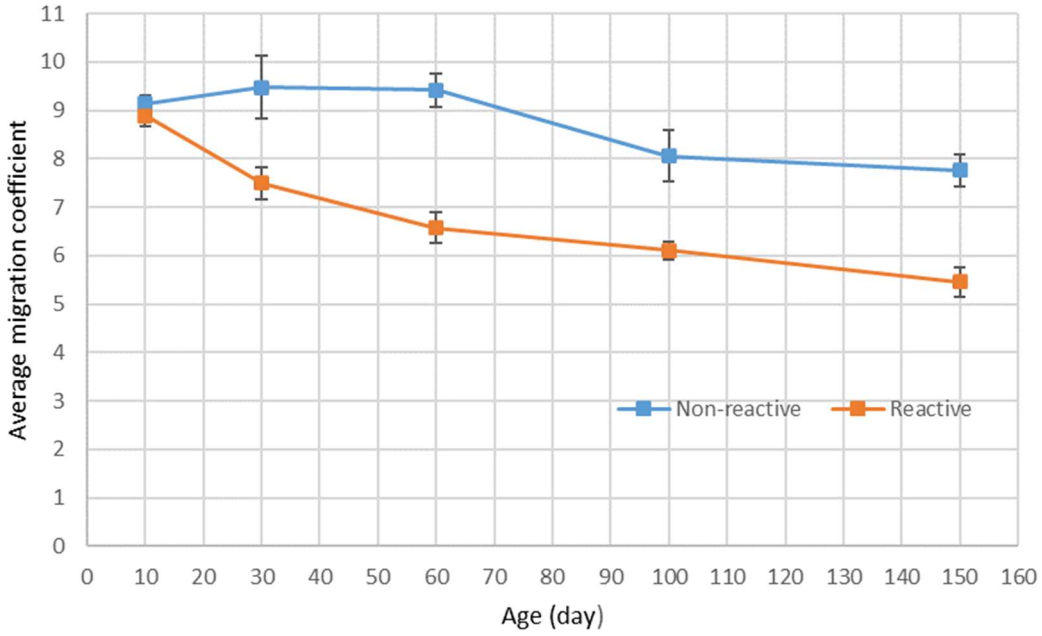

Figure 4-24 Average migration coefficient at different curing ages

At the age of 100 days, the specimens containing reactive aggregate showed signs of microcracking on the surface and AR gel deposits after extracting the specimens from the vacuum chamber. Some of the ASR gel deposits and microcracking were not detectable before putting them inside the vacuum chamber and submerging them in calcium hydroxide $Ca(OH)_2$. ASR gel deposits and microcracks are presented in Figure 4-25.

Figure 4-25 (Left) White ASR gel deposits on the surface of the NT build 492 test specimens at the age of 100-day and (Right) Side view of the same specimen which contains microcracks

The average penetration depth of reactive specimens was lower than that of non-reactive specimens starting from day 30, resulting in a lower diffusion coefficient for reactive specimens Figure 4-26, this trend was persistent through the rest of the tests.

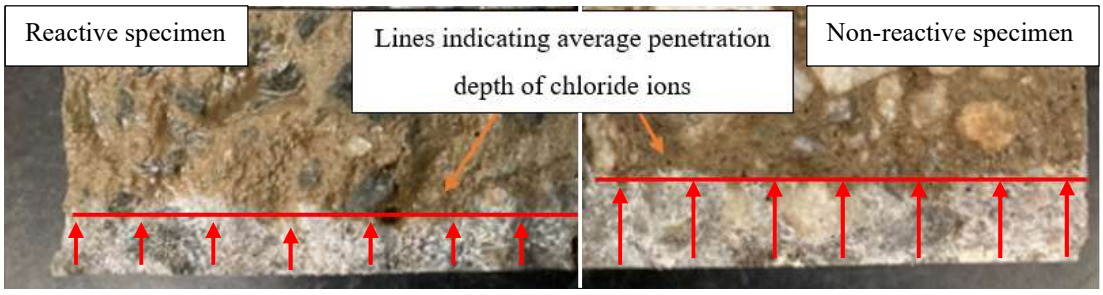

Figure 4-26 Axially split reactive and non-reactive specimens at 90-day of curing age undergone NT build 492 test indicating a lower penetration depth in reactive specimens on the left compared to the non-reactive specimen on the right after spraying them with 0.1 silver nitrate

A low migration and diffusion coefficient value indicate that the concrete is less porous and can better survive external attacks in harsh environments such as tidal zones.

There is a considerable difference in the migration coefficient of reactive and non-reactive specimens starting from the curing age of 30-day, based on Figure 4-24 Average migration coefficient at different curing ages The lowering in migration

coefficient in reactive specimens compared to non-reactive specimens is a good indication of ASR gel affecting the chloride ions migration/diffusivity in the concrete environment. An Improvement of 23.78%, 30.14%, 24% and 29.63% in chloride diffusion coefficient can be seen in 30-day, 60-day, 100-day and 150-day, respectively.

This can be explained by ASR gel blocking chloride ions' ingress due to filling the void gaps (Berndt, 2019; Tordoff, 1990; Trejo et al., 2017). The experimental study conducted by Trejo et al. (2017) shows that in addition to ASR gel reducing the chloride diffusion, it also lowers the critical chloride threshold, which reduces the chloride initiation time due to ASR lowering the pH of the concrete environment. The lowering in migration coefficient and critical chloride threshold in reactive specimens can set an equilibrium in the result of corrosion initiation time and lead to the same corrosion initiation time in reactive and non-reactive specimens.

4.9 Summary

In this chapter, the results of the experimental program were presented. The effect of ASR on concrete mechanical properties was experimented along with the combined effect of ASR and chloride-induced corrosion in reactive and non-reactive specimens utilizing ACIC test. The effect of ASR gel in retarding the ingress of chloride ions in concrete was also measured using NT build 492 standards for non-steady-state chloride migration coefficient measurement. From the gained results, it is evident that ASR influences the ingress of chloride and time to chloride-induced corrosion crack in reactive specimens utilizing accelerated test methods. ASR cracks were also observed in specimens containing reactive aggregate.

4.9.1 Fresh Concrete Properties

The results of the slump test, density, and air volume measurements in creating multiple batches show the concrete has good homogeneity and workability in both reactive and non-reactive mixes.

4.9.2 Concrete Mechanical Properties

The mechanical properties of reactive and non-reactive specimens were examined over a 150-day curing age. The reactive cylindrical specimens expanded by 0.12%.

Results show that ASR did not significantly impact the concrete compressive strength and indirect tensile strength. However, an average reduction of 22.56% in Young's modulus of elasticity was observed in reactive specimens affected by ASR. This indicates that ASR damage is sensitive to Young's modulus of elasticity and is a good indicator of ASR progress in concrete.

4.9.3 Durability Performance

Preliminary ACIC tests have been conducted on non-reactive specimens to assess pre and post crack behaviour of specimens undergoing the test and calculate rebar mass loss, minimum and maximum crack width that occurs at the time of chloride-induced corrosion crack. No signs of the crack were detected before any sudden rise in voltage which indicates cover cracking has occurred in concrete. However, a reduction in rebar mass was detected in pre-crack specimens. Post-crack specimens show that as time passes, crack width and rebar mass loss increases after the initial crack has occurred. It is essential to remove the specimens from the device as soon as any indications of a sudden rise in voltage occur to be able to measure the minimum and maximum crack width on the concrete cover and the percentage of the rebar mass loss accurately.

To investigate the combined effect of ASR and chloride-induced corrosion on time to chloride induced-corrosion crack in concrete cover, tests were conducted on reactive and non-reactive reinforced cylinders over 10-day, 30-day, 60-day, 100-day and 150-day curing ages. The results show that the reactive specimens take a significantly longer time to chloride-induced corrosion crack on the concrete cover and are about 68% more resistant to cover cracking at later ages compared to non-reactive specimens due to corrosion. The water content can also heavily impact the ACIC test as it is observed that RB1 with a higher W/C ratio showed faster crack time due to corrosion than its counterpart with a normal W/C ratio. The rebar mass loss and minimum and maximum crack width have been measured throughout all the experiments. The

average crack width and rebar mass loss in reactive and non-reactive specimens were in the same range.

Chloride migration coefficient tests on reactive and non-reactive specimens have been conducted in 10-day, 30-day, 60-day, 100-day and 150-day curing ages. Reactive specimens show a reduction in migration coefficient compared to non-reactive specimens as time passes. Results gained on non-steady-state migration confidant show that as ASR progresses within the concrete, ASR gel may fill the gaps and block the movement of chloride ions in concretes interconnected pore, resulting in lower migration coefficient in reactive specimens affected by ASR, making it more resilient against chloride ions penetration.

Chapter 5
Summary and Conclusion

5.1 Overview

ASR is a harmful long-term concrete durability issue and has been searched to a reasonable extent in the past years since its discovery. However, its combined effect with another deleterious phenomenon such as chloride-induced corrosion, which can devastate RC structures, has not been well researched, and there are a limited number of publications regarding their combined effects influence on mechanical properties and durability performance.

This study has investigated the influence of ASR and chloride-induced corrosion in RC structures and gives an insight into how their combined effects can influence a structure suffering from both deleterious effects.

A complete literature review has been conducted on the effects of ASR on RC structure serviceability, corrosion and their combined effects.

A preliminary mix design was conducted to ensure the characteristic compressive strength (f_c') of specimens were not below 40 MPa for the main concrete mix.

Mechanical properties consisting of compressive strength, tensile strength and Young's modulus of elasticity have been conducted on reactive and non-reactive specimens over 150 days to assess the impact of ASR on concrete mechanical properties along with expansion measurement on cylindrical specimens.

Accelerated Chloride-Induced Corrosion (ACIC) tests have been conducted on reactive and non-reactive cylindrical specimens embedded with rebar to evaluate the combined effects of ASR and chloride-induced corrosion on time to cracking of concrete cover. Additionally, non-steady-state chloride migration coefficients of non-reactive and reactive specimens have been measured utilizing NT build 492 to assess the effect of ASR by-product, ASR gel, on the transportation of chloride ions in concrete.

It is worth mentioning that there are no standards for evaluating the combined effects of ASR and chloride-induced concrete corrosion. There has been very limited research regarding the combined effects of ASR and chloride-induced corrosion throughout the literature, and none of them utilizes accelerated methods making this a novel research.

5.2 Conclusions

- Reactive cylindrical specimens stored in 38°C climate chamber in 1M sodium hydroxide solution showed signs of ASR-induced microcrack with ASR gel exuding out of the concrete cover at the age of 120 days of curing. Expansion of the reactive and non-reactive specimens was measured. The maximum expansion of reactive specimens were 0.12%, while non-reactive specimens showed no signs of expansion over 150-day of curing.
- The compressive strength of reactive specimens affected by ASR showed relatively no reduction in compressive strength compared to non-reactive specimens throughout the curing ages of 10-day, 30-day, 56-day, 90-day and 150-day. ASR has not affected the concretes compressive strength throughout the experiment.

- Indirect tensile strength tests have been conducted to measure the tensile strength of reactive and non-reactive cylindrical specimens throughout the curing ages of 10-day, 30-day, 56-day, 90-day and 150-day. Results show a minimal amount of reduction in tensile strength in reactive specimens.
- Young's modulus of elasticity of reactive and non-reactive specimens were also measured at the ages of 10-day, 30-day, 56-day, 90-day and 150-day. The average modulus of elasticity of the reactive specimens were lower in comparison with non-reactive specimens by 22.5%, indicating that ASR is sensitive to the modulus of elasticity test and can be a good criterion in evaluating the ASR progression in concrete.
- Accelerated Chloride-Induced Corrosion (ACIC) tests were conducted to assess the combined effects of ASR and chloride-induced corrosion in time to chloride-induced corrosion crack on the concrete cover in cylindrical specimens embedded with rebar. The obtained results indicate that as time passes, the time to chloride-induced corrosion of reactive specimens increases by a significant amount in comparison with non-reactive specimens by 64.58% at the age of 150-day. All specimens show an average rebar mass loss of 4.86 with pitting corrosion signs and were relatively consistent throughout the experiment. The maximum and minimum crack width of the reactive and non-reactive specimens were in the same range throughout the ACIC tests. The water content of the concrete can significantly influence the result of the ACIC test as well, as the water content of concrete increases the time to chloride-induced corrosion crack in concrete cover decreases as well.
- The chloride migration officiant of reactive and non-reactive specimens were measured utilizing NT build 492. The results show that both reactive and non-reactive specimens migration officiant lower as time passes because of the concrete hydration process filling up the pores and gaps within the concrete. The reactive specimens show a lower migration officiant than non-reactive specimens with an average of 23.78%, 30.14%, 24% and 29.63% in 30-day, 60-day, 100-day and 150-day, respectively. This indicates that ASR and its by-product ASR gel can influence the

chloride migration in concrete and lower its value as ASR progresses within the concrete environment.

5.3 Recommendations for Future Studies

More research is needed on the topic of combined effects of ASR and chloride-induced corrosion as there are very limited number of publications on this topic. ASR and Chloride-induced corrosion are both time-consuming deteriorating effects, making it very challenging to simulate them in the laboratory environment for the results to correlate with structure in the field damaged by combined effects of ASR and chloride-induced corrosion as there are no universal standards on this topic. Experiments such as surface chloride content and critical chloride threshold level can also be evaluated in future studies. Longer-term test duration is also recommended for better results as there were time restrictions because this was a master's degree project, and the tests were conducted during the Covid peak.

The addition of Supplementary Cementitious Material (SCM) such as ground granulated blast furnace slag, fly ash, and silica fume can be assessed in concrete, and tests such as ACIC and chloride migration coefficient can be conducted. Additionally, diffusion tests such as ponding can be conducted in a longer period of two to three years to evaluate better the effect of chloride diffusion on concrete affected by ASR as ASR progress takes a long time in concrete.

The influence of different types of aggregate with different reactivity and sizes can also be evaluated on the combined effects of ASR and chloride-induced corrosion as different reactive aggregate sizes and reactivity types may influence the combined effects of ASR and chloride-induced corrosion. Additionally, further tests can be conducted on full-scale structures to achieve a more realistic result.

Accelerated autoclave test can also be utilized to accelerate the ASR progress in a much shorter duration to evaluate the combined effects of ASR and chloride-induced corrosion and evaluate the migration or diffusion confidant. Petrographic and

Scanning Electron Microscopy analysis can also be conducted to evaluate the effect of ASR gel on preventing the ingress of chloride ions.

References

Ahmed, T., Burley, E., Rigden, S., & Abu-Tair, A. I. (2003). The effect of alkali reactivity on the mechanical properties of concrete. *Construction and Building Materials, 17*(2), 123-144. https://doi.org/10.1016/S0950-0618(02)00009-0

Alaud, S., & van Zijl, G. P. (2016). Effects on Concrete Properties by ASR Deterioration under Different Exposure Conditions. Proceedings of the Sixth International Conference on Structural Engineering, Mechanics, and Computation (SEMC), Cape Town, South Africa.

Alonso, M. C., & Sanchez, M. (2009). Analysis of the variability of chloride threshold values in the literature. *Materials and Corrosion, 60*(8), 631-637. 10.1002/maco.200905296

Andrade, C., Alonso, C., & Molina, F. (1993). Cover cracking as a function of bar corrosion: Part I-Experimental test. *Materials and Structures, 26*(8), 453-464.

Angst, U., Elsener, B., Larsen, C. K., & Vennesland, Ø. (2009). Critical chloride content in reinforced concrete — A review. *Cement and Concrete Research, 39*(12), 1122-1138. https://doi.org/10.1016/j.cemconres.2009.08.006

ASCE. (2017). America's infrastructure report card 2017.

Babaee, M., & Castel, A. (2018). Chloride diffusivity, chloride threshold, and corrosion initiation in reinforced alkali-activated mortars: Role of calcium, alkali, and silicate content. *Cement and Concrete Research, 111*, 56-71. https://doi.org/10.1016/j.cemconres.2018.06.009

Barbosa, R. A., Hansen, S. G., Hansen, K. K., Hoang, L. C., & Grelk, B. (2018). Influence of alkali-silica reaction and crack orientation on the uniaxial compressive strength of concrete cores from slab bridges. *Construction and Building Materials, 176*, 440-451. https://doi.org/10.1016/j.conbuildmat.2018.03.096

Berndt, M. L. A. (2019). Lucinda Jetty revisited: alkali-silica reaction and corrosion in prestressed concrete. *Proceedings of the Institution of Civil Engineers - Structures and Buildings, 0*(0), 1-12. 10.1680/jstbu.18.00148

Bertolini, L. (2013). *Corrosion of steel in concrete prevention, diagnosis, repair* (2nd. completely rev. & enl. ed. ed.). Wiley-VCH.

Bérubé, M.-A., Duchesne, J., Dorion, J. F., & Rivest, M. (2002). Laboratory assessment of alkali contribution by aggregates to concrete and application to concrete structures affected by alkali–silica reactivity. *Cement and Concrete Research, 32*(8), 1215-1227. https://doi.org/10.1016/S0008-8846(02)00766-4

Bhargava, K., Ghosh, A. K., Mori, Y., & Ramanujam, S. (2006). Model for cover cracking due to rebar corrosion in RC structures. *Engineering Structures, 28*(8), 1093-1109. https://doi.org/10.1016/j.engstruct.2005.11.014

Binal, A. (2015). The Pessimum Ratio and Aggregate Size Effects on Alkali Silica Reaction. *Procedia Earth and Planetary Science, 15*, 725-731. https://doi.org/10.1016/j.proeps.2015.08.103

Böhni, H. (2005). *Corrosion in reinforced concrete structures*. Elsevier.

Cao, C., Cheung, M. M. S., & Chan, B. Y. B. (2013). Modelling of interaction between corrosion-induced concrete cover crack and steel corrosion rate. *Corrosion Science, 69*, 97-109. https://doi.org/10.1016/j.corsci.2012.11.028

Cao, J., Gowripalan, N., Sirivivatnanon, V., & South, W. (2021). Accelerated test for assessing the potential risk of alkali-silica reaction in concrete using an autoclave. *Construction and Building Materials, 271*, 121871. https://doi.org/10.1016/j.conbuildmat.2020.121871

Courtier, R. H. (1990). The assessment of ASR-affected structures. *Cement and Concrete Composites, 12*(3), 191-201. https://doi.org/10.1016/0958-9465(90)90020-X

Crank, J. (1975). The Mathematics of Diffusion. *Clarendon Press*.

Cui, Z., & Alipour, A. (2018). Concrete cover cracking and service life prediction of reinforced concrete structures in corrosive environments. *Construction and Building Materials, 159*, 652-671. https://doi.org/10.1016/j.conbuildmat.2017.03.224

Davis, P. D., Parbrook, G. D., & Kenny, G. N. C. (1995). CHAPTER 7 - Diffusion and Osmosis. In P. D. Davis, G. D. Parbrook, & G. N. C. Kenny (Eds.), *Basic Physics and Measurement in Anaesthesia (Fourth Edition)* (pp. 89-102). Butterworth-Heinemann. https://doi.org/10.1016/B978-0-7506-1713-0.50012-3

Dron, R., & Brivot, F. (1992). Thermodynamic and kinetic approach to the alkali-silica reaction. Part 1: Concepts. *Cement and Concrete Research, 22*(5), 941-948. https://doi.org/10.1016/0008-8846(92)90118-F

Fan, S., & Hanson, J. M. (1998). Effect of alkali silica reaction expansion and cracking on structural behavior of reinforced concrete beams. *ACI Structural Journal, 95*, 498-505.

French, W. J. (1980). Reactions between aggregates and cement paste—an interpretation of the pessimum. *Quarterly Journal of Engineering Geology and Hydrogeology, 13*(4), 231-247.

Funahashi, M. (1990). Predicting corrosion-free service life of a concrete structure. *ACI Mater. J, 87*, M62.

GHD. (2015). Infrastructure maintenance–A report for Infrastructure Australia. GHD Sydney, Australia.

Giaccio, G., Zerbino, R., Ponce, J. M., & Batic, O. R. (2008). Mechanical behavior of concretes damaged by alkali-silica reaction. *Cement and Concrete Research, 38*(7), 993-1004. https://doi.org/10.1016/j.cemconres.2008.02.009

Giannini, E. R., Sanchez, L. F. M., Tuinukuafe, A., & Folliard, K. J. (2018). Characterization of concrete affected by delayed ettringite formation using the stiffness damage test. *Construction and Building Materials, 162*, 253-264. https://doi.org/10.1016/j.conbuildmat.2017.12.012

Gillott, J. E. (1975). Alkali-aggregate reactions in concrete. *Engineering Geology, 9*(4), 303-326. https://doi.org/10.1016/0013-7952(75)90013-7

Gjørv, O. E. (2014). *Durability Design of Concrete Structures in Severe Environments*. Taylor & Francis Group.

Güneyisi, E., Gesoğlu, M., Karaboğa, F., & Mermerdaş, K. (2013). Corrosion behavior of reinforcing steel embedded in chloride contaminated concretes with and without metakaolin. *Composites Part B: Engineering, 45*(1), 1288-1295. https://doi.org/10.1016/j.compositesb.2012.09.085

Hansson, C. M., Poursaee, A., & Laurent, A. (2006). Macrocell and microcell corrosion of steel in ordinary Portland cement and high performance concretes. *Cement and Concrete Research, 36*(11), 2098-2102. https://doi.org/10.1016/j.cemconres.2006.07.005

Hou, X., Struble, L. J., & Kirkpatrick, R. J. (2004). Formation of ASR gel and the roles of C-S-H and portlandite [Article]. *Cement and Concrete Research, 34*(9), 1683-1696. 10.1016/j.cemconres.2004.03.026

ISE. (1992). Structural Effects of Alkali-Silica Reaction – Technical Guidance on the Appraisal of Existing Structures. *Institution of Structural Engineers, London*.

Islam, M. S., & Ghafoori, N. (2018). A new approach to evaluate alkali-silica reactivity using loss in concrete stiffness. *Construction and Building Materials, 167*, 578-586. https://doi.org/10.1016/j.conbuildmat.2018.02.047

Ji, Y.-s., Zhao, W., Zhou, M., Ma, H.-r., & Zeng, P. (2013). Corrosion current distribution of macrocell and microcell of steel bar in concrete exposed to chloride environments. *Construction and Building Materials, 47*, 104-110. https://doi.org/10.1016/j.conbuildmat.2013.05.003

Jones, A. E. K., & Clark, L. A. (1998). The effects of ASR on the properties of concrete and the implications for assessment. *Engineering Structures, 20*(9), 785-791. https://doi.org/10.1016/S0141-0296(97)00125-9

Kongshaug, S. S., Oseland, O., Kanstad, T., Hendriks, M. A. N., Rodum, E., & Markeset, G. (2020). Experimental investigation of ASR-affected concrete – The influence of uniaxial loading on the evolution of mechanical properties, expansion and damage indices. *Construction and Building Materials, 245*, 118384. https://doi.org/10.1016/j.conbuildmat.2020.118384

Kreitman, K. L. (2011). *Nondestructive evaluation of reinforced concrete structures affected by alkali-silica reaction and delayed ettringite formation*.

Latifee, E. (2013). *Miniature concrete prism test-A new test method for evaluating the ASR potential of aggregates, the effectiveness of ASR mitigation and the job mixture* Clemson University].

Latifee, E. R., & Rangaraju, P. R. (2015). Miniature Concrete Prism Test: Rapid Test Method for Evaluating Alkali-Silica Reactivity of Aggregates. *Journal of Materials in Civil Engineering, 27*(7), 04014215. doi:10.1061/(ASCE)MT.1943-5533.0001183

Li, Z., Afshinnia, K., & Rangaraju, P. R. (2016). Effect of alkali content of cement on properties of high performance cementitious mortar. *Construction and Building Materials, 102*, 631-639. https://doi.org/10.1016/j.conbuildmat.2015.10.110

Maage, M., Helland, S., Poulsen, E., Vennesland, O., & Carl, J. E. (1996). Service life prediction of existing concrete structures exposed to marine environment. *Materials Journal, 93*(6), 602-608.

Maia Neto, F. M., Andrade, T. W. C. O., Gomes, R. M., Leal, A. F., Almeida, A. N. F., Lima Filho, M. R. F., & Torres, S. M. (2021). Considerations on the effect of temperature, cation type and molarity on silica degradation and implications to ASR assessment. *Construction and Building Materials, 299*, 123848. https://doi.org/10.1016/j.conbuildmat.2021.123848

Maraghechi, H. (2014). Development and assessment of alkali activated recycled glass-based concretes for civil infrastructure.

Maraghechi, H., Shafaatian, S.-M.-H., Fischer, G., & Rajabipour, F. (2012). The role of residual cracks on alkali silica reactivity of recycled glass aggregates. *Cement and Concrete Composites, 34*(1), 41-47. https://doi.org/10.1016/j.cemconcomp.2011.07.004

Marzouk, H., & Langdon, S. (2003). The effect of alkali-aggregate reactivity on the mechanical properties of high and normal strength concrete. *Cement and Concrete Composites, 25*(4), 549-556. https://doi.org/10.1016/S0958-9465(02)00094-X

Mazarei, V., Trejo, D., Ideker, J. H., & Isgor, O. B. (2017). Synergistic effects of ASR and fly ash on the corrosion characteristics of RC systems. *Construction and Building Materials, 153*, 647-655. https://doi.org/10.1016/j.conbuildmat.2017.07.097

McCormac, J., & Brown, R. (2016). *Design of reinforced concrete* (Tenth edition, ACI 318-14 code edition. ed.). John Wiley & Sons, Inc.

Mehta, P. K., & Monteiro, P. J. (2017). *Concrete microstructure, properties and materials*.

Mikata, Y., Fukutani, S., Hideaki, T., & Susumu, I. (2018). Effect of combined deterioration due to ASR and corrosion on flexural capacity of RC beams.

Mikata, Y., Matoba, R., Ura, T., & Fumoto, T. (2020). EFFECT OF COMBINED DETERIORATION DUE TO ASR AND CORROSION ON SHEAR CAPACITY OF RC BEAMS.

Mohammadi, A., Ghiasvand, E., & Nili, M. (2020). Relation between mechanical properties of concrete and alkali-silica reaction (ASR); a review. *Construction and Building Materials, 258*, 119567. https://doi.org/10.1016/j.conbuildmat.2020.119567

Multon, S., Cyr, M., Sellier, A., Leklou, N., & Petit, L. (2008). Coupled effects of aggregate size and alkali content on ASR expansion. *Cement and Concrete Research, 38*(3), 350-359. https://doi.org/10.1016/j.cemconres.2007.09.013

Nabavi, S. F. (2014). *Performance of polymer-concrete composites in service life of maritime structures*.

Neville, A. (1995). Chloride attack of reinforced concrete: an overview. *Materials and Structures, 28*(2), 63.

Nixon, P. J., & Sims, I. (2016). *RILEM Recommendations for the Prevention of Damage by Alkali-aggregate Reactions in New Concrete Structures: State-of-the-art Report of the RILEM Technical Committee 219-ACS*. Springer.

Pacheco-Torgal, F., Labrincha, J., Leonelli, C., Palomo, A., & Chindaprasit, P. (2014). *Handbook of alkali-activated cements, mortars and concretes*. Elsevier.

Pantazopoulou, S. J., & Papoulia, K. (2001). Modeling cover-cracking due to reinforcement corrosion in RC structures. *Journal of engineering mechanics, 127*(4), 342-351.

Philibert, J. (2005). One and a Half Century of Diffusion: Fick, Einstein, Before and Beyond. *The Open-Access Journal for the Basic principles of Diffusion Theory, Experiment and Application*.

Poole, A. B., & Sims, I. (2016). *Alkali-Aggregate Reaction in Concrete: A World Review*. Taylor & Francis.

Portland Cement Association. (2002). Types and causes of concrete deterioration. *Portland Cement Association: Skokie, IL, USA*.

Pullar-Strecker. (1987). Corrosion damaged concrete assessment and repair. *Construction Industry Research and Information Association*.

Rajabipour, F., Giannini, E., Dunant, C., Ideker, J. H., & Thomas, M. D. (2015). Alkali–silica reaction: current understanding of the reaction mechanisms and the knowledge gaps. *Cement and Concrete Research, 76*, 130-146.

Rivard, P., Ballivy, G., Gravel, C., & Saint-Pierre, F. (2010). Monitoring of an hydraulic structure affected by ASR: A case study. *Cement and Concrete Research, 40*(4), 676-680. https://doi.org/10.1016/j.cemconres.2009.09.010

Saetta, A. V. (2005). Deterioration of Reinforced Concrete Structures due to Chemical–Physical Phenomena: Model-Based Simulation. *Journal of Materials in Civil Engineering, 17*(3), 313-319. doi:10.1061/(ASCE)0899-1561(2005)17:3(313)

Sagüés, A. A., Sánchez, A. N., Lau, K., & Kranc, S. C. (2014). Service life forecasting for reinforced concrete incorporating potential-dependent chloride threshold [Article]. *Corrosion, 70*(9), 942-957. 10.5006/1286

Saint-Pierre, F., Rivard, P., & Ballivy, G. (2007). Measurement of alkali–silica reaction progression by ultrasonic waves attenuation. *Cement and Concrete Research, 37*(6), 948-956. https://doi.org/10.1016/j.cemconres.2007.02.022

Sanchez, L., Fournier, B., Jolin, M., & Bastien, J. (2015). Evaluation of the Stiffness Damage Test (SDT) as a tool for assessing damage in concrete due to alkali-silica reaction (ASR): Input parameters and variability of the test responses. *Construction and Building Materials, 77*, 20-32.

Sanchez, L. F. M., Fournier, B., Jolin, M., & Bastien, J. (2014). Evaluation of the stiffness damage test (SDT) as a tool for assessing damage in concrete due to ASR: Test loading and output responses for concretes incorporating fine or coarse reactive aggregates. *Cement and Concrete Research, 56*, 213-229. https://doi.org/10.1016/j.cemconres.2013.11.003

Sanchez, L. F. M., Fournier, B., Jolin, M., Bastien, J., & Mitchell, D. (2016). Practical use of the Stiffness Damage Test (SDT) for assessing damage in concrete infrastructure affected by alkali-silica reaction. *Construction and Building Materials, 125*, 1178-1188. https://doi.org/10.1016/j.conbuildmat.2016.08.101

Sanchez, L. F. M., Fournier, B., Jolin, M., & Duchesne, J. (2015). Reliable quantification of AAR damage through assessment of the Damage Rating Index (DRI). *Cement and Concrete Research, 67*, 74-92. https://doi.org/10.1016/j.cemconres.2014.08.002

Saouma, V. E. (2020). *Diagnosis and Prognosis of AAR Affected Structures: State-Of-the-Art Report of the RILEM Technical Committee 259-ISR* (Vol. 31). Springer International Publishing AG.

Schmidt, J. W., Hansen, S. G., Barbosa, R. A., & Henriksen, A. (2014). Novel shear capacity testing of ASR damaged full scale concrete bridge. *Engineering Structures, 79*, 365-374. https://doi.org/10.1016/j.engstruct.2014.08.027

Sinno, N., & Shehata, M. H. (2021). Role of temperature on Alkali-Silica reaction and the efficacy of supplementary cementitious materials. *Construction and Building Materials, 313*, 125427. https://doi.org/10.1016/j.conbuildmat.2021.125427

Somerville, G. (1985). *Engineering Aspects of Alkali-Silica Reaction*.

Stanton, T. E. (1940). *Expansion of concrete through reaction between cement and aggregate* Proc. Am. Soc. Civ. Eng.

Swamy, R. (1991). *The Alkali-Silica Reaction in Concrete*. CRC Press.

Tapas, M. J. (2020). *Role of Supplementary Cementitious Materials in Mitigating Alkali-Silica Reaction*.

Thomas, M. (2019). Alkali-silica reaction: Eighty years on. 5th fib Congress, FIB 2018.

Thomas, M., Fournier, B., Folliard, K., Ideker, J., & Shehata, M. (2006). Test methods for evaluating preventive measures for controlling expansion due to alkali–silica reaction in concrete. *Cement and Concrete Research, 36*(10), 1842-1856. https://doi.org/10.1016/j.cemconres.2006.01.014

Thomas, M. D., Folliard, K. J., Fournier, B., Rivard, P., Drimalas, T., & Garber, S. I. (2013). *Methods for Evaluating and Treating ASR-Affected Structures: Results of Field Application and Demonstration Projects: Volume II-Details of Field Applications and Analysis*.

Thomas, M. D., Fournier, B., & Folliard, K. J. (2008). *Report on determining the reactivity of concrete aggregates and selecting appropriate measures for preventing deleterious expansion in new concrete construction*.

Thomas, M. D., Fournier, B., & Folliard, K. J. (2013). *Alkali-aggregate reactivity (AAR) facts book*.

Thomas, M. D., Fournier, B., Folliard, K. J., & Resendez, Y. (2011). *Alkali-Silica Reactivity Field Identification Handbook*.

Tordoff, M. A. (1990). Assessment of pre-stressed concrete bridges suffering from alkali-silica reaction. *Cement and Concrete Composites, 12*(3), 203-210. https://doi.org/10.1016/0958-9465(90)90021-O

Trejo, D., Mazarei, V., Ideker, J. H., & Isgor, O. B. (2017). Influence of Alkali-Silica Reaction Reactivity on Corrosion in Reinforced Concrete. *ACI Materials Journal, 114*(5), 723.

Wang, H., & Gillott, J. E. (1991). Mechanism of alkali-silica reaction and the significance of calcium hydroxide. *Cement and Concrete Research, 21*(4), 647-654. https://doi.org/10.1016/0008-8846(91)90115-X

Win, P. P., Watanabe, M., & Machida, A. (2004). Penetration profile of chloride ion in cracked reinforced concrete. *Cement and Concrete Research, 34*(7), 1073-1079. https://doi.org/10.1016/j.cemconres.2003.11.020

Zhang, R., Castel, A., & François, R. (2010). Concrete cover cracking with reinforcement corrosion of RC beam during chloride-induced corrosion process. *Cement and Concrete Research, 40*(3), 415-425. https://doi.org/10.1016/j.cemconres.2009.09.026